Published in final edited form as:
Chem Rev. 2016 July 13; 116(13): 7642–72. doi:10.1021/acs.chemrev.5b00736.

Protons and Hydroxide Ions in Aqueous Systems

Noam Agmon[†], **Huib J. Bakker**[‡], **R. Kramer Campen**[§], **Richard H. Henchman**[‖], **Peter Pohl**[⊥], **Sylvie Roke**[#], **Martin Thämer**[▽,§], **Ali Hassanali**[*,○]

[†]The Fritz Haber Research Center, Institute of Chemistry, The Hebrew University of Jerusalem, Jerusalem 91904, Israel [‡]FOM Institute AMOLF, Science Park 104, 1098 XG Amsterdam, The Netherlands [§]Fritz Haber Institute of the Max Planck Society, Faradayweg 4-6, 14195 Berlin, Germany [‖]Manchester Institute of Biotechnology, School of Chemistry, The University of Manchester, Oxford Road, Manchester M13 9PL, United Kingdom [⊥]Johannes Kepler University Linz, Institute of Biophysics, Gruberstrasse 40, 4020 Linz, Austria [#]Laboratory for Fundamental BioPhotonics (LBP), Institute of Bioengineering (IBI), and Institute of Material Science (IMX), School of Engineering (STI), and Lausanne Centre for Ultrafast Science (LACUS), École Polytechnique Fédérale de Lausanne (EPFL), CH-1015, Lausanne, Switzerland [▽]Department of Chemistry, Institute for Biophysical Dynamics, and James Franck Institute, The University of Chicago, Chicago, Illinois 60637, United States [○]CMSP Section, The Abdus Salaam International Center for Theoretical Physics, I-34151 Trieste, Italy

Abstract

Understanding the structure and dynamics of water's constituent ions, proton and hydroxide, has been a subject of numerous experimental and theoretical studies over the last century. Besides their obvious importance in acid-base chemistry, these ions play an important role in numerous applications ranging from enzyme catalysis to environmental chemistry. Despite a long history of research, many fundamental issues regarding their properties continue to be an active area of research. Here, we provide a review of the experimental and theoretical advances made in the last several decades in understanding the structure, dynamics, and transport of the proton and hydroxide ions in different aqueous environments, ranging from water clusters to the bulk liquid and its interfaces with hydrophobic surfaces. The propensity of these ions to accumulate at hydrophobic surfaces has been a subject of intense debate, and we highlight the open issues and challenges in this area. Biological applications reviewed include proton transport along the hydration layer of various membranes and through channel proteins, problems that are at the core of cellular bioenergetics.

1 Introduction

It has been known for more than a century that protons (H^+) and hydroxide (OH^-) ions in aqueous solutions are critical in a wide variety of industrial, biological, and environmental

[*]**Corresponding Author** ahassana@ictp.it.

Notes
The authors declare no competing financial interest.

Europe PMC Funders Author Manuscripts

processes. [1–3] Driven by this appreciation, much work has been devoted to understanding the molecular-scale structure and dynamics of H^+ and OH^- in aqueous environments.[4–6] Despite extensive efforts, achieving detailed, molecular-scale insight has been challenging, partly because the structure and dynamics of protons and hydroxide ions is inextricably linked with the hydrogen bond (HB) dynamics of water, and thus, insight into the former requires a detailed understanding of the latter. Driven, in part, by massive improvements in computational and experimental techniques, the last 20 years have seen a dramatic enhancement in our understanding of both systems. In this paper we review these fundamental developments.

We begin by briefly describing the founding experiments of the field. These observations strongly suggested that H^+ and OH^- are unlike other ions in water: e.g., their solvation and transport properties differ dramatically. To understand how molecular-scale structure controls these macroscopic effects, experimental and theoretical tools are required that allow interrogation of molecular-scale structure and dynamics of both ions. Partly in an effort to develop such tools, numerous experimental and theoretical studies of gas-phase charged clusters have been conducted. Because these systems are cold and contain only small numbers of water molecules, experimental observables, most notably the infrared (IR) spectrum, are hopefully straightforward to interpret and computation is possible at very high levels of theory.

Armed with the insights from cluster studies, we next discuss computational and experimental studies of H^+ and OH^- in bulk liquid water. On the theoretical front, we review results from semiempirical and ab initio molecular dynamics (AIMD) methodologies concerning the solvation patterns of these ions and, particularly, the abnormal proton mobility occurring via a chain of proton transfer (PT) events. Although most simulations of the H^+ and OH^- treat the nuclei classically, there is a growing appreciation of the role of nuclear quantum effects (NQE) in hydrogen-bonded systems, and we highlight the importance of some these effects. On the experimental side, we emphasize the ability of femtosecond time-resolved IR spectroscopy to directly probe the dynamics of H^+ and OH^- in real time. These are complemented by time-resolved fluorescence techniques that can monitor excited photoacids transferring their proton to the water solvent or a base molecule over 3–5 orders of magnitude in time and intensity.

Because water structure and dynamics at interfaces and in one-dimensional channels differ significantly from that in the bulk liquid, it is expected that H^+ and OH^- structure and dynamics in such systems, which depend on that of the water solvent, should also differ from those in bulk water. To highlight these issues, we first review studies of H^+ and OH^- at extended hydrophobic surfaces, where we will show that the interpretation of experimental results at short-length scales near interfaces is extremely challenging. We will then briefly review the importance of understanding the structure and dynamics of protons in biological systems, such as membranes and transmembrane proteins. In spite of this wide range of different systems, the basic observation of abnormally fast proton transport through the HB network appears to carry over from bulk water to biological systems.

2 Structure and Dynamics of H^+ and OH^- in Bulk Water

2.1 Foundational Experiments

The first studies addressing the dynamics of PT between water molecules were experimental measurements of ionic conductivities, from which it was possible to derive the mobility of protons and hydroxide ions in water.[7–10] Results from the first half of the previous century are summarized in textbooks, for example, by Robinson and Stokes.[11] They reveal anomalously high mobilities (3.62×10^{-3} cm^2 V^{-1} s^{-1} for H^+ and 1.98×10^{-3} cm^2 V^{-1} s^{-1} for OH^- at room temperature) as compared to other ions. For example, the mobilities of Rb^+ and Cs^+ are just 22% that of the proton. The hydroxide anion also shows an abnormally high mobility, though to a lesser extent than the proton:[11] at room temperature, its mobility is 57% that of a proton, while the mobility of Br^- is 39% that of OH^-.

Further information about the dynamics of the solvated proton was obtained in the 1960s by nuclear magnetic resonance (NMR) measurements of acidic and basic aqueous solutions performed by Meiboom.[12] Since the chemical shift of the proton is highly sensitive to the local environment, the resonance frequencies of the excess proton and water hydrogen atoms are slightly different. While this technique has only millisecond time resolution, a careful analysis of the line shape using a very simple model for the line width (i.e., the NMR relaxation time) as a function of solution pH and temperature suggested that protons in bulk water move on a picosecond time scale, in good agreement with the proton mobility measurements. The mobility can be extracted by combining the Nernst and Einstein equations without assuming anything about the characteristic jump length of the proton. At room temperature, the results of this type of analysis give a PT time of 1.7 ps in acid solutions and 4.7 ps in bases.[12] This study has been extended to obtain the temperature dependence of these rate constants.[13] The measured Arrhenius plots gave low activation enthalpies, 2.4 and 2.1 kcal mol^{-1} for H^+ and OH^-, respectively. These values are similar to the enthalpy of the HB in bulk liquid water (2.6 kcal mol^{-1}, according to some Raman measurements)[14] and smaller than the activation enthalpy (4.5 kcal mol^{-1}) for the dielectric relaxation of water (see ref 15).

To summarize, early experiments suggested that the proton and hydroxide are unique among ions in aqueous solution with regard to their high mobilities. To understand *why* this is so requires development of a molecular-scale treatment of the solvated proton and hydroxide structures and an examination of how they change in time. The development of theoretical and computational tools that allow this insight have benefitted enormously from experimental work on gas-phase clusters.

2.2 Gas Phase Experiments and their Theoretical Interpretation

2.2.1 Infrared Spectra of Protonated Water Clusters—Much effort has been put into studying both neutral and charged water clusters, particularly in the context of interpreting infrared (IR) spectra, since it is easier to disentangle the molecular origins of specific modes of systems with a relatively small number of degrees of freedom. The difference in the IR spectra of liquid water and acidic water is quite featureless, with wide bands that are difficult to assign to particular conformers (see section 2.3.4 below). In

contrast, gas-phase protonated water clusters at low temperatures exhibit sharp IR features that may help disentangle the convoluted liquid spectrum.

Attempts to describe the molecular structure of the proton in water have typically revolved around two structural motifs proposed by Eigen and Zundel. Eigen viewed the proton as localized on a single water molecule,[16,17] with the resulting H_3O^+ being further solvated by three water molecules, yielding $H_3O^+(H_2O)_3$, the Eigen cation, E. In contrast, Zundel advocated[18] a structure proposed earlier by Huggins,[19] in which the proton is equally shared between two water molecules ($H_5O_2^+$, the Zundel cation, Z), which he believed gave rise to the broad IR continuum in concentrated acids. The isolated Z and E cations are depicted in Figure 1 by structures A and C, respectively.

An experimental breakthrough occurred with the introduction of the predissociation messenger method by Lee and collaborators,[21] which was subsequently perfected by the Johnson group using an argon messenger technique, where Ar atoms are weakly bound to the ultracold water clusters.[20,22] These Ar atoms are shaken off after an infrared photon is absorbed, and the daughter cluster is detected with a mass spectrometer. Using this highly sensitive technique, the IR spectra of the $H_5O_2^+$ and $H_9O_4^+$ structures (and the other clusters in Figure 1) were measured.

In the protonated water dimer, i.e. the Zundel complex, the features of the shared (excess) proton were clearly identified around 1050 and 1760 cm^{-1}. The first corresponds to the proton rattling between the two oxygen atoms. The second mode involves strong coupling of the proton motion to the HOH bending of the flanking water molecules. Before proceeding, we present a brief overview of theoretical methods used for vibrational spectroscopy calculations as applied to protonated water clusters. Recent reviews (specifically, for biological molecules) are available.[23,24]

The accuracy of all computational methods depends sensitively on the accuracy of the interaction potential (the “potential energy surface”, PES). Empirical force fields currently do not have spectroscopic accuracy, since most do not account explicitly for polarizability, which is particularly important for floppy systems like clusters. Thus, we only consider “first-principles” PES calculated by solving the Schrödinger equation for the electrons using either wave functions or density functional theory (DFT).

We broadly divide the computational methods into “static” and “dynamic”. Static methods utilize the PES only near its global minimum. High-level quantum chemistry methods can be utilized in these types of calculations. If the potential is expanded up to quadratic terms, the second derivatives of the potential can be used to find harmonic normal modes (NMs) and their characteristic frequencies. Expanding up to quartic terms enables a perturbation expansion around the harmonic solution, which corrects the frequencies and intensities for anharmonicities. This is the idea behind the second-order vibrational perturbation theory (VPT2) method, which gives quite accurate frequencies provided a sufficiently accurate quantum chemistry method is used and the quartic approximation for the potential is valid. It may nevertheless break down for very floppy and very anharmonic modes. Signs of a suspicious VPT2 output can be infinite anharmonic intensities (often due to energetic

degeneracies), unexpectedly large anharmonic frequency shifts, or imaginary frequencies. A competing methodology used less frequently for clusters, and extensively for biomolecules, is the vibrational self consistent field (VSCF) method.[24] It is based on a separability ansatz for the vibrational wave function and a mean field approximation in which each vibrational mode feels an averaged interaction due to all other modes.

Dynamic methods use the whole PES, namely, all the regions accessible energetically at a given energy or temperature. A time-dependent trajectory of all atoms is used to calculate the dipole moment autocorrelation function (DACF), whose Fourier transform (FT) yields the IR spectrum. Thus, this method inherently includes all anharmonic effects, including conformational changes and temperature effects not sampled in the 0 K spectrum. In addition, the bands are expected to widen with increasing temperature as more nuclear configurations become accessible to the simulation, an effect commonly referred to as thermal broadening. An accurate depiction of such effects therefore depends on the ability to calculate the full PES in all the nuclear degrees of freedom.

For small clusters, a large number of ab initio points on the PES can be calculated and fit to an analytical function. Alternately, ab initio molecular dynamics (AIMD), particularly the so-called Born-Oppenheimer molecular dynamics (BOMD) method, solves the whole electronic problem for each nuclear configuration along the trajectory of the nuclei and calculates the required forces using the Hellman-Feynman theorem. This usually cannot be done with a very high level quantum chemistry method, and one typically uses DFT techniques. The computational efficiency is because the electronic density is a function of only the three Cartesian coordinates and not of all the nuclear degrees of freedom of the system. However, the accuracy is limited by the suitability of the exchange “density functional”. In addition, the nuclear dynamics is classical, so that NQE, which is important for light atoms like hydrogen, are not included. A somewhat older AIMD approach is the Car-Parrinello molecular dynamics (CPMD),[25] which propagates the initial electronic wave-function together with the nuclei using a “fictitious mass” for the electrons. DACF spectra have also been computed with the CPMD method. Besides using DFT, there are also other methods for determining the electronic structure and IR spectrum, such as self-consistent tight-binding DFT (SCC-DFTB), which allows for much more exhaustive statistical sampling than DFT.[26]

The comparison between the different methods is summarized in Table 1. It is seen that no single method suffices for capturing all the aspects of the vibrational spectrum, so that a combination of static and dynamic methods may be recommended. An exception is perhaps the multiconfiguration time-dependent Hartree method (MCTDH), which solves the time-dependent nuclear Schrödinger equation on an ab initio generated PES. It is mentioned in passing that DFT-BOMD and DFT-CPMD can be coupled with methods such as ring-polymer molecular dynamics (RPMD), which allow for an explicit inclusion of quantum dynamics and hence, in principle, allow for the computation of IR spectra with NQE.[27] All of these types of calculations are, however, very computationally expensive.

For the $H_5O_2^+$ cluster, CPMD yielded spectra agreeing semiquantitatively with experiment.[28,29] Yet full quantitative agreement in the peak positions of the spectra between

experiments and theory was obtained when all the 15 nuclear degrees of freedom were treated quantum mechanically using the MCTDH method.[30] In particular, the 1047/928 cm $^{-1}$ doublet was shown to be a Fermi resonance between the proton transfer mode (PTM) and a combination band. This result is not easily obtained from AIMD, which normally produces only fundamentals, and when combination bands and overtones appear, they are of extremely weak intensities. However, the computational effort invested in this MCTDH project is so great[31] that full-dimensional MCTDH calculations were not done for clusters larger than $H_5O_2^+$. For larger systems, partial-dimensionality MCTDH calculations can be performed, but then some of the vibrational modes are not reproduced.[32,33]

In larger protonated water clusters, $H^+(H_2O)_n$, multiple isomers may exist like in bulk water. The existence of both Z and E cations was demonstrated for the protonated water hexamer.[34] Thus, some researchers consider $n = 6$ as the smallest n for which multiple isomers coexist in the molecular beam. This has been contested for both the tetramer[35] and pentamer.[36] Of particular interest is the protonated water tetramer ($n = 4$), by consensus the E cation in Figure 1C. This is the lowest-energy isomer for $n = 4$. Its computed spectrum exhibits strong absorption near 2850 cm^{-1} due to the stretch vibrations of the three hydrogen-bonded OH moieties but not the Zundel-type lower energy bands near 1050 and 1760 cm^{-1}. These latter features could be reproduced with DACF/AIMD computations for a linear four-water isomer that harbors a Z core in its center (Figure 2).[35] Its “dangling” (non-hydrogen-bonded) OH stretch appears above 3500 cm $^{-1}$. Red-shifted from it is the OH stretch of the hydrogen-bonded OH moieties (Z_{1a}), and, finally, the shared proton (Z_0) that contributes at two above-mentioned frequencies.

More recent hole-burning experiments show that only one isomer is present.[6] VPT2 anharmonic calculations for the E and Z isomers (Figure S1 of ref 6), at the B3LYP/6-31+G(d) level of theory, exhibit good agreement with experiment for the E but not the Z isomer spectrum. Aside from the problem that the VPT2 quartic ansatz might not be suitable for the Z isomer, which is likely too floppy (e.g., undergoing cis-trans isomerization), the use of DFT with a small basis set forsakes the relative advantage of VPT2 over AIMD. It remains to be shown that the VPT2 spectra do not change when computed with more accurate methods that account for electron correlation, as well as with larger basis sets, which are critical when using VPT2.[37]

Unlike the protonated tetramer, the protonated trimer ($n = 3$) can have only one isomer, which is linear. In the experiment, a prominent peak near 1880 cm^{-1} is observed.[38] VSCF calculations[20] reproduce it at 1984 cm^{-1}, while AIMD calculations[39] position this peak at around 2400 cm^{-1}. Since anharmonicity is already taken into account and VSCF, which solves a quantum mechanical vibrational problem, generates a considerably red-shifted frequency compared to AIMD, an intriguing possibility is that the experimentally observed large red shift is due to NQE[39] within a “mega-Zundel” cation in which two protons are delocalized over three water molecules. The shift may also be sensitive to the Ar binding site; note that in the VSCF calculations of this trimer,[20] argon atoms were not included. Similar behavior has been proposed for the protonated water trimer in benzene and dichloroethane solutions (see Figure 20 of ref 40), concluding that “contrary to general

expectation, neither E- nor Z-type ions are present. Rather, the core species is the $H_7O_3^+$ ion".[40]

Recently, the IR spectrum of the "magic number" cluster, $n = 21$ (magic number clusters have noticeably larger abundance in the mass spectrum than their neighbors), has been studied. Its predissociation spectrum was recently measured with enhanced detail[6,41] and interpreted as resulting from an E cation localized on the surface of the 21-water cluster. The main peaks of the experimental spectra appear to be reproduced quite well by anharmonic VPT2 calculations, although, as mentioned earlier, the broadening of the spectra is not captured with these approaches. It should be noted that in these calculations, only the Eigen isomer contributes to the spectra.

Whether or not a single isomer contributes to the IR spectra in the magic number cluster will require theory and simulations where broadening effects on the spectra are explicitly taken into account. In this regard, it is curious to observe that a closer inspection of this spectrum reveals peaks near 2300 and 1900 cm^{-1}, which are seen in the trimer but not in other clusters.[20] Besides the broadening coming from thermal fluctuations, there is also the question of the role of NQE. Although the dominant molecular structure may remain as Eigen-like, the effect of quantum fluctuations from this structure on the spectra remains an open question. Since in the trimer the proton is more delocalized, one possibility is that the proton on the cluster's surface may involve quantum mechanical delocalization over several water molecules. We mention this possibility without direct computational support at this point since an accurate modeling of the full quantum dynamics at the ab initio level remains quite challenging for large protonated clusters. As we will show later, the necessity of such a treatment is anticipated, since nuclear quantum effects have already been shown to significantly enhance the delocalization of protons in numerous hydrogen-bonded systems.[30,42–46]

Despite the importance of NQE, it should be mentioned that the classical treatment of the nuclei for calculating spectroscopic features remains a valuable tool in unraveling the molecular origins underlying the spectra. In particular, besides the quantum treatment of the nuclei, there are also other approximations, such as the quality of the electronic structure method as well as the role of adequate sampling of the configurational space, which can also affect the IR spectra. For example, for the protonated ammonia dimer it has been argued that only quantum dynamics (MCTDH) can explain the IR spectrum,[32,33] but recent classical AIMD simulations allowed the assignment of all of the fundamental peaks in this spectrum as well as some of the combination bands.[47]

2.2.2 Hydroxide Water Clusters—The properties of OH^- clusters, $OH^-(H_2O)_n$, have also been addressed in several studies, although not as extensively as clusters containing the excess proton. The electronic structure of the hydroxide is rather peculiar compared to that of the proton, because it is characterized by a "ring" of electron density around the OH^- axis on the oxygen side, to which different numbers of water molecules (typically 3, 4, or 5) may form a HB (Figure 3 in ref 48). This is analogous to the crescent of electron density (the "negativity track") between the lone pairs of a water molecule to which two or three water molecules may HB.[48,49] The presence of a "ring" of electron density poses challenges for

the calculation of the solvation structure of OH^-, since it is capable of adopting a much wider array of solvation structures. Concomitantly, the observed structures were found to depend quite sensitively on the density functional employed.[4,50]

Small gas-phase $OH^-(H_2O)_n$ clusters ($n \leq 5$) have been studied both theoretically[51] and experimentally.[52,53] It was found that up to $n = 3$ the water ligands enter into the first solvation shell of the hydroxide anion, but the fourth water enters already into the second solvation shell, donating HBs to two of the water molecules in the first shell (and possibly accepting a HB from the third one). Rather large clusters are required for a fourth water molecule to enter the first solvation shell. For example, quantum chemistry calculations of Bankura and Chandra have shown how OH^- solvation changes with cluster size.[54] In small clusters with less than 16 water molecules, OH^- mostly resides on the surface, tending to accept three HBs through its oxygen atom, whereas in larger clusters the ion has an increasing propensity to accept four HBs. For $n = 20$, Bankura and Chandra found an internalized state, where the hydroxide also donates a HB through its hydrogen atom.[4] However, their AIMD simulations indicated that this structure "melts" at room temperature, and the hydroxide moves to the surface of the cluster.[54]

A recent study used DACF from AIMD simulations ("dynamic spectra"), as well as normal-mode analysis, to determine the IR spectra of $OH^-(H_2O)_{20}$ of different motifs corresponding to local minima on the potential energy surface where the hydroxide ion can be either on the surface or buried in a cavity (i.e., the H atom of the OH^- is either pointing to the vacuum or to the cluster).[55,56] Interestingly, the potential energy of the motif where the OH^- accepts three HBs and is surface-bound (3A0DS; see Figure 4) is quite similar to the energy of an OH^- that is buried and accepts four HBs (4A1DB there). In the IR spectrum of 3A0DS (Figure 5), the stretch modes appear to mix with the bend mode due to the presence of a very strong HB that is donated to the OH^-, leading to a peak that is centered around but broader than the bend mode at 1600 cm^{-1}. On the other hand, the broad continuum between 1500 and 3000 cm^{-1} appears to come from clusters with the hydroxide ion having different local solvation environments (see Figure 4). Unfortunately, IR experiments on large hydroxide ion clusters have not been performed, so that one-to-one comparisons with calculations cannot be currently done. However, the spectra obtained for the different types of hydroxide ion structures determined with AIMD appear to account for the spectra that are experimentally observed for concentrated NaOH solutions.[57,58]

2.3 Proton and Hydroxide Ions in Bulk Liquid Water

Armed with insights from cluster studies on proton and hydroxide structural motifs, we next return to the central motivation outlined above: understanding why protons have an anomalously high mobility in liquid water relative to other cations and why the activation enthalpy for proton transport appears to be correlated with the energetics of HB breakage. In what follows, we first discuss conceptual models for proton transport in liquid water and the degree to which they account for these observations and then review work that explicitly probes proton and hydroxide mobility in simulation and experiment.

2.3.1 Interpretations of Experimental Data—The anomalously high proton mobility in acid solutions implies that it cannot be described by hydrodynamic diffusion.[2,59–61] In order to relate the experimental mobilities discussed earlier to a molecular picture of PT, structural information about the solvated proton and hydroxide is required. In 1905, Danneel explained proton mobility in water as occurring along onedimensional water chains, followed by water rotation ("turn") to allow the next proton transfer.[62] Thereby he revived the 1806 model of Grotthuss for water (OH, as then believed) electrolysis as parallel rows of O and H atoms, exchanging partners and moving to the positive and negative electrodes, respectively.[2,63] Today the term "Grotthuss mechanism" is used for any proton-hopping mechanism, regardless of whether it occurs along "water wires" in confined environments or in the bulk. In addition, there is a smaller component of "vehicular diffusion", namely, hydrodynamic motion of the protoncarrying water complex.

In bulk water, where there are many potential pathways for proton migration, there is no need to wait for Danneel's "turn" step, which could make the migration quite slow. Early interpretations of the conductivity data were based on a scenario of a rotating hydronium or water molecule. In 1928, Hückel suggested that after a water molecule picks up a proton to become H_3O^+ it rotates to deliver the proton to a neighboring water molecule.[64] This rotation requires cleaving of the three HBs to the hydronium, each considerably stronger than a water-water HB.[65,66] In 1933, Bernal and Fowler suggested, instead, that a water molecule rotates in the solvation shell of the hydronium until it acquires the right orientation to pick up the proton.[67] This, again, requires cleavage of several HBs. Subsequently, in 1958, Eigen and De Maeyer[16] proposed that the protonic charge fluctuates quickly back and forth within a finite hydrogen-bonded complex (such as a water wire) and that the reorientation of water molecules at the periphery of this complex is required for diffusion. They termed the restructuring of HBs as "structural diffusion".[16] Because all of these models for proton transport require the breaking of more than one bulk water HB, the low activation enthalpy from the NMR studies of Luz and Meiboom[13] suggests that one must look elsewhere.

Agmon proposed a model for proton mobility that does not require HB cleavage in the first solvation shell of H_3O^+, hence explaining its low activation energy discussed above.[59] In this picture, the Grotthuss mechanism in bulk liquid water involves an E cation "resting state" that is converted by second-shell HB loss to a Z intermediate, which by second-shell HB formation is in turn converted to an E cation centered on a neighboring water molecule (Figure 6). In this "E–Z–E mechanism", the activation enthalpy for proton mobility equals approximately the strength of one HB in bulk liquid water, because the broken HB is in the *second* solvation shell of the H_3O^+ cation, unlike first-shell HBs that are considerably stronger (about twice the enthalpy, according to ref 65).

2.3.2 Numerical Simulations—Proton motion via structural diffusion involves the breakage and formation of covalent bonds. In order to model this type of process with an atomistic simulation, electronic degrees of freedom must be explicitly described, making it computationally very challenging. The CPMD method[25] provided, for the first time, a way to achieve this description of the electronic degrees of freedom, thereby offering much

needed insights into the molecular mechanism of proton and hydroxide diffusion in liquid water.

2.3.2.1 Hydronium: The first CPMD simulations of an excess proton in liquid water consisted of a proton in a periodic box of 32 water molecules simulated for a couple of picoseconds.[60,69] These early calculations provided a first glimpse into the two postulated dominant structures of the excess proton in water, namely, the E and Z cations. In particular, the simulations showed that the E cation involved an $H_9O_4^+$ complex including the hydronium and three tightly bound water molecules. It could easily convert into the Z cation, since the proton rattled on the femtosecond time scale with one particular neighboring water, closest to the hydronium, referred to as the "special pair". These simulations revealed the detailed solvation environment of the E and Z cations as seen in the O*-H radial distribution function (RDF), where O* is the oxygen atom that hosts the excess proton (Figure 7).[69] These results showed that the O*−H covalent bonds in the hydronium are slightly longer (and weaker) as compared to bulk water, whereas the OH peak for the Z cation is split, indicating that the average OH^+ distances in the $H_2O\text{-}H^+\text{-}OH_2$ complex are not precisely equal. Additionally, the oxygen atoms of both the E and Z cations are weaker acceptors of HBs compared to neutral water. Besides characterizing structural properties, these simulations showed that proton transport in liquid water[16] proceeds via an interchange of E and Z forms.[59]

Subsequently, the understanding of the specific microscopic details of the Grotthuss mechanism has undergone significant refinement due to both the advancement in numerical algorithms and computational resources allowing for bigger and longer AIMD simulations and the development of sophisticated empirical potentials capable of modeling chemical reactions. In particular, later CPMD simulations run for over 70 ps showed that the E–Z–E mechanism also involved concerted HB dynamics, whereby the E cation begins to accept a HB from a nearby water molecule while simultaneously (within 50 fs) the proton accepting water loses one of its acceptor HBs[70] (see Figure 8).

Extracting dynamical properties such as diffusion constants requires averaging over long time scales. Hence, using CPMD to characterize proton transport is still computationally expensive. One way to circumvent this problem is to turn to empirical-based potentials that allow for the dissociation and formation of bonds.

The most popular approach is the multistate empirical valence bond (MS-EVB) methodology, where a certain number of valence bond states define the main chemical groups, and the potential energy surface along radial or angular coordinates is fitted to ab initio data.[5,71–73] For the H^+ in water, the longer simulation times of MS-EVB offered additional insight into the transport mechanism. For example, they revealed that the hydronium resting state involves, besides proton rattling, an exchange of the special partner among the three water ligands in the first solvation shell[68] driven by the HB cleavage event envisioned in ref 59 (see Figure 6). This "special pair dance" (SPD) scenario is depicted schematically in Figure 9.

The average time constant for special partner exchange was found to be 40 fs from classical MS-EVB simulations and 45 fs when the nuclei were quantized, as deduced from the plateau in Figure 7B of ref 68. Because the time scale for PT is a few picoseconds, the hydronium undergoes dozens of partner exchange events before a Z intermediate is formed and PT takes place. These can involve just two partners for a while, and only after several cycles one of them gets replaced by the third partner. This leads to oscillatory motion of the excess charge (between the two partners) with a period of about 90 fs (twice 45 fs), corresponding to about 360 cm^{-1}, which might give rise to an IR band at the indicated frequency (the “SPD band”).

While conventional IR measurements do not easily get below 500 cm^{-1}, recent terahertz Fourier transform infrared (FTIR) measurements on concentrated aqueous HCl and HBr solutions by Decka et al.[74] have located a band at 340 cm^{-1}, which they assigned to the SPD (Figure 10). They find for this mode a relaxation time of 60 fs, close to the theoretical values quoted above. As depicted in Figure 9, the SPD is controlled by cleavage of a second-shell HB. These HBs become a few percent stronger in heavy water (as deduced from the 2% increase in the heat of vaporization of D_2O compared to H_2O). Hence, one expects the SPD to slow down slightly in heavy water. Indeed, Figure 10 shows a few percent red shift of the SPD band upon deuteration.

MS-EVB simulations also revealed that a successful PT event (in which the proton is eventually transferred to one of the special partners) requires collective solvent fluctuations involving the reorganization of the second-shell water molecules around the Z cation.[75] These help destabilize the proton on the previous oxygen center while stabilizing it on the new oxygen center, sometimes before the transfer actually occurs (“presolvation”). The participation of so many water molecules in the Z cation dynamics leads to a wide distribution of its lifetimes (averaging to 380 fs).[75] Indeed, another terahertz time-domain spectroscopy study has found that the addition of protons to water leads to a very strong decrease of the water dielectric response, corresponding to about 19 water molecules per dissolved proton.[76] This is about the number of water molecules involved with the Z complex up to its second hydration shell (see Figure 14 in ref 75).

Thus far, proton diffusion was described as hopping from one molecule to the next in a stepwise fashion. In confined environments, such as carbon nanotubes and biological membranes, extended chains of water molecules (water wires) provide pathways for concerted proton jumps; PT in these systems is not stepwise.[77] Recently, AIMD simulations have found evidence for the presence of water wires that allow for concerted proton hopping events across several HBs in liquid water.[61] The fluctuations of the wires play an important role in triggering these events. For example, it has been shown that for the recombination of the hydronium and hydroxide ions, namely, the time-reversed process of ionization,[78] the collective compression of three HBs forming a wire between the ions was needed to trigger a concerted PT event.[77]

The HB network of liquid water is made up of a distribution of closed rings with specific directional correlations of waters within the rings, leading to different types of topological patterns; see Figure 11 showing two six-membered rings. The proton also participates in several closed rings, the segments of which create the architecture for water wires leading to

more complex proton-hopping mechanisms. Rather than occurring at a constant frequency, there are periods of rapid succession of PT events ("bursts"), separated by quiescence ("rest") periods during which few such events occur; see Figure 12 for an example of such a trajectory. Regions of the HB network where the proton is surrounded by a fewer number of rings tend to result in longer traps. The burst activities involve two or three rapid protons hopping over several HBs through the water wires, facilitated by the collective compressions of these wires, as illustrated in Figure 13. The concerted motion of two protons can occur when successive HBs along the proton wire decrease by about 0.25 Å. In the discussions below, we will make reference to a PT coordinate, δ, that corresponds to the difference in distance between the transferring proton and the oxygens it is connected to; therefore, when the PT coordinate is 0, the proton is equally shared between the waters.

This type of analysis makes clear that determining the reaction coordinates associated with PT is very complex. For example, a recent AIMD study[79] has found that the presence of the burst and rest states correlates with the presence or absence of a fourth water molecule (4WM) donating a HB to the hydronium oxygen atom (Figure 14a). When such a bond exists the burst probability is high (b). When the 4WM is further away from the hydronium (c), the latter is stabilized and few PT events occur.

Along similar lines, recent work has highlighted the importance of the umbrella inversion mode of the hydronium ion in PT in bulk water. Molecules such as ammonia and hydronium can turn inside out, and this inversion mode leads to a characteristic signature in the IR spectrum.[32–35] Figure 15 examines the role of the inversion mode for a situation where the hydronium is trapped in one part of the HB network, making it easier to focus the analysis on the motion of the proton between two water molecules only. Since inversion occurs on a faster time scale than solvent reorganization, the position along this coordinate change the PT potentials quite significantly. Because the PT barriers change quite substantially as a function of the inversion coordinate, they can couple with features such as the burst and rest behavior. More work is needed to understand how all these various coordinates couple together to form the Grotthuss mechanism.

Although we have focused on simulation results coming from AIMD and MS-EVB approaches, there are also efforts placed in developing more sophisticated empirical water potentials that allow its dissociation.[81–88] Some of these models capture many of the features observed in the AIMD and MS-EVB simulations. The reader is referred to those references for more details.

2.3.2.2 Hydroxide: As for clusters, the structural and dynamical properties of OH^- in bulk water are less well understood than those of H^+, partly because anionic species are more challenging to model with DFT. Before the first CPMD simulations of OH^- in water, the Grotthuss diffusion of the OH^- was thought to be a mirror image of that of the proton, implying that it would only accept three HBs.[89] Later, X-ray diffraction and core level electron spectroscopy experiments indicated that the OH^- could accept four HBs and possibly even donate a weak HB, thus yielding a hypercoordinated species. In their CPMD simulations, Tuckerman and co-workers[48] found that the dominant state of OH^- was the hypercoordinated species that accepts four HBs in a square planar arrangement, as illustrated

in Figure 16. The hopping mechanism involved a decrease of the coordination number of the hydroxide to form the short-lived transient species shown in the bottom panel of Figure 16. In this transient species, the OH^- accepts three HBs and donates a weak HB, thus forming a locally tetrahedral environment.[60]

Subsequently, it was found that three popular (generalized gradient) density functionals, BLYP, PW91 and HCTH, yield qualitatively different solvation structures, diffusion constants, and molecular mechanisms for OH^- migration in water.[4,50] For example, BLYP yields a diffusion constant of 1.92, PW91 gives 18.5, and HCTH gives 0.14, in comparison to the experimental value of 5.3 (all in units of 10^{-9} m^2 s^{-1}). Clearly more work is needed in this area, for example, with the use of multireference ab initio and quantum Monte Carlo calculations, which will allow for a more rigorous treatment of electron correlation effects.

2.3.3 The Importance of the Nuclear Quantum Effects (NQE)—In most of the previously discussed studies, the electrons were treated quantum mechanically (i.e., by solving the electronic Schrödinger equation at some level of approximation), whereas the nuclei were treated classically (i.e., the evolution of their position in time was computed from Newton's equations of motion). This may not always suffice. For example, the zero point energy of the O-H stretch mode in liquid water is about 0.2 eV, which is significant compared to the thermal energy at room temperature ($k_B T$ = 0.026 eV). The effects of NQE in bulk liquid water are reflected in the significant broadening of the O-H radial distribution function compared to what one observes when the nuclei are treated classically.[90,91]

A first-principles quantum mechanical treatment of both the electrons and nuclei for protons in liquid water can be achieved by the use of ab initio path integral molecular dynamics (PIMD) simulations, which are computationally quite expensive. Over a decade ago, Tuckerman and Marx performed the first ab initio PIMD simulations of the excess proton and hydroxide ion in liquid water.[48,92] The zero-point energy of the proton significantly lowered the barrier for transition between the E and Z cations to a point that the Z cation was no longer a true intermediate in the interconversion between these two states. Similarly, for the hydroxide ion, PIMD simulations also lowered the barrier, by ~1 kcal mol^{-1}, for the motion of the proton hole along the HB where PT occurs (see Figure 17). In addition, it was found that in the classical simulations PT occurred over a narrower range of OH^- orientations, as compared with the PIMD studies.

These earlier PIMD studies were limited by short simulation times and small system sizes. The design of more sophisticated and efficient algorithms to treat both electrons and nuclei quantum mechanically has resulted in more numerical studies examining the role of NQE in various hydrogen-bonded systems.[93–95] These studies showed, for example, that NQE strengthen strong HBs and weaken the weak HBs,[94] and that in both bulk liquid water and confined water NQE cause proton delocalization over several water molecules, partly washing away the distinction between the E and Z cations.[95]

Evidence for proton delocalization can be seen in Figure 18, which shows the probability of finding a particular protonated "cluster" in acidified bulk water.[45] Unlike in classical simulations, in simulations including NQE the proton can sometimes delocalize over more

than two water molecules, moving without requiring the correct presolvation at all places in the network. Although the probability of finding the proton delocalized over three water molecules is still small, the difference compared to the classical simulations is statistically significant. The role of these rare fluctuations on proton dynamics and hence the diffusion constant remains an open issue.

2.3.4 Time-Resolved IR Studies—As presented above, our current understanding of the specific molecular configurations and structures has relied on input from simulations and experiments. In the gas phase, such protonated water clusters have been identified primarily by infrared spectroscopy (section 2.2). However, the interpretation of the IR spectra in the liquid phase is a major challenge. This is due to the large number of hydrogen-bonding configurations, which give rise to very broad and rather featureless absorption bands, as well as the ultrafast dynamics that drives the interchange between these configurations and contributes to the observed line shapes. Especially remarkable is the growth of a continuum-like absorption spanning almost the entire mid-IR region (see Figure 19) when protons are added to water.[18]

However, by combining our knowledge from the cluster experiments discussed earlier (e.g., Figure 2) with results from ab initio calculations and liquid phase simulations,[22,28–30,34,96–98] the absorption in several spectral regions can be correlated to vibrations of different solvation structures (Figure 19). The Z complex gives rise to the characteristic absorption features at 3200 cm^{-1} (O-H stretch vibration of the flanking water molecules), at 1760 cm^{-1} (HOH bending motion of the flanking water molecules coupled to excess proton oscillations between them), and at 1150 cm^{-1} (proton-shuttling motion), whereas the E structure shows an absorption peak around 2700 cm^{-1} (O-H stretch vibration). Distortions of the Eigen geometry with one shortened HB lead to absorption frequencies that span the entire range between 1000 and 3200 cm^{-1} giving rise to the acid continuum absorption.[35,97]

Deeper experimental insight into the structures and dynamics of solvated protons and hydroxide ions requires a combination of structural sensitivity with time resolution in the same experiment. The advent of ultrafast lasers made it recently possible to perform ultrafast (femtosecond) IR measurements with a time resolution that suffices to resolve the fast fluctuations of the HB network that drive the structural changes. A number of experiments have been performed on acids and bases using transient absorption IR[100] and two-dimensional infrared (2DIR) techniques,[57,101] with the goal of identifying different solvation structures and determining their persistence time and rate of interchange.

Woutersen and Bakker performed two-color transient absorption experiments on isotopically dilute acid solutions, finding evidence for an ultrafast interconversion between E and Z species on a time scale of <50 fs.[100] By exciting the O–H stretch vibration of the Eigen core at 2935 cm^{-1} with a femtosecond infrared pulse, an instantaneous response of the Zundel species was observed (Figure 20). In the left panel of Figure 20, the absorption spectrum of an isotopically diluted (H:D = 1:20) solution of 5 M HCl in water is shown. In the right panel the responses at 2850 and 3300 cm^{-1} are shown as a function of delay between the excitation and the probing pulses. It is seen that the excitation of the vibrations of the E structure leads to a direct response at ~3300 cm^{-1}, which is associated with water molecules

flanking the Z proton. The quasiinstantaneous rise of this signal indicates that the interconversion between E and Z takes place on a time scale of <50 fs.

More recent experiments on solvated protons and hydroxide ions employed ultrafast 2DIR spectroscopy, where the temporal evolution of the induced vibrations can be monitored as a function of an excitation and a probe frequency.[57,101] The frequency correlation spectra obtained with this technique contain information about the inhomogeneous broadening of the IR absorption peaks, which is crucial for identifying the different solvation species contributing to these broad spectral features. Additionally, information about the dynamics of chemical exchange processes can be obtained by analyzing a series of 2D spectra with varying time delays. Measurements of isotopically dilute HOD in NaOD/D_2O solutions revealed strong evidence for the formation of a Z-like transition state ($H_3O_2^-$) during the proton transfer reaction which persists on a 110 fs time scale.[57] The identification of this transition species is based on the observation of a fast-decaying off-diagonal broadening of the 2D line shape in the spectral region of the O-H stretch vibration of the solvating HOD molecules. The interpretation was supported by calculations of vibrational frequencies of the $[DO\text{-}H\text{-}OD]^-$ complex during the PT event using MS-EVB simulations.

In a subsequent 2DIR study on this system, the temporal evolution of the cross-peak regions (off diagonal regions) that report on the proton/deuterium exchange processes between different deuterated water and hydroxide species was analyzed in more detail. In order to extract the molecular dynamics of these exchange processes, a model for calculating 2D line shapes was constructed that includes the most significant effects contributing to the 2DIR spectra.[101] Fitting the model parameters to the experimental data, a lower limit of the proton transfer time in basic solutions of approximately 3 ps was extracted, in good agreement with the results of the conductivity studies discussed earlier.

Even with the additional information content of a 2DIR spectrum, unambiguous identification of specific solvation structures can be challenging. One approach to this problem is to recognize that if a specific solvation structure is present, all modes associated with it must appear in the spectrum and could be coupled (i.e., apparent as off-diagonal cross-peaks in a 2D spectrum). One example of this is the stretch and bend vibrational modes of a Z complex. In order to perform such experiments, a very broad spectral bandwidth, which spans the entire mid-IR region, has to be probed because of the 1500 cm^{-1} separation of these modes. The development of broadband 2DIR has made these measurements possible.[102]

In studies of HCl/H_2O solutions using this broadband method, it was indeed possible to identify the spectral signature of $H_5O_2^+$.[99] By analyzing the region of the stretch-bend crosspeaks in the 2D spectra, it could be shown that the spectral feature at 1760 cm^{-1} is coupled to O-H stretch frequencies in the range between 3000 and 3200 cm^{-1} (Figure 21). This observation confirms that both vibrations stem from the same molecular species, namely the Z complex of the solvated proton. By analyzing time-dependent shifts of this cross-peak, a lower bound of 480 fs for the persistence time of the Z complex could be extracted, suggesting a rather stable Zundel species. At first glance, this observation seems to contradict the ultrashort lifetimes of protonated water structures found in the transient

absorption measurements.[100] However, it is possible that the results from the transient absorption measurements report on fast structural fluctuations, whereas the recent 2DIR results describe only the long-range PT events.[99] This may be in accord with MS-EVB simulations that found a wide distribution of lifetimes for the Z complex mediating PT in water: from ca. 50 fs to over 1 ps (Figures 9 and 7, respectively, in ref 75). With 2DIR it should also be possible to identify cross-peaks for the E cation,[103] allowing for a more quantitative identification of the Z and E cations in liquid water than ever before.

2.3.5 Excited State Proton Transfer by Proton Mobility and Water Wires—

Another active area of research involves the mechanisms of PT occurring upon electronic excitation, namely, excited state proton transfer (ESPT). When a molecule capable of releasing a proton after absorbing a photon (e.g., a photoacid) is excited, the emitted proton goes either to the solvent (ESPT to solvent, “by proton mobility”) or to another molecule (a base) that serves as a proton acceptor (“by water wires”). These processes are of practical interest in initiating chemical reactions, such as polymerization, by a photon-induced pH jump. ESPT also offers a convenient way of studying fundamental issues in PT reactions that are initiated, synchronously, by a laser pulse.

Photoacids are dye molecules that decrease their pK_a value upon photoexcitation.[104,105] A typical ROH photoacid might have a hydroxy group coupled to an electronic π-system. An example is 2-naphthol (Figure 22), the pK_a value of which decreases from 9.5 in the ground state to 2.8 in its first excited singlet state, S_1. The secret behind photoacidity is intramolecular charge transfer (ICT) in S_1, from the proximal ring that harbors the OH substituent to the distal ring, stabilizing the RO^- product of the ESPT reaction.[106] In “superphotoacids”, such as 5,8-dicyano-2-naphthol, electron-withdrawing substituents on the distal ring further stabilize the negative charge.[107,108] ICT makes dissociation in the excited-state more downhill, shifting the anion fluorescence to the red (lower energies) as compared with the acid. Such “dual emission”, consisting of two fluorescence frequencies (wiggly arrows in Figure 22), is the hallmark of ESPT.

2.3.5.1 ESPT to Solvent: Water is a receptive solvent to protons. Therefore, a relatively weak photoacid, like 2-naphthol, will transfer its proton to water (on the 100 ps time scale) but not, for example, to alcohols. Stronger photoacids dissociate faster (the fastest known to date is about 100 fs in water) and are capable of emitting protons to alcohols and other nonaqueous solutions.[107–109] Proton dissociation occurs adiabatically, leaving behind an *excited* anion. However, it is not necessarily irreversible, which would lead to exponential decay of the excited ROH fluorescence. Attracted by the charged RO^- base, the proton may recombine adiabatically on the S_1 potential energy surface several times before its eventual escape.

The ensuing reversible geminate recombination process can be described quantitatively by a reversible diffusion model,[110,111] involving a spherically symmetric, time-dependent Smoluchowski equation with “back-reaction” boundary conditions (Figure 23).[112] The parameters in this approach include the proton diffusion coefficient (taken from the conductivity measurements discussed above), its Coulomb attraction with the excited anion (determined from the solvent dielectric constant), and the two rate coefficients (for proton

dissociation and recombination). The long-time behavior is a $t^{-3/2}$ decay of the ROH signal (a straight line on a log–log scale), reflecting the probability of the random walker (the proton) to return to the origin of its random walk (the excited anion).

This behavior for ESPT kinetics has been verified after the detection technique was upgraded from streak-cameras to time-correlated single-photon counting.[113] Stronger photoacids are monitored nowadays using the up-conversion technique, because they emit their proton on a much faster time scale. For example, the time-resolved fluorescence of the dye dubbed QCy7 is due to proton ejection to water in about 0.5 ps.[114] The asymptotic power-law behavior shown in Figure 23 is modified upon moving from pure water to more complex systems, such as water in reverse micelles,[115] mesoporous surfaces,[116] or near proteins undergoing conformational changes.[117]

One wonders whether spherically symmetric diffusion for a single translational coordinate (the proton–photobase separation, r) is not an oversimplified model for PT reactions in liquids.[115] In comparison, molecular simulations follow the location and velocity of every atom, so one may search for an analogous mechanism there. For simplicity, let us consider H_3O^+ as the proton donor. Then, from a given trajectory of protonated water one may compute a correlation function, $c(t)$, that depicts the probability of the excess proton to reside at time t on the *same* H_3O^{*+} oxygen, O*, to which it was bound at $t = 0$.[118] The result in Figure 24 shows similar behavior to the experimental $t^{-3/2}$ asymptotic decay. However, it fits a slightly more complex model, with a distance-dependent diffusion coefficient, $D(r)$, for the relative H^+O^* motion. At small separations $D(r)$ diminishes, reflecting the stronger HBs near the excess charge (cf. the O_0O_1 HB in Figure 6).[65]

2.3.5.2 ESPT to Base: The PT reaction from a photoacid (HPTS) to an accepting base (acetate) in liquid water has been studied with femtosecond mid-IR laser pulses.[119–125] In this approach, PT is probed by detecting the vibrational resonances of the photoacid, the conjugate photobase, the hydrated proton, and the accepting base with time-delayed infrared probe pulses. Thereby a complete picture of the PT reaction can be obtained. The time the proton needs to leave the photoacid is detected by measuring the responses of the photoacid and its conjugate photobase. The uptake of the proton in water is detected by measuring the transient response of the hydrated proton, and the arrival at the base is detected by measuring the vibrational response of the conjugate acid of the accepting base (acetic acid).

In Figure 25, the vibrational response of the proton/deuteron vibrations is shown as a function of delay with respect to the excitation of HPTS for different acetate base concentrations. The PT reaction is observed to be highly nonexponential, which can be explained by the presence of a distribution of acid-base distances in solution before the excitation by the pump pulse.[119–125] PT will be fast if the nearest accepting base is close to the excited photoacid and slow when the nearest base is separated by many water molecules.

The distribution of reaction rates for different photoacid-base separations has been modeled in different ways. In one approach, the generation and reaction rate of each water-separated acid-base complex was described independently from the other acid-base complexes, which results in a large number of independent rate constants.[119–121] In another approach, the PT

dynamics is described with a model in which the PT rate coefficient decreases by the same factor for every additional water molecule separating the acid from the base.[122,123,125] For the acetate base it was found that, at a concentration of 1 M, most PT events take place in reaction complexes in which the photoacid and the acetate base are separated by two or three water molecules.

The comparison of the left and right panels of Figure 25 shows that PT to the base has a significant kinetic isotope effect (KIE) of 1.5 (note the difference in horizontal time axes). This KIE suggests that the reaction rate is *not* determined by diffusion of the base, as proposed earlier.[126,127] In such a scenario, one would expect to find a KIE of ~1.2, the ratio of the viscosities of D_2O and H_2O. A KIE of 1.5 is very similar to that of the mobility of free hydrated protons/deuterons in H_2O/D_2O. This supports PT via a Grotthuss-type conduction mechanism. The PT from the photoacid to the base thus likely involves conduction via short-lived wires of water molecules connecting the photoacid and the base (short time scale) or that the proton is first transferred to water and later taken up (scavenged) by the base (longer time scales). At low concentrations and for weak bases, it was shown that the second conducting channel becomes more pronounced,[128] indicating that the pK_a difference between acid and base plays a role in determining the strength of the water wires connecting them.[128]

The temperature dependence of photoacid to base PT kinetics is shown in Figure 26.[124] A generalized Smoluchowski model is capable of fitting this data over the whole time regime (fs to ps). Smoluchowski theory[129,130] treats the irreversible reaction A + B → products, for a single, static A molecule surrounded by a uniform distribution of B molecules. The survival probability of A (i.e., the probability that it has not reacted with any of the B's by time t) is then calculated from the probability distribution of an AB pair, $p(r,t)$. The latter obeys a spherically symmetric diffusion equation with a "sink term", $k(r)$, depicting PT within an AB pair separated by distance r. For very short times (say, $t < 1$ ps) diffusion can be neglected, and then $p(r,t) = \exp[-k(r)t]$ is a function of the distance, r, at which the pair was "born". Those born at short separations give rise to the sharp initial decay seen in Figure 26. The slowing down at longer times is due to pairs born at larger distances that require mass diffusion to bring them to distances amenable to PT.

Interestingly, the fit to the experimental data reveals an inverse temperature dependence of $k(r)$, which decreases with increasing temperature, T. This suggests concerted proton translocation along water wires: raising T disrupts the wires, rendering concerted PT less probable. Unlike proton hops between water molecules, here proton translocation involves a strong driving force from the photoacid to the acetate base. These scenarios have been tested by first-principles simulations of model acid-base pairs[131] (or just proton–base pairs),[132] finding evidence for both concerted and stepwise acid-to-base PT along water wires in liquid water. Concerted proton translocation occurs when the water molecules along the water wire are all four-coordinated, so that they cannot stabilize the proton as a transient hydronium cation.

Europe PMC Funders Author Manuscripts

3 H^+ and OH^- at Extended Hydrophobic Interfaces

Reducing the dimensionality of the liquid from the bulk (3D) to an extended surface (2D, with a radius of curvature that is larger relative to molecular dimensions) has notable effects on the properties of the excess proton and hydroxide ion. In general, it is thought that chemical reactivity occurs more readily at an interface than in a bulk phase. Since OH^- and H^+ are involved in numerous biochemical reactions, it is also useful to understand the interfacial structure and dynamics of H^+ and OH^- and how this might be relevant in biological systems. We address the first question in this section, while the function of protons in a related biological system (the membrane/water interface) is considered in the next section. Despite the significance of the interfacial structure of acidic and basic aqueous solutions in contact with hydrophobic phases, virtually every aspect of the structure and dynamics of the excess proton and hydroxide ion at hydrophobic interfaces is either contentious or incompletely understood. In the following, we review experimental and theoretical views that have attempted to shed light on the structure of acidic and basic solutions in contact with hydrophobic materials. In contrast to the previous sections of this review, far fewer studies have been conducted on this topic. For example, even the question whether excess protons and hydroxide ions reside at the interface and under which conditions is heavily debated, let alone what will be the exact structure. For this reason, after reviewing the literature, we end this section with a discussion of challenges.

3.1 Experimental Probes for H^+ and OH^- on Surfaces

3.1.1 Macroscopic Measurements—Surface tension measurements probe the equilibrium reversible work needed to create a unit surface area of liquid/vapor interface from bulk water and are therefore in general sensitive to changes in both the bulk and surface structure of water. Solubility and partitioning data provide information about the exclusion or accumulation of solutes near a homogeneous nonpolar/water interface. The surface tension of the air/neat water interface is 72.7 mN m^{-1} at 293 K and varies weakly between pH 3 and 10 on the addition of acid or base (i.e., between 72.6 and 72.9 mN m^{-1}).[133] With continued addition of acid below pH 1, the surface tension reduces to 71.4 mN m^{-1}, and with addition of base above pH 13, it increases to 73.4 mN m^{-1}.[133,134] In comparison, adding 1 M of NaCl to neat water increases the surface tension to 74 mN m^{-1}. Surface tension and solubility data for NaOH and HCl in water (for ionic strengths >0.1 M) were analyzed in the framework of a two-state approximation, in which water in contact with air was divided into a bulk water and a surface water region, with each having a certain concentration of ions. Partitioning coefficients for H^+ and OH^- of 1.5 and 0.5 for the air/water interface and 0.6 and 0.9 for the toluene/water interface, respectively, were obtained.[135] In the absence of additional information, these observations suggest that at sufficiently low pH the excess proton tends to adsorb to the air/water interface, while at sufficiently high pH the OH^- is excluded from it. For the oil/water interface, both ionic species appear to be repelled from the interface at high pH, but OH^- less so than H^+.

Because we wish to gain insight into the presence of charged species at an interface, one might expect electrokinetic mobility to also offer insight into proton and hydroxide interfacial abundance. In such measurements, the mobility of bubbles, droplets, or particles

in an electric field is measured. The mobility is proportional to an electrostatic potential, the ζ-potential, which is generally interpreted as the potential at the edge of the diffuse electric double layer.[136] Indeed, many years[137] of electrokinetic measurements on air[138] and N_2 [139] bubbles, oil droplets,[139,140] or extended hydrophobic surfaces all tell a similar story: that the air/water or oil/water interface has a vanishing ζ-potential at pH ≈2–3. With increasing pH, the ζ-potential becomes increasingly negative, indicating that the interface retains negative charge. This behavior is observed for many compounds,[138,141] some of which are represented in Figure 27. If the excess proton or OH^- are the only charged moieties in the system, it is natural to interpret these measurements as indicating that OH^- adsorbs with a free energy of adsorption of 12–20 $k_B T$ to the air/water interface: the air(hydrophobic)/water interface is strongly basic.[142,143] Beattie et al. have argued that there is no discrepancy between the surface tension and electrokinetic measurements by noting that the surface excess of H^+ and OH^- is coupled via the autodissociation constant of water and the Gibbs adsorption equation, and that they both change in similar but opposite ways when the pH is altered (provided that charge neutralization occurs via counterions whose nonideality can be described by bulk activity).[133] For strongly acidic/basic solutions (at pH <1 and >13, i.e., those that have a pH-dependent surface tension), it is not clear that this is a reasonable assumption.[144] However, even for solutions at more moderate pH values, much recent work, discussed in detail below, suggests that interface-induced ion pair formation may occur. Such effects imply that even at relatively low bulk concentrations, the analysis of the electrokinetic mobility data may need to be revisited. It is also worth noting that a recent measurement of the potential of the quiescent air/water interface using a Kelvin probe by Shapovalov and co-workers found essentially no surface potential change between pH 4 and 9.[145] However, as noted by the authors, despite experimental care, such measurements are susceptible to possible contamination by impurities that may suppress an otherwise changing surface potential.

Clearly, part of the difficulty in this discussion is that one is attempting to infer molecular-scale interfacial properties, the surface excess of H^+ or OH^-, from macroscopic observables. Presumably, application of experimental techniques that allow extraction of molecular-scale observables of the interfacial excess proton or OH^- might help clarify the appropriate molecular level interpretation of these macroscopic observables.

3.1.2 Molecular-Scale Measurements—Probing OH^- and the excess proton at the air/water interface experimentally is challenging in part because one needs to distinguish these moieties at the interface from the much larger number of both species in the adjoining bulk liquid phase. The laser-based techniques of second-harmonic generation (SHG) and vibrational sum frequency generation (SFG) spectroscopy are interface-specific by their symmetry selection rules (see, for example, the review by Lambert and co-workers for details[146]) and are thus conventional methods to address this problem. SFG/SHG spectroscopy is sensitive to both vibrational resonance (SFG) and electronic resonances (SHG) of interfacial species, as well as interfacial molecular order (orientational correlations along the surface normal of all active species, SFG as well as resonant and nonresonant SHG). As such, a variety of possible changes in spectral observables, such as frequency and intensity of resonances and their change with polarization of the optical beams as a function

of pH, might be expected. Petersen and Saykally conducted resonant SHG experiments on surfaces of strongly acidic and basic solutions.[147,148] These measurements probed interfacial OH^- via its charge transfer band, and the excess protons, via resonant excitation of counterion charge transfer bands (in absence of a direct resonance on H^+). The results are consistent with a scenario in which interfacial adsorption of the excess proton from strongly acidic solutions is energetically favorable, while in strongly basic solutions, OH^- adsorption is either weak or unfavorable. In contrast, a nonresonant SHG study[149] of the hexadecane/water interface found that the SHG intensity increases above pH 9 and levels off from 10 to 12, whereas the signal from NaCl solutions remained flat throughout this region (see Figure 28A). This signal was interpreted by the authors to be the result of the increasing order of interfacial water with pH increasing from 8 to 10. One possible cause of such increasing order could be adsorption of OH^-, which increases the interfacial electrostatic field and hence increases the order of water molecules.[149]

Several authors have measured or attempted to compute the SFG spectrum of the air/water interface, since the interfacial OH stretch response should contain details about the excess of H^+/OH^- ions.[150–153] The direct detection of the interfacial excess proton or OH^- via their characteristic vibrational resonances is in principle possible, since both species give rise to distinct spectral features in both IR[20,57] and Raman spectroscopy. Within the OH stretch response, as discussed above, increasing H^+ concentrations lead to an increase in intensity in the red part of the spectrum, while basic solutions display an increasing spectral intensity on the blue side as well as a narrow resonance at ~3625 cm^{-1} (~2705 cm^{-1}) for H_2O (D_2O).[154] SFG results for strongly (pH <2) acidic solutions at the air/water interface are consistent with a scenario in which the excess proton is present at the interface. In basic solutions, interfacial water order decreases and OH^- is, at most, only weakly adsorbed. Similar to the SHG measurements on both the air/water and hexadecane/water interfaces, SFG measurements at the air/water interface do not find a significant signal change that is attributable to interfacial H^+/OH^- at pHs at which electrokinetic measurements are made, which suggests that the surface should be strongly charged (i.e., pH 6–9).

The planar CCl_4/water interface was measured by Richmond and co-workers using SFG spectroscopy for aqueous phases at pH 9.87 and 2.45 and under pH-neutral conditions.[155] Here, as can be seen from Figure 28B, at high pH there are changes in the blue part of the spectrum, while at low pH there are changes in the red part of the spectrum. As described above, these observations are consistent with the presence of H^+/OH^- at low/high pH at the air/water interface but are indirect (the subtle changes in line shape observed may also have other origins). SFG spectra from octadecyltrichlorosilane (OTS)/water films were also shown to change as a function of bulk pH[156,158] (Figure 28C). The main features that change with pH are the broad OH stretch band around 3200 cm^{-1}, which increases with pH, and the phase difference between the imaginary and real part of the OH and the CH modes of the OTS molecules (not shown in the figure). In the first study of this system by Ye et al., these pH-dependent changes were attributed to changes in water structure involving defects in the monolayer.[158] Subsequently, Tyrode and Liljeblad,[159] monitoring the quality of OTS monolayer formation via advancing, retreating, and static contact angle measurements, confirmed that the peak intensity around 3300 cm^{-1} likely originates from defects in the OTS monolayer (although they did not address the pH dependence of their response). In a

subsequent paper from the Shen group on the pH dependence of the silica/OTS/water interfacial OH stretch response, the influence of monolayer defects on the spectral response was not considered.[156] Instead the observed spectral changes were attributed to water structure changes with H^+/OH^- adsorption at low/high pH with OH^- adsorption being more favorable (see Figure 28C). The planar polydimethylsiloxane (PDMS)/water interface was investigated as a function of pH by Bakker and co-workers. They found a similar trend as on the OTS/water interface: an increasing SFG signal with increasing pH.[160] While the line shape of the spectral response also appears to be pH-dependent, the low spectral resolution made it difficult to correlate their observations with interfacial H^+ or OH^- populations.

While most electrokinetic measurements have been performed on bubbles or droplets, most SHG/SFG measurements have been performed on planar interfaces. In an attempt to remove any possible differences in the acid/base properties of hydrophobic/water interfaces as a result of interfacial curvature, SFG scattering and electrokinetic measurements were performed on the same (hexadecane) droplet system.[161] While this particular study found behavior similar to that observed in Figure 27 for the electrokinetic measurements, in the high-frequency range at high pH values (9, 12.5), no change in the SFG intensity was seen (see Figure 28D). To summarize, while interfacial populations of H^+/OH^- at low/high pH at hydrophobic/water interfaces are consistent with most SHG/SFG measurements of these systems, the great majority of measurements find little or no change in spectral response from pH 2 to 9, a pH range over which most electrokinetic measurements find a large change in surface potential.

In addition to these all-optical probes, surface-specific information has been gained by applying synchrotron-based X-ray photoemission spectroscopy (XPS) to liquid water microjets. In contrast to SFG/SHG spectroscopy, the surface sensitivity in these experiments is limited by the mean free path of electrons in liquid water, which is a function of electron kinetic energy. Hence it can be tuned by changing the incident photon energy, enabling one to extract a “surface” and “bulk” signal from the same measurement.[162] In spite of the different probing depths of the all-optical and XPS approaches, the latter experiments tell a story similar to that of the former, as probed both via the OH^- $2p\pi$ valence electron and O 1s core electron response; these results suggest that OH^- is either not enriched or weakly repelled from the air/water interface at elevated pH.[163]

Similar to the all-optical SHG measurements, X-ray-based probes can also be applied to probe the interfacial activity of H^+/OH^- indirectly, through the presence of counterions. In an example of this approach, XPS spectra (of the carbon 1s orbital) collected from solutions of formic, acetic, and butyric acid strongly suggest that both formic and acetic acids exist at the interface as fully protonated species (at the half-equivalence point) while butyric acid coexists with butyrate.[164] Collectively, these measurements thus suggest that adsorption of the excess proton at the air/water interface is favorable: the air/water interface is acidic. While in this case the counterion was the acid’s conjugate base, in a subsequent study, the XPS spectrum of iodine in solution at pH values of 1, 6.8, and 13 (pH adjusted by HCl/NaOH) was concluded to suggest that interfacial concentrations of iodide were enhanced at both pH extremes.[165] On the basis of complementary molecular dynamics simulation, these measurements were taken to suggest that interfacial populations of I^- are enhanced at low

pH because of the surface activity of the excess proton and at high pH by a salting-out effect from OH^- in bulk (see Figure 29). Along similar lines, Shapovalov et al. have recently performed total reflection X-ray fluorescence measurements of solutions containing RbBr, at pH values of 4, 6, and 9, and found essentially no preferential enrichment of either species, suggesting that both the excess proton and OH^- at most weakly adsorb to the interface at these pH values.[145]

In addition to probing the presence of H^+/OH^- at the air/water interface via their optical response, one might also utilize mass spectrometric techniques. Recently, Colussi and coworkers have performed electrospray ionization mass spectrometry on liquid jets of heptanoic acid solutions.[166] In their experiments, systems in which the acid is dissolved in the aqueous solution used to form a liquid jet and those in which the acid is deposited via the gas phase on the jet's surface are probed via electrospray mass spectrometry.[166] By comparing the two types of samples, they conclude that, as a function of bulk pH, the surface population of heptanoate is enhanced relative to that of the bulk. On the basis of cluster calculations, the authors then suggest that such surface excess is only possible if OH^- is enhanced at the air/water interface at nearneutral pH: the air/water interface is basic. Whether this novel approach directly or indirectly probes interfacial H^+/OH^- still remains an open question. In particular, the relative time scales of autoionization and diffusional equilibrium at the interface remain unclear. Furthermore, the similarity between the electronic and dielectric properties of neat interfacial water and those inferred from the presence of interfacial carboxylate also remains an open question.[167]

3.2 Theoretical Description

Proton adsorption at the air/water interface has been modeled coarsely by Levin and co-workers employing polarizable anion dielectric continuum theory (PA-DCT), in which the excess proton is treated as a point charge.[168,169] In this model, proton adsorption is the result of a square well potential positioned at ~1 HB length from the interface. Given this ansatz, a square well potential chosen so as to give a proton adsorption free energy of −7.5 kJ/mol results in calculated surface tensions that reproduce the experimental values for solutions of most hydrohalous acids. While useful, it is clear that such an approach assumes a lack of specific proton/anion interactions that for some systems is not correct, as discussed below.

Clearly, the first step toward studying surface partitioning of OH^- or the excess proton from an atomistic simulation perspective is to develop an appropriate model for both species. As discussed above, developing such a model for the bulk is already challenging. This challenge is amplified at the air/water, and indeed all, extended interfaces. Molecular dynamics simulations used to study the air/water interface need to be larger than those appropriate for bulk properties and must additionally sample slower interfacial structural degrees of freedom and therefore have to be simulated longer. A variety of workers have modeled the proton using classical fixed charge or polarizable models. Because such models are not reactive, typically such analyses assume that the proton exists in its E form.[170–172] In this spirit, initial work by Dang found that the adsorption of the E cation is not favorable at the air/water interface.[170] However, other polarizable force fields suggest that H_3O+ has a favorable free energy of adsorption of ~12.6 kJ mol^{-1}.[172] Jungwirth and co-workers have recently

demonstrated that the favorability of E cation adsorption at the air/water interface sensitively depends on the interaction of the hydronium oxygen with adjoining water molecules.[171] If the hydronium accepts a weak HB, the free energy of adsorption is substantially less favorable. However, as discussed above, an essential feature of the excess proton in bulk water is its structural flexibility. As confinement to a two-dimensional surface will likely influence these structural dynamics, there is little evidence that a single E form is an appropriate description.

To address this limitation, a variety of workers have applied MS-EVB models designed to capture the E–Z interconversion. Notably, Voth and co-workers have demonstrated that excess proton adsorption at the air/water interface is favorable by 2.1–8.4 kJ mol^{-1} (depending on the model parametrization).[173–175] The excess proton in their model is slightly delocalized. As a result, Z is more favorable at the interface than in the bulk. Köfinger and Dellago reached similar conclusions with a differently parametrized MS-EVB model.[176] Neither of these models, however, explicitly account for electronic polarization. Wick developed such an MS-EVB variant and found that explicitly accounting for polarizability results in an essentially flat potential of mean force as the proton is brought from the bulk to the interface (see Figure 30); i.e., surface adsorption of the proton is not favored.[177] A more recent study with a new MS-EVB model indicates that the proton is found to be attracted to the air-water interface and that this is driven by favorable enthalpic contributions. In contrast, the hydroxide ion is repelled from the interface.[178]

There have been several studies examining H^+ and OH^- near water/hydrophobic interfaces from AIMD simulations. Such simulations are computationally demanding, and as a result, initial efforts by Buch et al.[179] and Kudin and Car[180] did not quantify the proton's free energy of adsorption. On the basis of limited statistics, the former found the excess proton to preferentially absorb to the air/water interface, while the latter found that both the H^+ and OH^- interact strongly with a hydrophobic surface. Potentials of mean force for adsorption of the excess proton at the air/water interface have been calculated in more recent work.[181,182] While the exchange/correlation functionals employed in the two studies differed, neither work found proton adsorption to be favorable, and the former found a 7.5 kJ mol^{-1} barrier for surface adsorption.

Several groups have also examined adsorption of OH^- at the air/water interface using empirical potentials.[172,183] In general, these works find that OH^- at the interface is 4.8–16.7 kJ mol^{-1} less stable than in the bulk. MS-EVB models [also called MS-RMD (reactive molecular dynamics)] developed in different ways find qualitatively similar but quantitatively different results: OH^- at the interface is 0–10.5 kJ mol^{-1} less stable than in the bulk.[184] Similar AIMD simulations predicted a 0.5 kcal mol^{-1} stabilization of OH^- at the air/water interface.[182,185]

3.3 Challenges for Interfacial Studies

From the previous sections, it is clear that there are a number of experimental findings that suggest contradictory interfacial affinities of OH^-/H^+. Partially, this can be ascribed to differences between the methods. First there is the sample preparation: given that planar surfaces typically have a small surface to volume ratio, it is possible that impurities from the

bulk phase (water, oil, solid film) influence the outcome of the experiment. Such an effect of impurities is to be suspected when subsequent experiments render different results or when they change over time.[186] Using an aqueous solution of nanodroplets/particles or bubbles in water in combination with an overall small volume can reduce this problem, but this also depends on the chosen chemicals, preparation procedure, and chemical purity. SHG[149] and SFG[187] measurements can detect the surface influence of impurities down to micromolar concentrations. On the basis of these data, it is reasonable to assume that negligibly detectable impurity-related changes occur when >99.8% pure oils are used. In addition, defects in supported films[159] or imperfect wetting in the case of oils[188] can have a significant influence on the experimental outcome and thus complicate the interpretation of, for example, the data reported in Figure 28A.

Second, method-related differences in the experimental observables can also play a role, for example, the probing depth of XPS, SHG, and SFG is not the same. Pulsed IR and 800 nm laser radiation can influence monolayer structure.[189]

Also, as nicely illustrated by Figure 28B,C, deconvoluting the spectral response of the excess proton or hydroxide ion from the broad OH stretch feature of interfacial water is not trivial. A third issue concerns the physical interpretation of experimental observables. Surface tension measurements are often thought to report on the properties of the surface state of water, but they equally report on properties of the bulk state of water.[190] Electrokinetic mobility data are interpreted to report on a surface potential using typically a point charge to replace the particle. It can also be shown that an E field across a particle with oriented water molecules generates a gradient in the chemical potential. Similar to the osmotic force, this gradient can lead to particle motion.[191] Also, mean field modeling of a hydrophobic surface with mobile charge and displaying a significant slip (relevant for the oil and gas bubbles as described above) shows that compared to hydrophilic interfaces smaller charges lead to larger mobility and thus electrokinetic potentials.[192] Clearly, the final verdict has not been given here, but it may well be possible that the surface charge necessary to predict the high electrokinetic mobility is much lower than what is commonly expected. For example, more sophisticated interfacial descriptions, such as a charge transfer mechanism instead of adsorbed ionic species, may rationalize the pH dependence.[161,193,194]

Another interpretational controversy might arise from the assumption that the excess proton and OH^- adsorb independently. Recent work has highlighted that for many solutions the counterion (anion for the excess proton and cation for OH^-) determines the stability of the interfacial excess proton and OH^-.[182,195,196] For example, in X-ray photoemission measurements and ab initio molecular dynamics studies of the air/water interface of nitric acid solutions, it was found that the undissociated acid is substantially more energetically favorable at the air/water interface than both the $H_3O^+ \ldots NO_3^-$ contact ion pair (CIP) and the fully dissociated forms.[197,198] Recent work calculating a potential of mean force from ab initio dynamics simulations quantifies this effect and confirms earlier qualitative conclusions from previous, less extensive, ab initio molecular dynamics studies: the molecular form is approximately 4 kcal mol^{-1} more stable than the CIP and more than 5.5 kcal mol^{-1} more stable than the fully dissociated form.[182,199,200] Along similar lines, combined X-ray absorption measurements and ab initio molecular dynamics simulations have been taken to

suggest that HCl forms persistent CIPs in solution over a wide range of acid concentrations.[201,202] A recently calculated ab initio potential of mean force suggests similar structures exist at the air/water interface: here the $H_3O^+…Cl^-$ CIP is 0.6 kcal mol^{-1} more stable than the molecular acid.[202] Such contact ion pair formation appears to be consistent both with molecular beam measurements at the solution/vapor interface[203] that have found slow isotope exchange between vapor-deposited DCl and H_2O and with VSF measurements that find essentially no interfacial molecular HCl at virtually all bulk concentrations.[204]

From a physical point of view, there is an increasing awareness that the potential of mean force for ion pair formation and acid deprotonation may differ significantly at the air/water and hydrophobic/water interface from that in bulk water. While such phenomena are clearly important chemically, e.g., effectively HNO_3 is a dramatically weaker acid at the air/water interface than in the bulk, their quantification may help to reconcile apparent inconsistencies between experimental observables. For example, undissociated acids/bases do not contribute to interfacial charging and thus will drastically decrease interfacial water ordering and the free energy of adsorption of subsequent counterions relative to their dissociated analogs. The exploration of such phenomena is in its infancy. X-ray photoemission measurements as a function of ion concentration and ion pair are capable of providing such insight as SFG measurements provide information about the internal vibrations. In the latter case, 2D IR-SFG measurements applied to intramolecular vibrations may provide similar insight into interfacial ion clustering and dynamics as that gained from 2D IR measurements in bulk (see discussion of both points elsewhere in this issue), although, with the average duration of the experiment being several hours, it may require heroic efforts in terms of purity and system stability.

To summarize, the behavior of water at hydrophobic interfaces in the context of the propensity for it to attract hydronium or hydroxide ions remains a hotly debated issue. Given experimental and simulation-based local probes, the pH-dependent surface charge at the air/water interface inferred from bubble and droplet surface potential measurements is difficult to understand. As mentioned in the above paragraphs, it may well be that the standard interpretation[205] needs adjustment. Ideally, experiments on the hydrophobic/water interface that provides simultaneous insight into surface charging and the interfacial structure of all constituents under conditions of controllable shear would be very insightful. Sum frequency scattering measurements combined with electrokinetic mobility measurements provide one ingredient to further build upon,[161] as well as SFG experiments in microfluidic devices probing hydrophilic interfaces under shear.[206] Combining surface charge and surface structure under carefully explained slip conditions would go a long way in clarifying some of the inconsistencies, as would further work on interpretational questions related, for example, to the probing depth of the various nonlinear optical methods. In addition, combining XPS and SHG/SFG experiments might help to disentangle the molecular structure of acidic, neutral, and basic aqueous interfaces.

4 Protons at the Membrane/Water Interface

In the previous section, we discussed the propensity of protons and hydroxide ions for hydrophobic surfaces like the air/water interface. Most of the evidence in this context

suggests that the binding free energy of protons to these interfaces is comparable to thermal energy at room temperature. In the current section, we discuss the properties of protons at the membrane/water interface, where apparently the propensity for protons appears to be significantly larger. This increased affinity is one of the many consequences of a profoundly altered interface structure: the hydrophobic membrane interior is shielded from water by polar moieties (e.g., carbonyl groups) and most often also by charged groups (e.g., phosphate moieties) (Figure 31), which are both able to attract protons. Second, membrane lipids are strongly hydrated, as indicated by the high penalty for removing all water separating lipid bilayers; e.g., an energy of 5 kcal per mole of lipid molecules is needed to bring egg phosphatidylcholine bilayers into contact.[207]

The more favorable binding free energy of protons to the water/membrane interface than to the air/water one enables membrane interfaces to act as proton pathways; i.e., protons are thought to move along membranes via a hopping mechanism. This is markedly different from proton diffusion in biological aqueous solutions, which usually contain buffers in concentrations that exceed the free proton concentration by orders of magnitude. Thus, under physiological conditions, proton transport through the bulk does not occur via a protonhopping mechanism but via the (much slower) diffusion of buffer molecules that carry the protons.

By providing the shortest pathway and the fastest means of transport, membrane surfaces gain special importance in bioenergetics: the first step in energy transduction in biological systems (e.g., photosynthetic bacteria, mitochondria) is proton pumping across a membrane by a specialized protein (e.g., bacteriorhodopsin, cytochrome *c* oxidase), creating a pH gradient that in a second step can be utilized to synthesize ATP (the energy “currency” of the cell) or provide the driving force for membrane transport (e.g., ion pumps, protein translocation channels).[3] The pumped protons may not be immediately released into the bulk of the aqueous phase but may migrate in the confinement of the membrane/water interface toward the proton-consuming membranal proteins, where they energize an enzymatic reaction, e.g., ATP synthesis. Such a link between sites of proton release and proton consumption is thought to be more efficient than the exchange via diffusion through the liquid bulk.[208] It also implies that pH does not equilibrate even in the small volume of the mitochondria. This offers the possibility of locally regulating the proton transmembrane chemical potential. For example, the proton transporter UCP4 (uncoupling protein 4) prevents excessive transmembrane pH differences, thereby limiting the production of reactive oxygen species by proton pumps.[209]

The molecular mechanism of proton movement in the confinement of near-membrane water layers is not well understood. For a long time, surface protons were considered to either hop between titratable membrane moieties[210,211] or along a HB network involving both titratable groups and interfacial water molecules.[212] The hypotheses came from experiments that were carried out with either lipid monolayers[213] or membrane fragments of purple bacteria.[214,215]

4.1 Proton Movement along Lipid Monolayers

In the early experiments by Teissie et al., protons were injected into the aqueous phase below a lipid monolayer, and their travel time was derived from the pH-dependent decline in

fluorescence intensity of lipid anchored dyes at a distance of several centimeters.[213] In the absence of the phosphatidylethanolamine monolayer, this time became significantly longer, as judged from the fluorescence of water-soluble dyes. The interfacial proton surface diffusion coefficient, D_p, in the presence of phosphatidylethanolamine monolayers, appeared to be larger than the proton diffusion coefficient in pure water. It varied between 1.5×10^{-4} [216] and 2×10^{-3} cm^2 s^{-1}.[213,216] This large variability suggested that convection, due to a rather large injection volume, may have influenced the results.[217]

Long-distance interfacial proton movement was also debated because the early experiments revealed no evidence for the delayed proton surface-to-bulk release that it requires.[217] That is, subsequent to their permeation through a lipid bilayer, weak acids dissociated adjacent to the membrane surface and buffer molecules from the bulk solution appeared to immediately pick up the released protons. In contrast, protons released by more hydrophobic weak acids first traveled over the bilayer surface and continued migrating along the lipids that covered the Teflon support before being observed in the bulk by double-barreled ion-selective microelectrodes.[218] The second barrel of the microelectrodes was sensitive to Ca^{2+} that these weak acids (i) picked up in exchange at one interface for twice as many released protons and (ii) released at the opposite interphase. In contrast to the H^+ release, the Ca^{2+} release was limited to the bilayer part of the membrane.

Support for a delayed proton surface-to-bulk release came also from measurements of the equilibrium electrical conductance of the aqueous layers in the immediate vicinity of a monolayer surface.[217] Two platinum electrodes enclosed the monolayer and reached a few millimeters into the aqueous phase. They revealed a much lower conductivity in the absence of the lipid monolayer.[219] These conductivity data translate into an increase in proton concentration from 2.6×10^{-6} M in the bulk to 0.18 M in a 1 nm thick volume element adjacent to a phosphatidylethanolamine monolayer! The calculations assume that (i) only short-range interaction forces may keep the proton at the bilayer surface and (ii) the protons retained bulk mobility.

However, it is questionable that protons were the only charge carriers that contributed to the electrical conductivity in the immediate vicinity of the lipid monolayers. The projected huge increase in proton surface concentration[219] is in sharp contrast to (i) pH profiles that were reported by lipid-anchored pH-sensitive dyes at distances between 0.2 and 1.3 nm from the membrane surface,[220] and (ii) direct measurements of the protonation rate of a fluorophore by fluorescence correlation spectroscopy.[221] It appeared to be equal for dyes that were anchored to an uncharged lipid bilayer and dyes that were placed into the bulk solution (for pH <7).[221]

Taken together, the controversially discussed monolayer experiments did not conclusively demonstrate proton migration along the monolayer/water interface. Additional experimental evidence was required to demonstrate that the membrane surface may serve as a proton pathway. Experiments carried out with bacterial membrane fragments provided some of the missing pieces.

4.2 Proton Diffusion along Bacterial Membrane Fragments

Long-range proton transfer was found along the surface of purple membrane fragments.[214,215] Protons that were photo-released to one (the extracellular) side of the membrane fragment by the integral membrane protein bacteriorhodopsin arrived at surface-bound pH-dependent dyes at the other (cytoplasmic) side of the fragment earlier than at aqueous dyes (pyranine) in the surrounding solution.[214,215] Different D_p values were calculated from proton's travel time and the dimensions of the membrane fragments: D_p varied from 1×10^{-6} [214] to 3×10^{-5} cm^2 s^{-1}.[214,215] This discrepancy is not the only weak point of these experiments: long-range proton transfer is only one possible interpretation of the data. A transient deprotonation on the cytoplasmic surface could also explain the observations.[222]

In order to remove this ambiguity, proton movement around a bacteriorhodopsin-lipid–detergent micelle was measured with lipids of different pK_a values. Accordingly, cysteine-anchored pH-dependent dyes demonstrated a pK_a-dependent change in signal amplitude that was taken as evidence for lateral diffusion along surface-bound buffer groups.[210] However, this conclusion is also not unambiguous, because the travel time around the micelle should have increased with pK_a. That is, if the protons would have moved by hopping from one headgroup to the next, their migration time should have depended on their dwell time on the lipid head groups, as the latter increases rapidly with the headgroup's pK_a.[223,224] The fact that an invariant D_p was observed in these experiments[210] could mean that (i) the proton does not travel along lipid head groups, or (ii) the system was out of equilibrium, or both.

4.3 Proton Migration along Lipid Bilayers

Assuming that protons move along the membrane surface by jumping between titratable lipid head groups (Figure 31), the lateral diffusion constant, D_p, was predicted from measurements[211] of the rate constant k_{off} for proton exchange between a pH-dependent fluorescent dye and the surrounding head groups as: [211]

$$D_p = k_{off} l^2/4 \quad (1)$$

where l is the average distance between two lipid molecules. To derive k_{off}, lipid vesicles were subjected to fluorescence correlation spectroscopy and the fluctuations attributable to dye protonation were observed. For vesicles made of phosphatidic acid, D_p amounted to only 2×10^{-7} cm^2 s^{-1}.[211] Thus, it was 1 or 2 orders of magnitude smaller than proton diffusivity adjacent to bacterial membrane fragments (compare section 4.2). The difference cannot be attributed to membrane proteins, as D_p on top of planar phosphatidylcholine bilayers was also much larger.[218]

In order to obtain the D_p value for planar lipid bilayers, protons were photoreleased from a hydrophobic membrane-bound caged compound[225] in a small membrane patch.[225] Membrane-anchored, pH-sensitive fluorescent dyes indicated the arrival of the protons at a distant membrane patch (Figure 32). The proton travel time between both sites was measured. D_p calculations were undertaken by a Monte Carlo algorithm that revealed a satisfactory fit to the experimental fluorescence kinetics for $D_p = 5.8 \times 10^{-5}$ cm^2 s^{-1}.[218]

It is impossible to explain the 2 orders of magnitude difference between measured[218] and predicted[211] D_p values as originating from the acidity of the lipid headgroups, because D_p appears to be independent of the pK_a.[226] This is best demonstrated by comparing proton mobilities on top of phosphatidyl ethanolamine (PE) and phosphatidylcholine (PC) bilayers. Assuming a diffusion-limited protonation reaction with the on-rate $k_{on} = 2 \times 10^{10}$ s^{-1} M^{-1} [223] and pK_a values of 9.6[227] and 2.5[223] for PE[227] and PC,[223] respectively, we find k_{off} values of $2 \times 10^{(10\text{-}9\ 6)}$ $s^{-1} \approx 5$ s^{-1} and $2 \times 10^{(10\text{-}25)}$ $s^{-1} \approx 6.3 \times 10^7$ s^{-1} and the corresponding D_p values of ~10^{-14} and ~10^{-7} cm^2 s^{-1}, respectively (Figure 31). Using the assay depicted in Figure 32, Springer et al. measured similar rates of proton diffusion for compositionally different lipid bilayers.[226] Fitting a system of reaction-diffusion equations to the experimental data was successful provided that an energy barrier that impedes proton surface to bulk release was artificially introduced. This procedure did not confirm the predicted 7 orders of magnitude difference between the D_p values.[226] It revealed a 2-fold D_p difference between PC and PE, indicating that the model of proton hopping between titratable residues along the membrane surface is invalid.[226] Instead, proton surface migration is likely to occur along ordered waters of membrane hydration.

To explain these results, two different migration models were proposed (Figure 33). According to the first model, proton surface-to-bulk release is irreversible.[228] That is, once a proton has left the surface, the probability of its return to the membrane surface is negligibly small. The second model envisions a quasi-equilibrium process; i.e., the released proton is allowed to return multiple times to the membrane surface.[229]

The Gibbs activation energy $\Delta G^{\ddagger}$ for proton surface-to-bulk release was considered to be on the order of 10 $k_B T$ in the quasi-equilibrium model.[229] The alternative model of an irreversible proton release from the membrane surface returns an off-rate on the order of 0.5 s^{-1}.[228] In the frame of transition state theory for rate processes at surfaces, such an off-rate would correspond to $\Delta G^{\ddagger} = -k_B T \ln(k_{off}/\nu_0) \approx 30\ k_B T$, if one assumes the value $\nu_0 \approx 10^{13}$ s^{-1} for the attempt frequency. Such an immense energy barrier cannot be explained by hydrogen bonding. An entropic barrier would be required. So far there is no experimental proof in favor of either model.

However, the hypothesis of an entropic component is favored by the observation of interfacial proton migration along the decane/water interface.[230] In these experiments the protons were microinjected close to the decane/water interface and their arrival at a distant spot was observed (Figure 34). Indeed, both D_p and k_{off} differed surprisingly little from the respective values measured at the membrane/water interface,[230] supporting the idea that the protons migrate along ordered interfacial water molecules. Such ordering was observed adjacent to lipid membranes as well as in the vicinity of organic solvents such as decane by vibrational sum frequency generation spectroscopy.[231]

The importance of interfacial proton movement was demonstrated by measuring the PT rate into the catalytic site of a proton pump.[232] The proton-coupled electron transfer was accelerated 7-fold when the pump cytochrome *c* oxidase (from *Rhodobacter sphaeroides*) was moved from a detergent solution into lipid vesicles (Figure 35). The membrane-accelerating effect was completely suppressed when the surface-exposed titratable residue

(glutamic acid) of the pump at position 101 was mutated to a nontitratable residue (alanine). The result suggested that Glu101 establishes a protonic contact between the intraproteinaceous proton pathway and the membrane surface.[232] That is, protons that accumulated on the membrane surface rushed directly into the proton channel of the proton pump.

4.4 Molecular Dynamics Simulations of Proton Movement along Membranes

Computational approaches using the MS-EVB model suggested that some of the interfacial protons are stabilized by charged or dipolar lipid moieties, i.e., by carbonyls or phosphate groups. Proton release from these groups was so slow that the hydrated proton essentially followed the lipid motion.[233,234] A second, more mobile fraction of surface protons was also found to be incapable of efficiently linking the membranal proton source and sink because it readily equilibrated with the bulk; i.e., the mobile protons were released from the interfacial region in less than 1 ns.[234]

Classical molecular dynamics simulations observed a much longer residence time of mobile protons on the membrane surface.[235] The Grotthuss proton-shuttling mechanism was included in the calculations by means of the HYDYN protocol. That is, a Monte Carlo criterion was used at regular intervals for the selection of a proton acceptor in the vicinity of a proton donor.[235] In these simulations, restricted diffusion of (i) lipid-bound protons or (ii) protons that were entrapped inside small water clusters, was interrupted by occasional proton excursions into the bulk that allowed for long-range diffusion intervals. With a diffusion constant of about 10^{-6} cm^2 s^{-1}, overall proton mobility was more than 1 order of magnitude smaller than in comparable experimental systems.[218,226]

Ab initio simulations revealed a more reasonable agreement with experiment.[230] However, the immense computational effort has so far restricted the simulations to the decane/water interface. Its simple structure allowed answering the question about how the requirements for proton attraction and high proton transport rate, which at first glance appear conflicting, may be simultaneously realized. The 75 ps long simulations show that the protons in direct contact with the hydrophobic liquid are immobile.[230] However, the protons in the second water layer are mobile and the in silico mobility is compatible with the D_p of the in vitro measurements.[230] The conclusion from these simulations is that fast proton migration occurs along the ordered waters of hydration. Interestingly, the same mode of transport, i.e., hopping along hydrogen-bonded water wires, has long been accepted as the preferential mode of proton movement through membrane channels, within carbon nanotubes[236,237] or through a protein.[238]

4.5 Proton Transport through Membrane Channels

The involvement of the proton jump mechanism along water wires was first shown in experiments with gramicidin-A channels.[239] These are small pentadecapeptides from *Bacillus brevis* that span the membrane upon dimerization at their N-termini. They conduct monovalent cations like protons, sodium, and potassium ions.[240] In response to an osmotic gradient, water flows through the channel and drags solvated cations with it.[241] Since this mechanism is cation-specific, a membrane potential builds up. This so-called streaming

potential is missing when sodium or potassium ions are replaced by protons.[239] It was concluded that protons are transported along water wires. That is, a proton jumps on to a water molecule at one end of the channel and due to the Grotthuss mechanism, another proton jumps off at the other end.[239] It is important to note that the ability of a membrane channel to conduct protons cannot be derived from the mere presence of a continuous row of water molecules in its lumen. For example, water channel proteins that belong to the aquaporin family exclude protons with an astonishing selectivity: The water-to-proton ratio is higher than 10^9:1.[242,243] The transport mechanism of aquaporins is reviewed in an accompanying paper in this issue.

On the other hand, there are proton-selective channels that are commonly unable to transport water, like the proton channel formed by the M2 protein from influenza A[244] or the voltage-sensitive HV_1 channel.[245] Their selectivity filter consists of titratable amino acids that protrude into the lumen, thereby physically occluding the channel. The water column in these channels is divided into two parts and the protons are handed over from one column to the other by one intervening amino acid[244] or by a pair of amino acids.[245] The inclusion of amino acids into the proton-conducting wire of HBs (see Figure 36) has the peculiar effect that proton conductivity depends only weakly on the proton concentration in the outside solution. While there is no problem in measuring single channel openings for gramicidin channels at acidic pH,[246] the conductance of proton-selective channels remains so small that electrophysiological recordings of single channels cannot be performed. The only report of single voltage-gated HV_1 proton channels indicated a pH-dependent conductivity of 38140 fS.[247] In contrast, fluorescence measurements of intravesicular pH changes estimated the conductivity of reconstituted channels to be on the order of 0.1 fS.[248]

5 Conclusions and Perspectives

In this review, we have provided a summary of both the experimental and theoretical progress made in understanding the structural and dynamical properties of protons and hydroxide ions in different aqueous environments. We began with a discussion of efforts made in disentangling the spectroscopic origins of protonated/deprotonated water clusters: Does the lowest energy isomer dominate at low temperatures, or is a mixture of isomers responsible for the observed IR spectra? These seemingly simple molecular systems still pose challenges especially from the view of the ability of theoretical models to reproduce features of the experimental IR spectra. Methods that provide excellent results for other systems are often ambiguous for these clusters, which exhibit a high degree of anharmonicity due to coupling between the vibrational modes. This can result in rather intense combination bands and Fermi resonances that render the assignment difficult. Both dynamic methods such as AIMD as well as static anharmonic approaches like VPT2 have challenges in reproducing these types of features. The hope is that a quantum mechanical treatment encompassing the nuclear degrees of freedom could provide the ultimate assignments, yet due to steep computational costs, this has been demonstrated only for the smallest system namely, the protonated dimer.

In liquid water, progress has been made in quantifying the structural diffusion process commonly referred to as the Grotthuss mechanism, such as via the special pair dance and the

E–Z–E mechanism. The complementary role of proton wires has been demonstrated for proton transfer in the bulk, for H^+/OH^- recombination and photoacid-to-base PT. Yet, fundamental issues are still debated, e.g., whether the E or Z forms (to an extent that protonated water can be approximated by these structures) dominate the acidic solutions. Time-resolved 2DIR offers new avenues for approaching this question, e.g., by direct monitoring of intermode couplings in the time domain.

For the hydroxide ion, even the coordination number remains debated, and different DFT functionals provide different results. Modeling the proton and hydroxide ions remains challenging also because their physical and chemical properties are inherently quantum mechanical, involving both the electronic and nuclear degrees of freedom. In particular, the importance of quantum fluctuations of the nuclei will be an important issue to consider in future studies.

The propensity of hydronium and hydroxide ions for the air/water or membrane/water interfaces remains an extremely muddy area with inconsistent and contradictory views coming from experiments and as well as theory. We have highlighted the challenges underlying the interpretations of various experiments and also proposed a possible way forward. From the computational side, besides exploring many fundamental questions regarding the structure and dynamics of protons and hydroxide ions at the air/water interface, as has been done in the bulk, the development of highly accurate dissociable empirical potentials that will allow for modeling of electrokinetic phenomena while at the same time allowing for spontaneous autoionization is certainly needed.

The computational challenges involved in elucidating the structure of the proton at the membrane/water interface are even larger. So far, there is no clear picture as to what constitutes the barrier opposing proton surface-to-bulk release. It is only clear that a proton's residence time at titratable residues is not compatible with fast surface proton migration. Further experimental and theoretical work is needed to reveal whether proton surface diffusion occurs either totally decoupled from the bulk or under conditions of rapid equilibrium between bulk and surface protons.

Besides the fascinating properties of the proton at the membrane/water interface, there are many other exciting problems in biophysics where both the thermodynamics and kinetics of proton transfer play an important role. Hydrogen-deuterium isotope exchange to probe the solvent accessibility of amide groups in proteins;[249] ground- and excited-state proton transfer in biological systems, such as green fluorescent protein,[250] amyloid proteins[251] and enzymes;[252] and, finally, the molecular origins of pK_a shifts of amino acids[253] are some of the many situations where both experimental and theoretical research is currently an active area of investigation.

Acknowledgments

This review was initiated during the Nordita (Nordic Institute for Theoretical Physics) scientific program "Water–the Most Anomalous Liquid" (October 2014). Additional financial support for this program was provided by the Royal Swedish Academy of Sciences through its Nobel Institutes for Physics and Chemistry, by the Swedish Research Council, and by the Department of Physics at Stockholm University. N.A. acknowledges support from the

Israel Science Foundation (grant number 766/12). R.H.H. acknowledges support from the BBSRC (grant number BB/K001558/1). P.P. is indebted to the Austrian Science Fund (grant number P25981) for support.

Biographies

Noam Agmon did his Ph.D. in theoretical chemistry on the topic of structure-reactivity correlations with R. D. Levine at the Hebrew University of Jerusalem (Jerusalem, Israel) in 1980. He moved to the United States for a short postdoctoral position with D. R. Herschbach at Harvard University (Cambridge, MA) and a longer one with J. J. Hop field at the California Institute of Technology (Pasadena, CA) on ligand binding to heme proteins. He then returned as a lecturer to the Hebrew University in 1983, being promoted to full professor of chemistry in 2000. His research interests are diffusion-influenced reactions (particularly for reversible reactions), excited-state proton transfer, mechanisms of proton transport in aqueous solutions and in proteins (such as the green fluorescent protein), infrared spectra of protonated water in the liquid and in gas-phase clusters.

Huib J. Bakker was born in Haarlem, The Netherlands. He did his Ph.D. studies in the group of Prof. Dr. Ad Lagendijk, at the FOM Institute for Atomic and Molecular Physics (AMOLF) (Amsterdam, The Netherlands). From 1991 to 1994, he worked as a postdoc in the group of Prof. Dr. Heinrich Kurz at the Institute of Semiconductor Electronics at the Technical University of Aachen (Aachen, Germany). In 1995, he became a group leader at AMOLF, heading the ultrafast spectroscopy group. The research work of the group includes the spectroscopic study of the structure and ultrafast dynamics of water interacting with ions and (bio)molecular systems and the study of the mechanism of proton transfer in aqueous media. In 2001 he became a full professor of physical chemistry at the University of Amsterdam, (Amsterdam, The Netherlands), and in 2003 he became head of the Molecular Nanophysics Department at FOM-AMOLF. In 2004, he received the Gold Medal of the Royal Netherlands Chemical Society for his work on the ultrafast dynamics of aqueous systems. Since February 1, 2016, he has been director of AMOLF.

R. Kramer Campen is currently a staff scientist at the Fritz Haber Institute of the Max Planck Society in Berlin, Germany. There he runs a research group that focuses on molecular structure, ultrafast dynamics, and chemical kinetics at gas/solid, air/liquid and solid/liquid interfaces. Currently, he spends his time trying to understand how water interacts with alumina, the mechanism of ion adsorption at hydrophobic aqueous interfaces, the mechanism of coupled proton/electron transfer across solid/water interfaces, what determines the thermal stability of small hydrocarbons on metal surfaces, and how solvent and surface potential control switching in photoswitchable self-assembled monolayers.

Richard H. Henchman obtained a B.Sc. Honours degree from the University of Sydney (Sydney, Australia), in 1996, and his Ph.D. from the University of Southampton (Southampton, UK), in 2000, supported by a Commonwealth Scholarship (supervised by Prof. Jonathan Essex). He did postdoctoral research with Prof. Andrew McCammon at the University of California, San Diego (San Diego, CA) and Howard Hughes Medical Institute from 2000 to 2004. Subsequently, he took a lecturer position at the University of Manchester (Manchester, UK), later being promoted to senior lecturer. He develops theories to calculate

Europe PMC Funders Author Manuscripts

the entropy of multimolecular systems such as liquids, solutions, and assemblies so as to understand their structure and stability.

Peter Pohl obtained his diploma in biophysics at the Pirogov Institute Moscow (Moscow, Russia) in 1989 and his M.D. at the Martin Luther University Halle (Saale, Germany) in 1994. After having completed his habilitation in 2001, he joined the Leibniz Institute of Molecular Pharmacology in Berlin, Germany, as Heisenberg Fellow of the Deutsche Forschungsgemeinschaft. He then became guest professor at the Institute of Biology of the Humboldt University of Berlin (Berlin,

Germany) in 2002-2003 and was appointed as full professor of biophysics in 2004 at the Physics Department of the Johannes Kepler University Linz (Linz, Austria). His research focuses on (i) membrane transport of water by aquaporins, ion channels, and cotransporters, (ii) proton migration along membranes, (iii) protein translocation through membranes, and (iv) the coupling of membrane leaflets.

Sylvie Roke obtained B.Sc. and M.Sc. degrees with highest honors in chemistry (2000) and physics (2000) from Utrecht University (Utrecht, The Netherlands) and a Ph.D. degree in natural sciences from Leiden University (Leiden, The Netherlands) in 2004, with highest honors. In 2005, she was awarded an independent research group leader (W2) position from the Max-Planck Society. In 2011 she moved to Ecole Polytechnique Fédérale de Lausanne (Lausanne, Switzerland), where she holds the Juli Jacobi chair in photomedicine. She received the Minerva Prize (2006), the Hertha Sponer Prize (2008), an ERC Starting Grant (2009), and an ERC Consolidator Grant (2014). Her research is focused on understanding aqueous systems, interfaces, soft matter, and biological systems using a variety of spectroscopic and imaging methods.

Martin Thämer graduated from the University of Munster (Munster, Germany) in 2006. He then joined the group of Prof. U. Heiz at TU Munich (Munich, Germany), where he received his Ph.D. in physical chemistry in 2012. His Ph.D. work focused on surface-sensitive spectroscopy of supported size-selected metal clusters. From 2013 to 2015 he worked as a postdoctoral fellow (DAAD fellowship) with Prof. A. Tokmakoff at MIT (Cambridge, MA) and later at the University of Chicago (Chicago, IL). During this time he studied hydrogen-bonded systems by employing ultrafast multidimensional spectroscopy. Since 2015, he has been a postdoc with Prof. M. Wolf at the Fritz-Haber-Institute in Berlin, Germany. His current research interests focus on time-resolved spectroscopy of ultrafast surface reactions.

Ali Hassanali was born in Tanzania and grew up in Kenya. He received his Ph.D. in biophysics at The Ohio State University in Columbus, OH, in 2010, under Sherwin Singer and Dongping Zhong. He then did a postdoc with Michele Parrinello at ETH-Zürich (Zürich, Switzerland) and at the University of Lugano (Lugano, Switzerland), where he began to work on fundamental problems in acid-base chemistry in water. He is currently a staff scientist at the International Center for Theoretical Physics in Trieste, Italy. His research interests lie in the area of the structure, dynamics, and IR and optical spectroscopy of water and aqueous solutions, as well as mechanistic details of chemical reactions like proton transfer in these and biological systems like DNA and amyloid proteins.

References

(1). Kreuer KD. Proton Conductivity: Materials and Applications. Chem Mater. 1996; 8:610–641.

(2). Cukierman S. Et Tu, Grotthuss! And Other Unfinished Stories. Biochim Biophys Acta Bioenerg. 2006; 1757:876–885.

(3). Wraight CA. Chance and Design - Proton Transfer in Water, Channels and Bioenergetic Proteins. Biochim Biophys Acta Bioenerg. 2006; 1757:886–912.

(4). Marx D, Chandra A, Tuckerman ME. Aqueous Basic Solutions: Hydroxide Solvation, Structural Diffusion, and Comparison to the Hydrated Proton. Chem Rev. 2010; 110:2174–2216. [PubMed: 20170203]

(5). Knight C, Voth GA. The Curious Case of the Hydrated Proton. Acc Chem Res. 2012; 45:101–109. [PubMed: 21859071]

(6). Fournier JA, Wolke CT, Johnson MA, Odbadrakh TT, Jordan KD, Kathmann SM, Xantheas SS. Snapshots of Proton Accommodation at a Microscopic Water Surface: Understanding the Vibrational Spectral Signatures of the Charge Defect in Cryogenically Cooled $H^+(H_2O)_{n=2-28}$ Clusters. J Phys Chem A. 2015; 119:94259440.

(7). Noyes AA, Kato Y. The Equivalent Conductance of Hydrogen-Ion Derived from Transference Experiments with Nitric Acid. J Am Chem Soc. 1908; 30:318–334.

(8). Noyes AA, Melcher AC, Cooper HC, Eastman GW, Kato Y. The Conductivity and Ionization of Salts, Acids, and Bases in Aqueous Solutions at High Temperatures. J Am Chem Soc. 1908; 30:335–353.

(9). Johnston J. The Change of the Equivalent Conductance of Ions with the Temperature. J Am Chem Soc. 1909; 31:1010–1020.

(10). Gierer A, Wirtz K. Anomale H- und OH-Ionenbeweglichkeit im Wasser. Ann Phys. 1950; 441:257–304.

(11). Robinson, RA, Stokes, RH. Electrolyte Solutions. 2nd. Butterworths; London: 1959.

(12). Meiboom S. Nuclear Magnetic Resonance Study of Proton Transfer in Water. J Chem Phys. 1961; 34:375–388.

(13). Luz Z, Meiboom S. Activation Energies of Proton Transfer Reactions in Water. J Am Chem Soc. 1964; 86:4768–4769.

(14). Walrafen GE, Fisher MR, Hokmabadi MS, Yang WH. Temperature-Dependence of the Low-Frequency and High-Frequency Raman-Scattering from Liquid Water. J Chem Phys. 1986; 85:6970–6982.

(15). Agmon N. Hydrogen Bonds, Water Rotation and Proton Mobility. J Chim Phys Phys-Chim Biol. 1996; 93:1714–1736.

(16). Eigen M, De Maeyer L. Self-Dissociation and Protonic Charge Transport in Water and Ice. Proc R Soc London Ser A. 1958; 247:505–533.

(17). Eigen M. Proton Transfer, Acid-Base Catalysis, and Enzymatic Hydrolysis. I. Elementary Processes. Angew Chem Int Ed Engl. 1964; 3:1–499.

(18). Zundel G. Hydration Structure and Intermolecular Interaction in Polyelectrolytes. Angew Chem Int Ed Engl. 1969; 8:499–509.

(19). Huggins ML. Hydrogen Bridges in Ice and Liquid Water. J Phys Chem. 1936; 40:723–731.

(20). Headrick JM, Diken EG, Walters RS, Hammer NI, Christie RA, Cui J, Myshakin EM, Duncan MA, Johnson MA, Jordan KD. Spectral Signatures of Hydrated Proton Vibrations in Water Clusters. Science. 2005; 308:1765–1769. [PubMed: 15961665]

(21). Okumura M, Yeh LI, Myers JD, Lee YT. Infrared-Spectra of the Solvated Hydronium Ion: Vibrational Predissociation Spectroscopy of Mass-Selected $H_3O^+(H_2O)n(H_2)_m$. J Phys Chem. 1990; 94:3416–3427.

(22). Headrick JM, Bopp JC, Johnson MA. Predissociation Spectroscopy of the Argon-Solvated $H_5O_2^+$ "Zundel" Cation in the 1000–1900 cm^{-1} Region. J Chem Phys. 2004; 121:11523–11526. [PubMed: 15634115]

(23). Gaigeot M-P. Theoretical Spectroscopy of Floppy Peptides at Room Temperature. A DFTMD Perspective: Gas and Aqueous Phase. Phys Chem Chem Phys. 2010; 12:3336–3359. [PubMed: 20336243]

(24). Roy TK, Gerber RB. Vibrational Self-Consistent Field Calculations for Spectroscopy of Biological Molecules: New Algorithmic Developments and Applications. Phys Chem Chem Phys. 2013; 15:9468–9492. [PubMed: 23677257]

(25). Car R, Parrinello M. Unified Approach for Molecular-Dynamics and Density-Functional Theory. Phys Rev Lett. 1985; 55:2471–2474. [PubMed: 10032153]

(26). Yu HB, Cui Q. The Vibrational Spectra of Protonated Water Clusters: A Benchmark for Self-Consistent-Charge Density-Functional Tight Binding. J Chem Phys. 2007; 127:234504. [PubMed: 18154397]

(27). Habershon S, Manolopoulos DE, Markland TE, Miller TF. Ring-Polymer Molecular Dynamics: Quantum Effects in Chemical Dynamics from Classical Trajectories in an Extended Phase Space. Annu Rev Phys Chem. 2013; 64:387–413. [PubMed: 23298242]

(28). Park M, Shin I, Singh NJ, Kim KS. Eigen and Zundel Forms of Small Protonated Water Clusters: Structures and Infrared Spectra. J Phys Chem A. 2007; 111:10692–10702. [PubMed: 17910422]

(29). Kaledin M, Kaledin AL, Bowman JM, Ding J, Jordan KD. Calculation of the Vibrational Spectra of $H_5O_2^+$ and Its Deuterium-Substituted Isotopologues by Molecular Dynamics Simulations. J Phys Chem A. 2009; 113:7671–7677. [PubMed: 19368403]

(30). Vendrell O, Gatti F, Meyer HD. Full Dimensional (15Dimensional) Quantum-Dynamical Simulation of the Protonated Water Dimer. I. Infrared Spectrum and Vibrational Dynamics. J Chem Phys. 2007; 127:184303. [PubMed: 18020635]

(31). Niedner-Schatteburg G. Infrared Spectroscopy and Ab Initio Theory of Isolated $H_5O_2^+$: From Buckets of Water to the Schrodinger Equation and Back. Angew Chem Int Ed. 2008; 47:1008–1011.

(32). Asmis KR, Yang YG, Santambrogio G, Brummer M, Roscioli JR, McCunn LR, Johnson MA, Kuhn O. Gas-Phase Infrared Spectroscopy and Multidimensional Quantum Calculations of the Protonated Ammonia Dimer $N_2H_7^+$. Angew Chem Int Ed. 2007; 46:8691–8694.

(33). Yang Y, Kühn O, Santambrogio G, Goebbert DJ, Asmis KR. Vibrational Signatures of Hydrogen Bonding in the Protonated Ammonia Clusters $NH_4^+(NH_3)_{1-4}$. J Chem Phys. 2008; 129:224302. [PubMed: 19071911]

(34). Heine N, Fagiani MR, Rossi M, Wende T, Berden G, Blum V, Asmis KR. Isomer-Selective Detection of Hydrogen-Bond Vibrations in the Protonated Water Hexamer. J Am Chem Soc. 2013; 135:8266–8273. [PubMed: 23662586]

(35). Kulig W, Agmon N. Both Zundel and Eigen Isomers Contribute to the IR Spectrum of the Gas-Phase $H_9O_9^+$ Cluster. J Phys Chem B. 2014; 118:278–286. [PubMed: 24344636]

(36). Kulig W, Agmon N. Deciphering the Infrared Spectrum of the Protonated Water Pentamer and the Hybrid Eigen-Zundel Cation. Phys Chem Chem Phys. 2014; 16:4933–4941. [PubMed: 24477279]

(37). Jacobsen RL, Johnson RD III, Irikura KK, Kacker RN. Anharmonic Vibrational Frequency Calculations Are Not Worthwhile for Small Basis Sets. J Chem Theory Comput. 2013; 9:951–954. [PubMed: 26588738]

(38). Olesen SG, Guasco TL, Roscioli JR, Johnson MA. Tuning the Intermolecular Proton Bond in the $H_5O_2^+$ 'Zundel Ion' Scaffold. Chem Phys Lett. 2011; 509:89–95.

(39). Kaledin M, Wood CA. Ab Initio Studies of Structural and Vibrational Properties of Protonated Water Cluster $H_7O_3^+$ and Its Deuterium Isotopologues: An Application of Driven Molecular Dynamics. J Chem Theory Comput. 2010; 6:2525–2535. [PubMed: 26613504]

(40). Stoyanov ES, Stoyanova IV, Tham FS, Reed CA. The Nature of the Hydrated Proton $H^+_{(aq)}$ in Organic Solvents. J Am Chem Soc. 2008; 130:12128–12138. [PubMed: 18700768]

(41). Fournier JA, Johnson CJ, Wolke CT, Weddle GH, Wolk AB, Johnson MA. Vibrational Spectral Signature of the Proton Defect in the Three-Dimensional $H^+(H_2O)_{21}$ Cluster. Science. 2014; 344:1009–1012. [PubMed: 24876493]

(42). Hassanali AA, Cuny J, Ceriotti M, Pickard CJ, Parrinello M. The Fuzzy Quantum Proton in the Hydrogen Chloride Hydrates. J Am Chem Soc. 2012; 134:8557–8569. [PubMed: 22500856]

(43). Ceriotti M, Cuny J, Parrinello M, Manolopoulos DE. Nuclear Quantum Effects and Hydrogen Bond Fluctuations in Water. Proc Natl Acad Sci U S A. 2013; 110:15591–15596. [PubMed: 24014589]

(44). Walewski L, Forbert H, Marx D. Revealing the Subtle Interplay of Thermal and Quantum Fluctuation Effects on Contact Ion Pairing in Microsolvated HCl. ChemPhysChem. 2013; 14:817–826. [PubMed: 23161850]

(45). Giberti F, Hassanali AA, Ceriotti M, Parrinello M. The Role of Quantum Effects on Structural and Electronic Fluctuations in Neat and Charged Water. J Phys Chem B. 2014; 118:13226–13235. [PubMed: 25286281]

(46). Mancini JS, Bowman JM. Effects of Zero-Point Delocalization on the Vibrational Frequencies of Mixed HCl and Water Clusters. J Phys Chem Lett. 2014; 5:2247–2253. [PubMed: 26279542]

(47). Wang H, Agmon N. J Phys Chem A. 2016; 120:3117–3135. [PubMed: 27124704]

(48). Tuckerman ME, Marx D, Parrinello M. The Nature and Transport Mechanism of Hydrated Hydroxide Ions in Aqueous Solution. Nature. 2002; 417:925–929. [PubMed: 12087398]

(49). Agmon N. Liquid Water: From Symmetry Distortions to Diffusive Motion. Acc Chem Res. 2012; 45:63–73. [PubMed: 21978022]

(50). Tuckerman ME, Chandra A, Marx D. Structure and Dynamics of $OH^-_{(aq)}$. Acc Chem Res. 2006; 39:151–158. [PubMed: 16489735]

(51). Pliego JR, Riveros JM. Ab Initio Study of the Hydroxide Ion-Water Clusters: An Accurate Determination of the Thermodynamic Properties for the Processes $nH_2O+OH^-(HO^-(H_2O)_n$ (n = 1–4). J Chem Phys. 2000; 112:4045–4052.

(52). Chaudhuri C, Wang YS, Jiang JC, Lee YT, Chang HC, Niedner-Schatteburg G. Infrared Spectra and Isomeric Structures of Hydroxide Ion-Water Clusters $OH^-(H_2O)_{1–5}$: A Comparison with $H_3O^+(H_2O)_{1–5}$. Mol Phys. 2001; 99:1161–1173.

(53). Robertson WH, Diken EG, Price EA, Shin JW, Johnson MA. Spectroscopic Determination of the OH-Solvation Shell in the $OH^-(H_2O)_n$ Clusters. Science. 2003; 299:1367–1372. [PubMed: 12543981]

(54). Bankura A, Chandra A. Hydration Structure and Dynamics of a Hydroxide Ion in Water Clusters of Varying Size and Temperature: Quantum Chemical and Ab Initio Molecular Dynamics Studies. Chem Phys. 2012; 400:154–164.

(55). Crespo Y, Hassanali A. Unveiling the Janus-Like Properties of OH^-. J Phys Chem Lett. 2015; 6:272–278. [PubMed: 26263462]

(56). Crespo Y, Hassanali A. Characterizating the Local Solvation Environment of OH^- in Water Clusters with AIMD. J Chem Phys. 2016; 144:074304. [PubMed: 26896983]

(57). Roberts ST, Petersen PB, Ramasesha K, Tokmakoff A, Ufimtsev IS, Martinez TJ. Observation of a Zundel-Like Transition State During Proton Transfer in Aqueous Hydroxide Solutions. Proc Natl Acad Sci U S A. 2009; 106:15154–15159. [PubMed: 19666493]

(58). Mandal A, Ramasesha K, De Marco L, Tokmakoff A. Collective Vibrations of Water-Solvated Hydroxide Ions Investigated with Broadband 2D-IR Spectroscopy. J Chem Phys. 2014; 140:204508. [PubMed: 24880302]

(59). Agmon N. The Grotthuss Mechanism. Chem Phys Lett. 1995; 244:456–462.

(60). Tuckerman ME, Laasonen K, Sprik M, Parrinello M. Ab-Initio Simulations of Water and Water Ions. J Phys: Condens Matter. 1994; 6:A93–A100.

(61). Hassanali A, Giberti F, Cuny J, Kuehne TD, Parrinello M. Proton Transfer Through the Water Gossamer. Proc Natl Acad Sci U S A. 2013; 110:13723–13728. [PubMed: 23868853]

(62). Danneel H. The Quicksilver Voltameter and the Electricity Meter “Electrolyte”. Z Elektrochem Angew Phys Chem. 1905; 11:139–145.

(63). von Grotthuss CJT. Sur la Decomposition de L’eau et des Corps Qu’elle Tient en Dissolution à L’aide de L’électricité Galvanique. Ann Chim. 1806; 58:54–73.

(64). Hückel E. Theorie der Beweglichkeiten des Wasserstoff-und Hydroxylions in Wässerlinger Lösung. Z Elektrochem. 1928; 34:546–562.

(65). Markovitch O, Agmon N. Structure and Energetics of the Hydronium Hydration Shells. J Phys Chem A. 2007; 111:2253–2256. [PubMed: 17388314]

(66). Chen C, Huang C, Waluyo I, Nordlund D, Weng TC, Sokaras D, Weiss T, Bergmann U, Pettersson LGM, Nilsson A. Solvation Structures of Protons and Hydroxide Ions in Water. J Chem Phys. 2013; 138:154506. [PubMed: 23614429]

(67). Bernal JD, Fowler RH. A Theory of Water and Ionic Solution, with Particular Reference to Hydrogen and Hydroxyl Ions. J Chem Phys. 1933; 1:515–548.

(68). Markovitch O, Chen H, Izvekov S, Paesani F, Voth GA, Agmon N. Special Pair Dance and Partner Selection: Elementary Steps in Proton Transport in Liquid Water. J Phys Chem B. 2008; 112:9456–9466. [PubMed: 18630857]

(69). Tuckerman M, Laasonen K, Sprik M, Parrinello M. Ab-Initio Molecular-Dynamics Simulation of the Solvation and Transport of Hydronium and Hydroxyl Ions in Water. J Chem Phys. 1995; 103:150–161.

(70). Berkelbach TC, Lee H-S, Tuckerman ME. Concerted Hydrogen-Bond Dynamics in the Transport Mechanism of the Hydrated Proton: A First-Principles Molecular Dynamics Study. Phys Rev Lett. 2009; 103:238302. [PubMed: 20366181]

(71). Warshel A, Weiss R. M. An Empirical Valence Bond Approach for Comparing Reactions in Solutions and in Enzymes. J Am Chem Soc. 1980; 102:6218–6226.

(72). Vuilleumier R, Borgis D. Transport and Spectroscopy of the Hydrated Proton: A Molecular Dynamics Study. J Chem Phys. 1999; 111:4251–4266.

(73). Voth GA. Computer Simulation of Proton Solvation and Transport in Aqueous and Biomolecular Systems. Acc Chem Res. 2006; 39:143–150. [PubMed: 16489734]

(74). Decka D, Schwaab G, Havenith M. A THZ/FTIR Fingerprint of the Solvated Proton: Evidence for Eigen Structure and Zundel Dynamics. Phys Chem Chem Phys. 2015; 17:11898–11907. [PubMed: 25872169]

(75). Lapid H, Agmon N, Petersen MK, Voth GA. A Bond-Order Analysis of the Mechanism for Hydrated Proton Mobility in Liquid Water. J Chem Phys. 2005; 122:014506.

(76). Tielrooij KJ, Timmer RLA, Bakker HJ, Bonn M. Structure Dynamics of the Proton in Liquid Water Probed with Terahertz Time-Domain Spectroscopy. Phys Rev Lett. 2009; 102:198303. [PubMed: 19519004]

(77). Hassanali A, Prakash MK, Eshet H, Parrinello M. On the Recombination of Hydronium and Hydroxide Ions in Water. Proc Natl Acad Sci U S A. 2011; 108:20410–20415. [PubMed: 22143756]

(78). Geissler PL, Dellago C, Chandler D, Hutter J, Parrinello M. Autoionization in Liquid Water. Science. 2001; 291:2121–2124. [PubMed: 11251111]

(79). Tse Y-LS, Knight C, Voth GA. An Analysis of Hydrated Proton Diffusion in *Ab Initio* Molecular Dynamics. J Chem Phys. 2015; 142:014104. [PubMed: 25573550]

(80). Hassanali AA, Giberti F, Sosso GC, Parrinello M. The Role of the Umbrella Inversion Mode in Proton Diffusion. Chem Phys Left. 2014; 599:133–138.

(81). Lee SH. Molecular Dynamics Simulation Study of the Ionic Mobility of OH^- Using the OSS2 Model. Bull Korean Chem Soc. 2006; 27:1154–1158.

(82). Webb MB, Garofalini SH, Scherer GW. Use of a Dissociative Potential to Simulate Hydration of Na^+ and Cl^- Ions. J Phys Chem B. 2009; 113:9886–9893. [PubMed: 19569628]

(83). Pinilla C, Irani AH, Seriani N, Scandolo S. Ab Initio Parameterization of an All-Atom Polarizable and Dissociable Force Field for Water. J Chem Phys. 2012; 136:114511. [PubMed: 22443781]

(84). Babin V, Leforestier C, Paesani F. Development of a “First Principles” Water Potential with Flexible Monomers: Dimer Potential Energy Surface, VRT Spectrum, and Second Virial Coefficient. J Chem Theory Comput. 2013; 9:5395–5403. [PubMed: 26592277]

(85). Babin V, Medders GR, Paesani F. Development of a “First Principles” Water Potential with Flexible Monomers. II: Trimer Potential Energy Surface, Third Virial Coefficient, and Small Clusters. J Chem Theory Comput. 2014; 10:1599–1607. [PubMed: 26580372]

(86). Geiger P, Dellago C. Neural Networks for Local Structure Detection in Polymorphic Systems. J Chem Phys. 2013; 139:164105. [PubMed: 24182002]

(87). Lockwood GK, Garofalini SH. Lifetimes of Excess Protons in Water Using a Dissociative Water Potential. J Phys Chem B. 2013; 117:4089–4097. [PubMed: 23565831]

(88). Medders GR, Babin V, Paesani F. Development of a “First-Principles” Water Potential with Flexible Monomers. III. Liquid Phase Properties. J Chem Theory Comput. 2014; 10:2906–2910. [PubMed: 26588266]

(89). Agmon N. Mechanism of Hydroxide Mobility. Chem Phys Lett. 2000; 319:247–252.

(90). Paesani F, Iuchi S, Voth G. A Quantum Effects in Liquid Water from an Ab Initio-Based Polarizable Force Field. J Chem Phys. 2007; 127:074506. [PubMed: 17718619]

(91). Morrone JA, Car R. Nuclear Quantum Effects in Water. Phys Rev Lett. 2008; 101:017801. [PubMed: 18764152]

(92). Marx D, Tuckerman ME, Hutter J, Parrinello M. The Nature of the Hydrated Excess Proton in Water. Nature. 1999; 397:601–604.

(93). Li X-Z, Probert MIJ, Alavi A, Michaelides A. Quantum Nature of the Proton in Water-Hydroxyl Overlayers on Metal Surfaces. Phys Rev Lett. 2010; 104:066102. [PubMed: 20366833]

(94). Li X-Z, Walker B, Michaelides A. Quantum Nature of the Hydrogen Bond. Proc Natl Acad Sci U S A. 2011; 108:6369–6373.

(95). Chen J, Li X-Z, Zhang Q, Michaelides A, Wang E. Nature of Proton Transport in a Water-Filled Carbon Nanotube and in Liquid Water. Phys Chem Chem Phys. 2013; 15:6344–6349. [PubMed: 23518762]

(96). Kim J, Schmitt UW, Gruetzmacher JA, Voth GA, Scherer NE. The Vibrational Spectrum of the Hydrated Proton: Comparison of Experiment, Simulation, and Normal Mode Analysis. J Chem Phys. 2002; 116:737–746.

(97). Xu J, Zhang Y, Voth GA. Infrared Spectrum of the Hydrated Proton in Water. J Phys Chem Lett. 2011; 2:81–86. [PubMed: 26295525]

(98). Kulig W, Agmon N. A ’Clusters-in-Liquid’ Method for Calculating Infrared Spectra Identifies the Proton-Transfer Mode in Acidic Aqueous Solutions. Nat Chem. 2013; 5:29–35. [PubMed: 23247174]

(99). Thämer M, De Marco L, Ramasesha K, Mandal A, Tokmakoff A. Ultrafast 2D IR Spectroscopy of the Excess Proton in Liquid Water. Science. 2015; 350:78–82. [PubMed: 26430117]

(100). Woutersen S, Bakker HJ. Ultrafast Vibrational and Structural Dynamics of the Proton in Liquid Water. Phys Rev Lett. 2006; 96:138305. [PubMed: 16712045]

(101). Roberts ST, Ramasesha K, Petersen PB, Mandal A, Tokmakoff A. Proton Transfer in Concentrated Aqueous Hydroxide Visualized Using Ultrafast Infrared Spectroscopy. J Phys Chem A. 2011; 115:3957–3972. [PubMed: 21314148]

(102). Petersen PB, Tokmakoff A. Source for Ultrafast Continuum Infrared and Terahertz Radiation. Opt Lett. 2010; 35:1962–1964. [PubMed: 20548353]

(103). Agmon N. Infrared Spectroscopy: The Acid Test for Water Structure. Nat Chem. 2016; 8:206–207. [PubMed: 26892549]

(104). Förster, Th. Die pH-Abhängigkeit der Fluoreszenz von Naphthalinderivaten. Z Elektrochem. 1950; 54:531–535.

(105). Weller A. Fast Reactions of Excited Molecules. Prog React Kinet. 1961; 1:187–214.

(106). Agmon N. Elementary Steps in Excited-State Proton Transfer. J Phys Chem A. 2005; 109:13–35. [PubMed: 16839085]

(107). Tolbert LM, Solntsev KM. Excited-State Proton Transfer: From Constrained Systems to “Super” Photoacids to Superfast Proton Transfer. Acc Chem Res. 2002; 35:19–27. [PubMed: 11790085]

(108). Szczepanik B. Protolytic Dissociation of Cyano Derivatives of Naphthol, Biphenyl and Phenol in the Excited State: A Review. J Mol Struct. 2015; 1099:209–214.

(109). Simkovitch R, Shomer S, Gepshtein R, Huppert D. How Fast Can a Proton-Transfer Reaction Be Beyond the Solvent-Control Limit? J Phys Chem B. 2015; 119:2253–2262. [PubMed: 25079251]

(110). Agmon N, Pines E, Huppert D. Geminate Recombination in Proton-Transfer Reactions. 2. Comparison of Diffusional and Kinetic Schemes. J Chem Phys. 1988; 88:5631–5638.

(111). Pines E, Huppert D, Agmon N. Geminate Recombination in Excited-State Proton-Transfer Reactions - Numerical-Solution of the Debye-Smoluchowski Equation with Backreaction and Comparison with Experimental Results. J Chem Phys. 1988; 88:5620–5630.

(112). Agmon N. Diffusion with Back Reaction. J Chem Phys. 1984; 81:2811–2817.

(113). Huppert D, Goldberg SY, Masad A, Agmon N. Experimental-Determination of the Long-Time Behavior in Reversible Binary Chemical-Reactions. Phys Rev Lett. 1992; 68:3932–3935. [PubMed: 10045841]

(114). Karton-Lifshin N, Presiado I, Erez Y, Gepshtein R, Shabat D, Huppert D. Ultrafast Excited-State Intermolecular Proton Transfer of Cyanine Fluorochrome Dyes. J Phys Chem A. 2012; 116:85–92. [PubMed: 22107595]

(115). Lawler C, Fayer MD. Proton Transfer in Ionic and Neutral Reverse Micelles. J Phys Chem B. 2015; 119:6024–6034. [PubMed: 25913559]

(116). Alarcos N, Cohen B, Douhal A. A Slowing Down of Proton Motion from HPTS to Water Adsorbed on the MCM-41 Surface. Phys Chem Chem Phys. 2016; 18:2658–2671. [PubMed: 26705542]

(117). Amdursky N. Photoacids as a New Fluorescence Tool for Tracking Structural Transitions of Proteins: Following the Concentration-Induced Transition of Bovine Serum Albumin. Phys Chem Chem Phys. 2015; 17:32023–32032. [PubMed: 26573990]

(118). Chen H, Voth GA, Agmon N. Kinetics of Proton Migration in Liquid Water. J Phys Chem B. 2010; 114:333–339. [PubMed: 19961199]

(119). Rini M, Magnes BZ, Pines E, Nibbering ETJ. RealTime Observation of Bimodal Proton Transfer in Acid-Base Pairs in Water. Science. 2003; 301:349–352. [PubMed: 12869756]

(120). Mohammed OF, Pines D, Dreyer J, Pines E, Nibbering ETJ. Sequential Proton Transfer through Water Bridges in Acid-Base Reactions. Science. 2005; 310:83–86. [PubMed: 16210532]

(121). Mohammed OF, Pines D, Nibbering ETJ, Pines E. Base-Induced Solvent Switches in Acid-Base Reactions. Angew Chem Int Ed. 2007; 46:1458–1461.

(122). Siwick BJ, Bakker HJ. On the Role of Water in Intermolecular Proton-Transfer Reactions. J Am Chem Soc. 2007; 129:13412–13420. [PubMed: 17935322]

(123). Siwick BJ, Cox MJ, Bakker HJ. Long-Range Proton Transfer in Aqueous Acid-Base Reactions. J Phys Chem B. 2008; 112:378–389. [PubMed: 18067280]

(124). Cox MJ, Timmer RLA, Bakker HJ, Park S, Agmon N. Distance-Dependent Proton Transfer Along Water Wires Connecting Acid-Base Pairs. J Phys Chem A. 2009; 113:6599–6606. [PubMed: 19449829]

(125). Cox MJ, Siwick BJ, Bakker HJ. Influence of Ions on Aqueous Acid-Base Reactions. ChemPhysChem. 2009; 10:236–244. [PubMed: 19130538]

(126). Pines E, Magnes BZ, Lang MJ, Fleming G. R Direct Measurement of Intrinsic Proton Transfer Rates in Diffusion-Controlled Reactions. Chem Phys Lett. 1997; 281:413–420.

(127). Genosar L, Cohen B, Huppert D. Ultrafast Direct Photoacid-Base Reaction. J Phys Chem A. 2000; 104:6689–6698.

(128). Cox MJ, Bakker HJ. Parallel Proton Transfer Pathways in Aqueous Acid-Base Reactions. J Chem Phys. 2008; 128:174501. [PubMed: 18465924]

(129). von Smoluchowski M. Versuch Einer Mathematischen Theorie der Koagulationskinetik Kolloider Lösungen. Z Phys Chem. 1917; 92:129–168.

(130). Szabo A. Theory of Diffusion-Influenced Fluorescence Quenching. J Phys Chem. 1989; 93:6929–6939.

(131). Maurer P, Thomas V, Iftimie R. A Computational Study of Ultrafast Acid Dissociation and Acid-Base Neutralization Reactions. II. The Relationship between the Coordination State of Solvent Molecules and Concerted Versus Sequential Acid Dissociation. J Chem Phys. 2011; 134:094505. [PubMed: 21384983]

(132). Cuny J, Hassanali A. A. Ab Initio Molecular Dynamics Study of the Mechanism of Proton Recombination with a Weak Base. J Phys Chem B. 2014; 118:13903–13912. [PubMed: 25415885]

(133). Beattie JK, Djerdjev AM, Gray-Weale A, Kallay N, Lutzenkirchen J, Preočanin T, Selmani A. pH and the Surface Tension of Water. J Colloid Interface Sci. 2014; 422:54–57. [PubMed: 24655828]

(134). Weissenborn PK, Pugh R. J. Surface Tension of Aqueous Solutions of Electrolytes: Relationship with Ion Hydration, Oxygen Solubility, and Bubble Coalescence. J Colloid Interface Sci. 1996; 184:550–563. [PubMed: 8978559]

(135). Pegram LM, Record MT Jr. Quantifying Accumulation or Exclusion of H^+, HO^-, and Hofmeister Salt Ions near Interfaces. Chem Phys Lett. 2008; 467:1–8. [PubMed: 23750042]

(136). Ottewill, RH, Rowell, RL, editors. Zeta Potential in Colloid Science. Academic Press; 1981.

(137). Carruthers JC. The Electrophoresis of Certain Hydrocarbons and Their Simple Derivatives as a Function of pH. Trans Faraday Soc. 1938; 34:300–307.

(138). Takahashi M. ζ-Potential of Microbubbles in Aqueous Solutions: Electrical Properties of the Gas-Water Interface. J Phys Chem B. 2005; 109:21858–21864. [PubMed: 16853839]

(139). Creux P, Lachaise J, Graciaa A, Beattie JK, Djerdjev A. Strong Specific Hydroxide Ion Binding at the Pristine Oil/Water and Air/Water Interfaces. J Phys Chem B. 2009; 113:14146–14150. [PubMed: 19810695]

(140). Marinova KG, Alargova RG, Denkov ND, Velev OD, Petsev DN, Ivanov IB, Borwankar R. P. Charging of Oil-Water Interfaces Due to Spontaneous Adsorption of Hydroxyl Ions. Langmuir. 1996; 12:2045–2051.

(141). Zimmermann R, Freudenberg U, Schweiss R, Kuettner D, Werner C. Hydroxide and Hydronium Ion Adsorption - a Survey. Curr Opin Colloid Interface Sci. 2010; 15:196–202.

(142). Gray-Weale A, Beattie JK. An Explanation for the Charge on Water's Surface. Phys Chem Chem Phys. 2009; 11:10994–11005. [PubMed: 19924335]

(143). Beattie JK, Djerdjev AN, Warr GG. The Surface of Neat Water Is Basic. Faraday Discuss. 2009; 141:31–39. [PubMed: 19227349]

(144). Winter B, Faubel M, Vácha R, Jungwirth P. Reply to Comments on Frontiers Article 'Behavior of Hydroxide at the Water/Vapor Interface'. Chem Phys Lett. 2009; 481:19–21.

(145). Shapovalov VL, Mohwald H, Konovalov OV, Knecht V. Negligible Water Surface Charge Determined Using Kelvin Probe and Total Reflection X-Ray Fluorescence Techniques. Phys Chem Chem Phys. 2013; 15:13991–13998. [PubMed: 23842782]

(146). Lambert AG, Davies PB, Neivandt DJ. Implementing the Theory of Sum Frequency Generation Vibrational Spectroscopy: A Tutorial Review. Appl Spectrosc Rev. 2005; 40:103–145.

(147). Petersen PB, Saykally RJ. Evidence for an Enhanced Hydronium Concentration at the Liquid Water Surface. J Phys Chem B. 2005; 109:7976–7980. [PubMed: 16851932]

(148). Petersen PB, Saykally RJ. Is the Liquid Water Surface Basic or Acidic? Macroscopic vs. Molecular-Scale Investigations. Chem Phys Lett. 2008; 458:255–261.

(149). Fang H, Wu W, Sang Y, Chen S, Zhu X, Zhang L, Niu Y, Gan W. Evidence of the Adsorption of Hydroxide Ion at Hexadecane/Water Interface from Second Harmonic Generation Study. RSCAdv. 2015; 5:23578–23585.

(150). Tarbuck TL, Ota ST, Richmond GL. Spectroscopic Studies of Solvated Hydrogen and Hydroxide Ions at Aqueous Surfaces. J Am Chem Soc. 2006; 128:14519–14527. [PubMed: 17090035]

(151). Gopalakrishnan S, Liu DF, Allen HC, Kuo M, Shultz MJ. Vibrational Spectroscopic Studies of Aqueous Interfaces: Salts, Acids, Bases, and Nanodrops. Chem Rev. 2006; 106:1155–1175. [PubMed: 16608176]

(152). Tian CS, Ji N, Waychunas GA, Shen Y. R Interfacial Structures of Acidic and Basic Aqueous Solutions. J Am Chem Soc. 2008; 130:13033–13039. [PubMed: 18774819]

(153). Imamura T, Ishiyama T, Morita A. Molecular Dynamics Analysis of NaOH Aqueous Solution Surface and the Sum Frequency Generation Spectra: Is Surface OH^- Detected by SFG Spectroscopy? J Phys Chem C. 2014; 118:29017–29027.

(154). Hermansson K, Bopp PA, Spangberg D, Pejov L, Bako I, Mitev PD. The Vibrating Hydroxide Ion in Water. Chem Phys Lett. 2011; 514:1–15.

(155). Scatena LF, Brown MG, Richmond GL. Water at Hydrophobic Surfaces: Weak Hydrogen Bonding and Strong Orientation Effects. Science. 2001; 292:908–912. [PubMed: 11340199]

(156). Tian CS, Shen Y. R Structure and Charging of Hydrophobic Material/Water Interfaces Studied by Phase-Sensitive Sum-Frequency Vibrational Spectroscopy. Proc Natl Acad Sci U S A. 2009; 106:15148–15153. [PubMed: 19706483]

(157). Samson JS, Scheu R, Smolentsev N, Rick SW, Roke S. Sum Frequency Spectroscopy of the Hydrophobic Nanodroplet/Water Interface: Absence of Hydroxyl Ion and Dangling OH Bond Signatures. Chem Phys Lett. 2014; 615:124–131.

(158). Ye S, Nihonyanagi S, Uosaki K. Sum Frequency Generation (SFG) Study of the pH-Dependent Water Structure on a Fused Quartz Surface Modified by an Octadecyltrichlorosilane (OTS) Monolayer. Phys Chem Chem Phys. 2001; 3:3463–3469.

(159). Tyrode E, Liljeblad JFD. Water Structure Next to Ordered and Disordered Hydrophobic Silane Monolayers: A Vibrational Sum Frequency Spectroscopy Study. J Phys Chem C. 2013; 117:17801790.

(160). Strazdaite S, Versluis J, Bakker HJ. Water Orientation at Hydrophobic Interfaces. J Chem Phys. 2015; 143:084708. [PubMed: 26328868]

(161). Vácha R, Rick SW, Jungwirth P, de Beer AGF, de Aguiar HB, Samson J-S, Roke S. The Orientation and Charge of Water at the Hydrophobic Oil Droplet-Water Interface. J Am Chem Soc. 2011; 133:10204–10210. [PubMed: 21568343]

(162). Ottosson N, Faubel M, Bradforth SE, Jungwirth P, Winter B. Photoelectron Spectroscopy of Liquid Water and Aqueous Solution: Electron Effective Attenuation Lengths and Emission-Angle Anisotropy. J Electron Spectrosc Relat Phenom. 2010; 177:60–70.

(163). Winter B, Faubel M, Vácha R, Jungwirth P. Behavior of Hydroxide at the Water/Vapor Interface. Chem Phys Lett. 2009; 474:241–247.

(164). Ottosson N, Wernersson E, Söderström J, Pokapanich W, Kaufmann S, Svensson S, Persson I, Öhrwall G, Björneholm O. The Protonation State of Small Carboxylic Acids at the Water Surface from Photoelectron Spectroscopy. Phys Chem Chem Phys. 2011; 13:12261–12267. [PubMed: 21633751]

(165). Ottosson N, Cwiklik L, Söderström J, Björneholm O, Öhrwall G, Jungwirth P. Increased Propensity of I_{aq}^{-} for the Water Surface in Non-Neutral Solutions: Implications for the Interfacial Behavior of $H_3O_{aq}^{+}$ and OH_{aq}^{-}. J Phys Chem Lett. 2011; 2:972–976.

(166). Mishra H, Enami S, Nielsen RJ, Stewart LA, Hoffmann MR, Goddard WA III, Colussi AJ. Brønsted Basicity of the Air-Water Interface. Proc Natl Acad Sci U S A. 2012; 109:18679–18683. [PubMed: 23112167]

(167). Saykally R. J. Air/Water Interface: Two Sides of the Acid-Base Story. Nat Chem. 2013; 5:82–84. [PubMed: 23344441]

(168). Tobias DJ, Stern AC, Baer MD, Levin Y, Mundy CJ. Simulation and Theory of Ions at Atmospherically Relevant Aqueous Liquid-Air Interfaces. Annu Rev Phys Chem. 2013; 64:339–359. [PubMed: 23331311]

(169). Levin Y, dos Santos AP. Ions at Hydrophobic Interfaces. J Phys.: Condens Matter. 2014; 26:203101. [PubMed: 24769502]

(170). Dang LX. Solvation of the Hydronium Ion at the Water Liquid/Vapor Interface. J Chem Phys. 2003; 119:6351–6353.

(171). Jagoda-Cwiklik B, Cwiklik L, Jungwirth P. Behavior of the Eigen Form of Hydronium at the Air/Water Interface. J Phys Chem A. 2011; 115:5881–5886. [PubMed: 21214229]

(172). Hub JS, Wolf MG, Caleman C, van Maaren PJ, Groenhof G, van der Spoel D. Thermodynamics of Hydronium and Hydroxide Surface Solvation. Chem Sci. 2014; 5:1745–1749.

(173). Petersen MK, Iyengar SS, Day TJF, Voth GA. The Hydrated Proton at the Water Liquid/Vapor Interface. J Phys Chem B. 2004; 108:14804–14806.

(174). Iuchi S, Chen HN, Paesani F, Voth GA. Hydrated Excess Proton at Water-Hydrophobic Interfaces. J Phys Chem B. 2009; 113:4017–4030. [PubMed: 18821788]

(175). Kumar R, Knight C, Voth GA. Exploring the Behaviour of the Hydrated Excess Proton at Hydrophobic Interfaces. Faraday Discuss. 2014; 167:263–278.

(176). Köfinger J, Dellago C. Biasing the Center of Charge in Molecular Dynamics Simulations with Empirical Valence Bond Models: Free Energetics of an Excess Proton in a Water Droplet. J Phys Chem B. 2008; 112:2349–2356. [PubMed: 18247589]

(177). Wick CD. Hydronium Behavior at the Air-Water Interface with a Polarizable Multistate Empirical Valence Bond Model. J Phys Chem C. 2012; 116:4026–4038.

(178). Tse YLS, Chen C, Lindberg GE, Kumar R, Voth GA. Propensity of Hydrated Excess Protons and Hydroxide Anions for the 2354 Air-Water Interface. J Am Chem Soc. 2015; 137:12610–12616. [PubMed: 26366480]

(179). Buch V, Milet A, Vácha R, Jungwirth P, Devlin JP. Water Surface Is Acidic. Proc Natl Acad Sci U S A. 2007; 104:7342–7347. [PubMed: 17452650]

(180). Kudin KN, Car R. Why Are Water-Hydrophobic Interfaces Charged? J Am Chem Soc. 2008; 130:3915–3919. [PubMed: 18311970]

(181). Lee HS, Tuckerman ME. Ab Initio Molecular Dynamics Studies of the Liquid-Vapor Interface of an HCl Solution. J. Phys Chem A. 2009; 113:2144–2151.

(182). Baer MD, Kuo IFW, Tobias DJ, Mundy CJ. Toward a Unified Picture of the Water Self-Ions at the Air-Water Interface: A Density Functional Theory Perspective. J Phys Chem B. 2014; 118:8364–8372. [PubMed: 24762096]

(183). Vácha R, Buch V, Milet A, Devlin P, Jungwirth P. Autoionization at the Surface of Neat Water: Is the Top Layer pH Neutral, Basic, or Acidic? Phys Chem Chem Phys. 2007; 9:4736–4747. [PubMed: 17712453]

(184). Wick CD, Dang LX. Investigating Hydroxide Anion Interfacial Activity by Classical and Multistate Empirical Valence Bond Molecular Dynamics Simulations. J Phys Chem A. 2009; 113:6356–6364. [PubMed: 19391589]

(185). Mundy CJ, Kuo IFW, Tuckerman ME, Lee HS, Tobias DJ. Hydroxide Anion at the Air-Water Interface. Chem Phys Lett. 2009; 481:2–8.

(186). Goebel A, Lunkenheimer K. Interfacial Tension of the Water/n-Alkane Interface. Langmuir. 1997; 13:369–372.

(187). Jena KC, Scheu R, Roke S. Surface Impurities Are Not Responsible for the Charge on the Oil/Water Interface. Angew Chem Int Ed. 2012; 51:12938–12940.

(188). Delcerro C, Jameson GJ. The Behavior of Pentane, Hexane, and Heptane on Water. J Colloid Interface Sci. 1980; 78:362–375.

(189). Backus EHG, Bonn D, Cantin S, Roke S, Bonn M. Laser-Heating-Induced Displacement of Surfactants on the Water Surface. J Phys Chem B. 2012; 116:2703–2712. [PubMed: 22324652]

(190). Adamson AW, Gast AP. Physical Chemistry of Surfaces. Wiley-Interscience. 1997

(191). Matyushov DV. Electrophoretic Mobility without Charge Driven by Polarisation of the Nanoparticle-Water Interface. Mol Phys. 2014; 112:2029–2039.

(192). Maduar SR, Belyaev AV, Lobaskin V, Vinogradova OI. Electrohydrodynamics near Hydrophobic Surfaces. Phys Rev Lett. 2016; 114:118301.

(193). Vácha R, Marsalek O, Willard AP, Bonthuis DJ, Netz RR, Jungwirth P. Charge Transfer between Water Molecules as the Possible Origin of the Observed Charging at the Surface of Pure Water. J Phys Chem Lett. 2012; 3:107–111.

(194). Wick CD, Lee AJ, Rick SW. How Intermolecular Charge Transfer Influences the Air-Water Interface. J Chem Phys. 2012; 137:154701. [PubMed: 23083178]

(195). Wick CD, Dang LX. Computational Observation of Enhanced Solvation of the Hydroxyl Radical with Increased NaCl Concentration. J Phys Chem B. 2006; 110:8917–8920. [PubMed: 16671694]

(196). Wick CD, Dang LX. The Behavior of NaOH at the Air-Water Interface: A Computational Study. J Chem Phys. 2010; 133:024705. [PubMed: 20632768]

(197). Lewis T, Winter B, Stern AC, Baer MD, Mundy CJ, Tobias DJ, Hemminger JC. Does Nitric Acid Dissociate at the Aqueous Solution Surface? J Phys Chem C. 2011; 115:21183–21190.

(198). Lewis T, Winter B, Stern AC, Baer MD, Mundy CJ, Tobias DJ, Hemminger JC. Dissociation of Strong Acid Revisited: X-Ray Photoelectron Spectroscopy and Molecular Dynamics Simulations of HNO3 in Water. J Phys Chem B. 2011; 115:9445–9451. [PubMed: 21688845]

(199). Shamay ES, Buch V, Parrinello M, Richmond GL. At the Water's Edge: Nitric Acid as a Weak Acid. J Am Chem Soc. 2007; 129:12910–12911. [PubMed: 17915872]

(200). Wang SZ, Bianco R, Hynes JT. Depth-Dependent Dissociation of Nitric Acid at an Aqueous Surface: Car-Parrinello Molecular Dynamics. J Phys Chem A. 2009; 113:1295–1307. [PubMed: 19173580]

(201). Fulton JL, Balasubramanian M. Structure of Hydronium (H_3O^+)/Chloride (Cl^-) Contact Ion Pairs in Aqueous Hydrochloric Acid Solution: A Zundel-Like Local Configuration. J Am Chem Soc. 2010; 132:12597–12604. [PubMed: 20731390]

(202). Baer MD, Fulton JL, Balasubramanian M, Schenter GK, Mundy CJ. Persistent Ion Pairing in Aqueous Hydrochloric Acid. J Phys Chem B. 2014; 118:7211–7220. [PubMed: 24837190]

(203). Brastad SM, Nathanson GM. Molecular Beam Studies of HCl Dissolution and Dissociation in Cold Salty Water. Phys Chem Chem Phys. 2011; 13:8284–8295. [PubMed: 21347480]

(204). Baldelli S, Schnitzer C, Shultz MJ. The Structure of Water on HCl Solutions Studied with Sum Frequency Generation. Chem Phys Lett. 1999; 302:157–163.

(205). Lyklema, J, editor. Elsevier; 2005. Fundamentals of Interface and Colloid Science.

(206). Lis D, Backus EHG, Hunger J, Parekh SH, Bonn M. Liquid Flow Along a Solid Surface Reversibly Alters Interfacial Chemistry. Science. 2014; 344:1138–1142. [PubMed: 24904160]

(207). Leikin S, Parsegian VA, Rau DC, Rand RP. Hydration Forces. Annu Rev Phys Chem. 1993; 44:369–395. [PubMed: 8257560]

(208). Williams RJP. Proton Circuits in Biological Energy Interconversions. Annu Rev Biophys. Biophys Chem. 1988; 17:71–97. [PubMed: 2840089]

(209). Klotzsch E, Smorodchenko A, Löfler L, Moldzio R, Parkinson E, Schütz GJ, Pohl EE. Superresolution Microscopy Reveals Spatial Separation of UCP4 and F0F1-ATP Synthase in Neuronal Mitochondria. Proc Natl Acad Sci U S A. 2015; 112:130–135. [PubMed: 25535394]

(210). Scherrer P, Alexiev U, Marti T, Khorana HG, Heyn MP. Covalently Bound pH-Indicator Dyes at Selected Extracellular or Cytoplasmic Sites in Bacteriorhodopsin. 1. Proton Migration Along the Surface of Bacteriorhodopsin Micelles and Its Delayed Transfer from Surface to Bulk. Biochemistry. 1994; 33:13684–13692. [PubMed: 7947777]

(211). Branden M, Sanden T, Brzezinski P, Widengren J. Localized Proton Microcircuits at the Biological Membrane-Water Interface. Proc Natl Acad Sci U S A. 2006; 103:19766–19770. [PubMed: 17172452]

(212). Tocanne JF, Teissie J. Ionization of Phospholipids and Phospholipid-Supported Interfacial Lateral Diffusion of Protons in Membrane Model Systems. Biochim Biophys Acta, Rev Biomembr. 1990; 1031:111–142.

(213). Teissie J, Prats M, Soucaille P, Tocanne JF. Evidence for Conduction of Protons Along the Interface between Water and a Polar Lipid Monolayer. Proc Natl Acad Sci U S A. 1985; 82:3217–3221. [PubMed: 2987914]

(214). Heberle J, Riesle J, Thiedemann G, Oesterhelt D, Dencher NA. Proton Migration Along the Membrane-Surface and Retarded Surface to Bulk Transfer. Nature. 1994; 370:379–382. [PubMed: 8047144]

(215). Alexiev U, Mollaaghababa R, Scherrer P, Khorana HG, Heyn MP. Rapid Long-Range Proton Diffusion Along the Surface of the Purple Membrane and Delayed Proton-Transfer into the Bulk. Proc Natl Acad Sci U S A. 1995; 92:372–376. [PubMed: 7831293]

(216). Gabriel B, Prats M, Teissie J. Lateral Proton Conduction in Mixed Monolayers of Phosphatidylethanolamine and Cetyltrimethylammonium Bromide. Biochemistry. 1991; 30:9359–9364. [PubMed: 1654096]

(217). Kasianowicz J, Benz R, McLaughlin S. How Do Protons Cross the Membrane-Solution Interface? Kinetic-Studies on Bilayer-Membranes Exposed to the Protonphore-S-13 (5-Chloro-3-Tert-Butyl-2'-Chloro-4'-Nitrosalicyclanilide). J Membr Biol. 1987; 95:73–89. [PubMed: 3031309]

(218). Serowy S, Saparov SM, Antonenko YN, Kozlovsky W, Hagen V, Pohl P. Structural Proton Diffusion Along Lipid Bilayers. Biophys J. 2003; 84:1031–1037. [PubMed: 12547784]

(219). Morgan H, Taylor DM, Oliveira ON Jr. Proton Transport at the Monolayer-Water Interface. Biochim Biophys Ada, Biomembr. 1991; 1062:149–156.

(220). Kraayenhof R, Sterk GJ, Wong Fong Sang HW. Probing Biomembrane Interfacial Potential and pH Profiles with a New Type of Float-Like Fluorophores Positioned at Varying Distance from the Membrane-Surface. Biochemistry. 1993; 32:10057–10066. [PubMed: 8399132]

(221). Sanden T, Salomonsson L, Brzezinski P, Widengren J. Surface-Coupled Proton Exchange of a Membrane-Bound Proton Acceptor. Proc Natl Acad Sci U S A. 2010; 107:4129–4134. [PubMed: 20160117]

(222). Scherrer P. Proton Movement on Membranes. Nature. 1995; 374:222–222. [PubMed: 7885441]

(223). Gutman M, Nachliel E. The Dynamic Aspects of Proton-Transfer Processes. Biochim Biophys Acta, Bioenerg. 1990; 1015:391–414.

(224). Nachliel E, Gutman M. Time-Resolved Proton-Phospholipid Interaction. Methodology and Kinetic Analysis. J Am Chem Soc. 1988; 110:2629–2635.

(225). Geissler D, Antonenko YN, Schmidt R, Keller S, Krylova OO, Wiesner B, Bendig J, Pohl P, Hagen V. (Coumarin-4-yl)methyl Esters as Highly Efficient, Ultrafast Phototriggers for Protons and Their Application to Acidifying Membrane Surfaces. Angew Chem, Int Ed. 2005; 44:1195–1198.

(226). Springer A, Hagen V, Cherepanov DA, Antonenko YN, Pohl P. Protons Migrate Along Interfacial Water without Significant Contributions from Jumps between Ionizable Groups on the Membrane Surface. Proc Natl Acad Sci U S A. 2011; 108:14461–14466. [PubMed: 21859952]

(227). Tsui FC, Ojcius DM, Hubbell WL. The Intrinsic pK Values for Phosphatidylserine and Phosphatydylethanolamine in Phosphatidylcholine Host Bilayers. Biophys J. 1986; 49:459–468. [PubMed: 3955180]

(228). Agmon N, Gutman M. Bioenergetics: Proton Fronts on Membranes. Nat Chem. 2011; 3:840–842. [PubMed: 22024877]

(229). Medvedev ES, Stuchebrukhov AA. Mechanism of Long-Range Proton Translocation Along Biological Membranes. FEBS Lett. 2013; 587:345–349. [PubMed: 23268201]

(230). Zhang C, Knyazev DG, Vereshaga YA, Ippoliti E, Nguyen TH, Carloni P, Pohl P. Water at Hydrophobic Interfaces Delays Proton Surface-to-Bulk Transfer and Provides a Pathway for Lateral Proton Diffusion. Proc Natl Acad Sci U S A. 2012; 109:9744–9749. [PubMed: 22675120]

(231). Strazdaite S, Versluis J, Backus EHG, Bakker HJ. Enhanced Ordering of Water at Hydrophobic Surfaces. J Chem Phys. 2015; 140:054711.

(232). Öjemyr LN, Lee HJ, Gennis RB, Brzezinski P. Functional Interactions between Membrane-Bound Transporters and Membranes. Proc Natl Acad Sci U S A. 2010; 107:15763–15767. [PubMed: 20798065]

(233). Smondyrev AM, Voth GA. Molecular Dynamics Simulation of Proton Transport near the Surface of a Phospholipid Membrane. Biophys J. 2002; 82:1460–1468. [PubMed: 11867461]

(234). Yamashita T, Voth GA. Properties of Hydrated Excess Protons near Phospholipid Bilayers. J Phys Chem B. 2010; 114:592–603. [PubMed: 19924872]

(235). Wolf MG, Grubmüller H, Groenhof G. Anomalous Surface Diffusion of Protons on Lipid Membranes. Biophys J. 2014; 107:76–87. [PubMed: 24988343]

(236). Cao Z, Peng YX, Yan TY, Li S, Li AL, Voth GA. Mechanism of Fast Proton Transport Along One-Dimensional Water Chains Confined in Carbon Nanotubes. J Am Chem Soc. 2010; 132:11395–11397. [PubMed: 20669967]

(237). Kaila VRI, Hummer G. Energetics and Dynamics of Proton Transfer Reactions Along Short Water Wires. Phys Chem Chem Phys. 2011; 13:13207–13215. [PubMed: 21701719]

(238). Shinobu A, Palm GJ, Schierbeek AJ, Agmon N. Visualizing Proton Antenna in a High-Resolution Green Fluorescent Protein Structure. J Am Chem Soc. 2010; 132:11093–11102. [PubMed: 20698675]

(239). Levitt DG, Elias SR, Hautman JM. Number of Water Molecules Coupled to Sodium, Potassium and Hydrogen Ions Via Gramicidin, Nonactin or Valinomycin. Biochim Biophys Acta, Biomembr. 1978; 512:436–451.

(240). Myers VB, Haydon DA. Ion Transfer across Lipid-Membranes in the Presence of Gramicidin-A. II. The Ion Selectivity. Biochim Biophys Acta, Biomembr. 1972; 274:313–322.

(241). Pohl P, Saparov SM. Solvent Drag across Gramicidin Channels Demonstrated by Microelectrodes. Biophys J. 2000; 78:2426–2434. [PubMed: 10777738]

(242). Pohl P, Saparov SM, Borgnia MJ, Agre P. Highly Selective Water Channel Activity Measured by Voltage Clamp: Analysis of Planar Lipid Bilayers Reconstituted with Purified AqpZ. Proc Natl Acad Sci U S A. 2001; 98:9624–9629. [PubMed: 11493683]

(243). Saparov SM, Tsunoda SP, Pohl P. Proton Exclusion by an Aquaglyceroprotein: A Voltage Clamp Study. Biol Cell. 2005; 97:545–550. [PubMed: 15850456]

(244). Sharma M, Yi MG, Dong H, Qin HJ, Peterson E, Busath DD, Zhou HX, Cross TA. Insight into the Mechanism of the Influenza a Proton Channel from a Structure in a Lipid Bilayer. Science. 2010; 330:509–512. [PubMed: 20966252]

(245). Musset B, Smith SME, Rajan S, Morgan D, Cherny VV, DeCoursey TE. Aspartate 112 Is the Selectivity Filter of the Human Voltage-Gated Proton Channel. Nature. 2011; 480:273–277. [PubMed: 22020278]

(246). Saparov SM, Antonenko YN, Koeppe PE, Pohl P. Desformylgramicidin: A Model Channel with an Extremely High Water Permeability. Biophys J. 2000; 79:2526–2534. [PubMed: 11053127]

(247). Cherny VV, Murphy R, Sokolov V, Levis RA, DeCoursey TE. Properties of Single Voltage-Gated Proton Channels in Human Eosinophils Estimated by Noise Analysis and by Direct Measurement. J Gen Physiol. 2003; 121:615–628. [PubMed: 12771195]

(248). Lee S-Y, Letts JA, MacKinnon R. Functional Reconstitution of Purified Human Hv1 H^+ Channels. J Mol Biol. 2009; 387:1055–1060. [PubMed: 19233200]

(249). Persson F, Halle B. How Amide Hydrogens Exchange in Native Proteins. Proc Natl Acad Sci U S A. 2015; 112:10383–10388. [PubMed: 26195754]

(250). Agmon N. Proton Pathways in Green Fluorescence Protein. Biophys J. 2005; 88:2452–2461. [PubMed: 15681647]

(251). Pinotsi D, Grisanti L, Mahou P, Gebauer R, Kaminski CF, Hassanali A, Kaminski Schierle GS. Proton Transfer and Structure-Specific Fluorescence in Hydrogen Bond-Rich Protein Structures. J Am Chem Soc. 2016; 138:3046–3057. [PubMed: 26824778]

(252). Wang L, Fried SD, Boxer SG, Markland TE. Quantum Delocalization of Protons in the Hydrogen-Bond Network of an Enzyme Active Site. Proc Natl Acad Sci U S A. 2014; 111:18454–18459. [PubMed: 25503367]

(253). Isom DG, Castaneda CA, Cannon BR, García-Moreno EB. Large Shifts in pKa Values of Lysine Residues Buried inside a Protein. Proc Natl Acad Sci U S A. 2011; 108:5260–5265. [PubMed: 21389271]

Europe PMC Funders Author Manuscripts

Europe PMC Funders Author Manuscripts

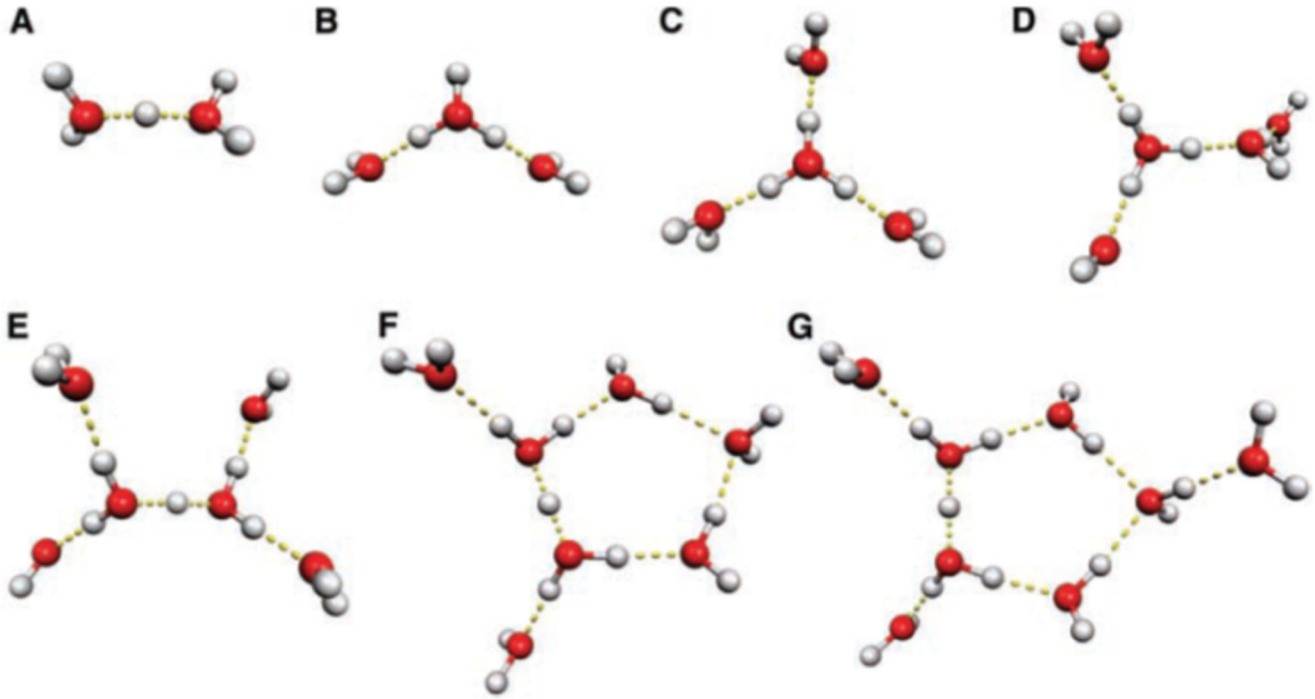

Figure 1.

Minimum-energy structures of small protonated water clusters, calculated at the MP2/aug-cc-pVDZ level of theory and possibly detected in the low-temperature IR spectra of ref 20. Structure A is the Zundel cation, C is the Eigen cation, D is an Eigen cation with one water molecule in its second solvation shell, and E is a Zundel cation with a complete first solvation shell. F and G are ring structures harboring a Zundel ion. Reprinted from ref 20 with permission. Copyright 2005 American Association for the Advancement of Science.

Europe PMC Funders Author Manuscripts

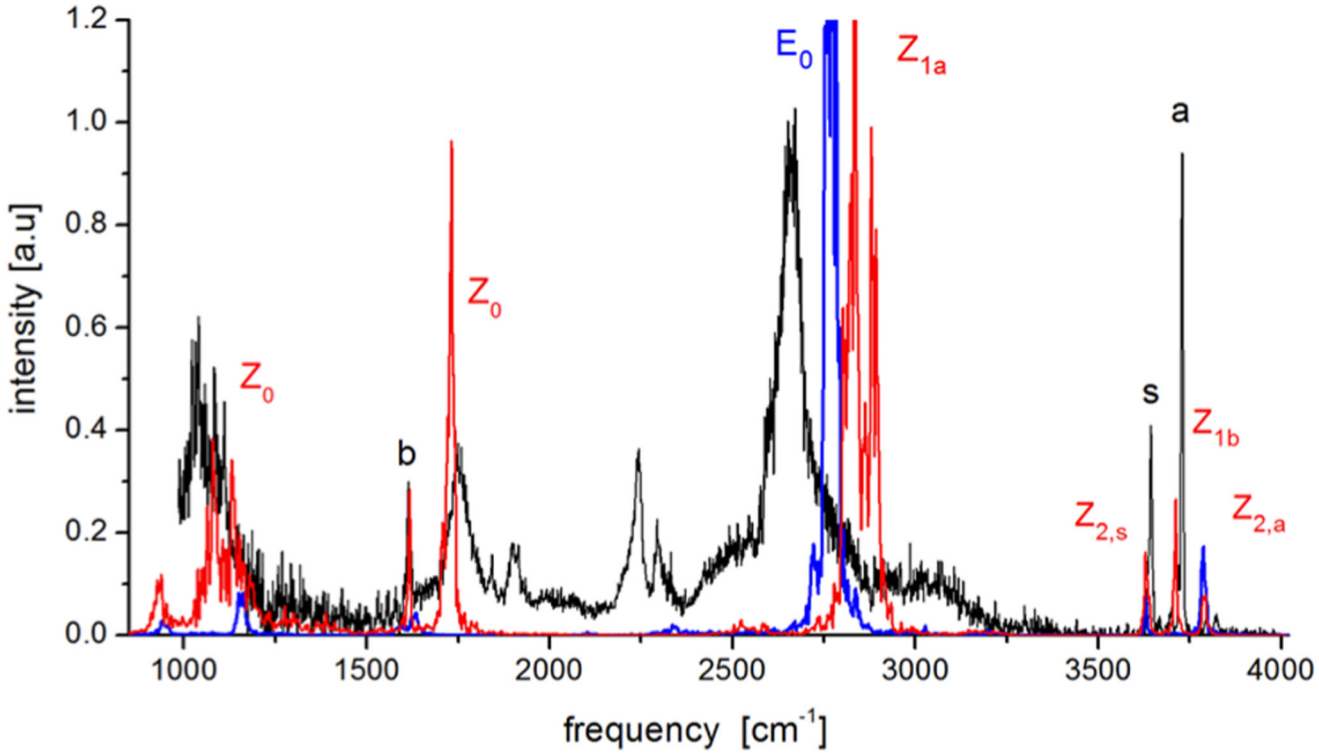

Figure 2.

Ar-predissociation IR spectrum of the $H^+(H_2O)_4$ cluster at 50 K (black line),[20] compared with simulated spectra (AIMD dipole autocorrelation) for the branched E isomer (blue) and a linear isomer with a Z core (red).[35] The labels a, s, and b (in black) on the experimental spectrum mark the antisymmetric and symmetric stretching and the bending band (respectively) of water molecules that do not donate any HB. The computed stretching bands of hydrogen-bonded OH moieties are denoted (in color) by E or Z (the isomer) with a numerical subscript (0, 1, or 2) for the solvation shell around the excess proton; see Figure 3 below for the detailed notation. $Z_{2,a}$ and $Z_{2,s}$ are the antisymmetric and symmetric stretching modes of the dangling hydrogens in the second shell, while Z_{1a} and Z_{1b} refer to the bonded and dangling OH in the first shell of the Z cation. Adapted from ref 35. Copyright 2014 American Chemical Society.

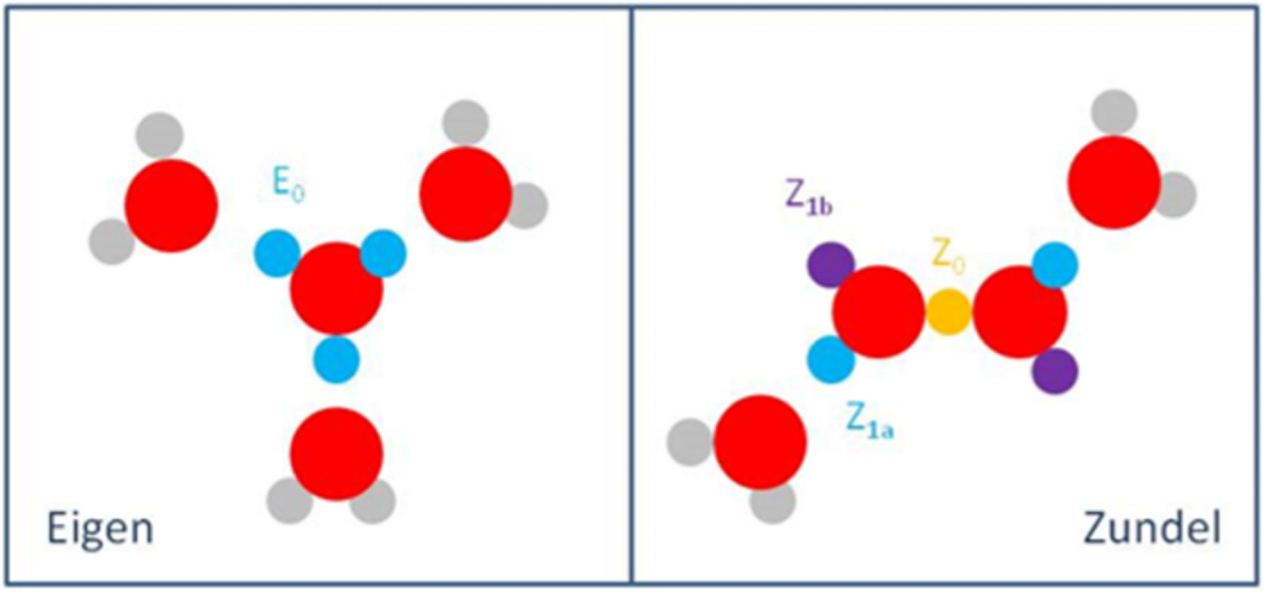

Figure 3.
Schematic depiction of the different proton classes of the E and linear Z cations of the protonated water tetramer whose IR spectra are shown in Figure 2

Europe PMC Funders Author Manuscripts

Europe PMC Funders Author Manuscripts

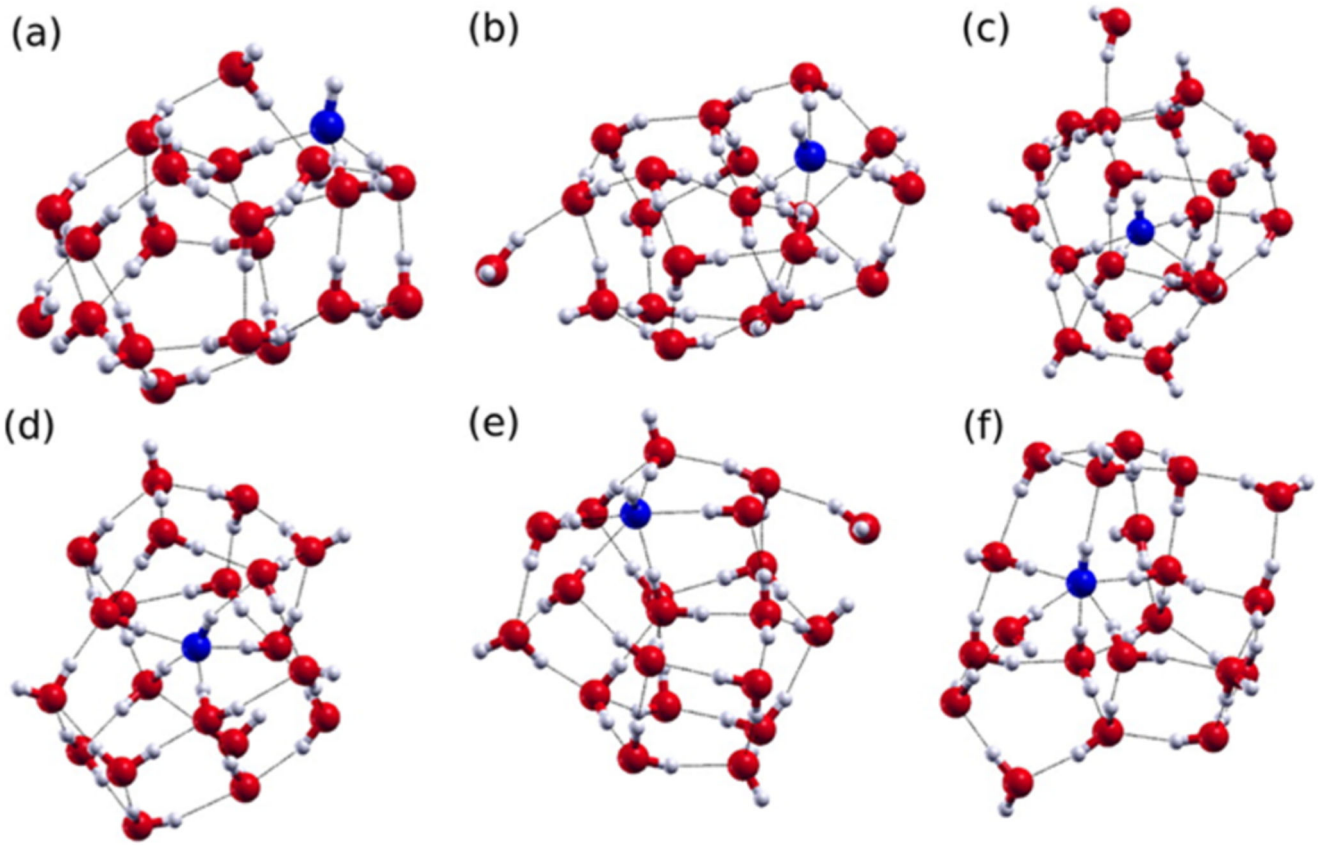

Figure 4.

Six motifs illustrating the amphiphilic character of the OH ion: (a) 3A0DS, (b) 4A0DS, (c) 4A0DB, (d) 4A1DB, (e) 5A0DS, and (f) 5A1DB. The number in front of A refers to the number of HBs that the hydroxide accepts, while the number in front of D refers to whether it donates a HB or not. Finally, the B and the S describe whether it is a buried or a surface state. Reproduced from ref 55 with permission. Copyright 2015 American Chemical Society

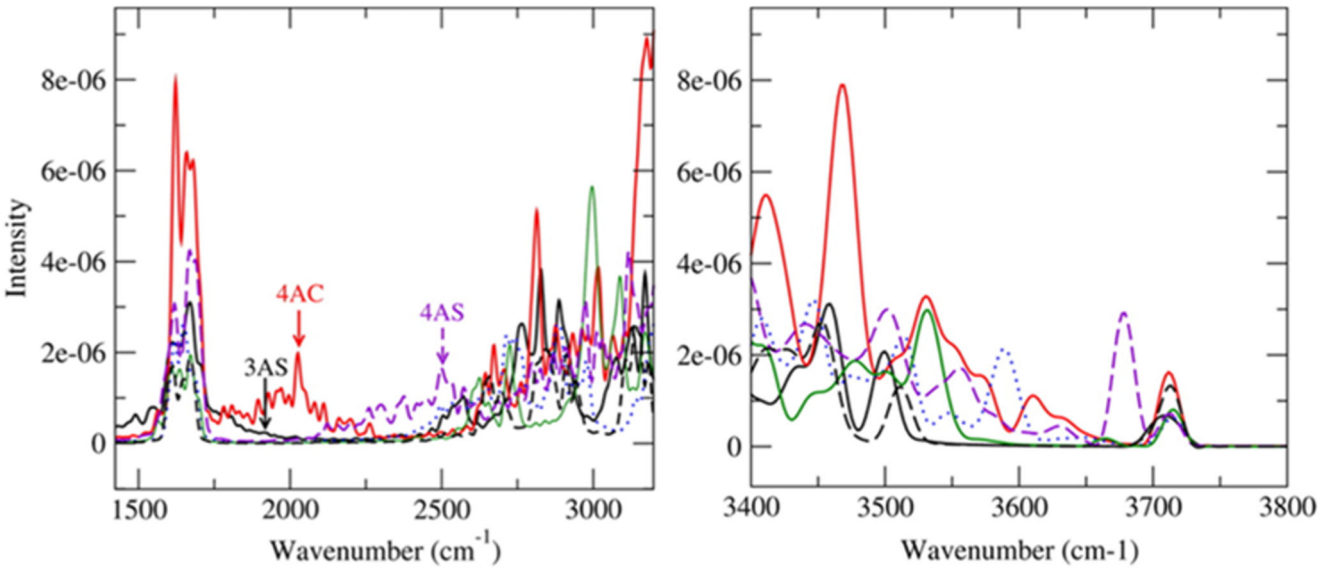

Figure 5.

Computed linear response theory IR spectra of hydroxide clusters shown earlier (a, left) between 1500 and 3200 cm^{-1} and (b, right) between 3400 and 3800 cm^{-1}. Color codes adopted here are the following: 3A0DS (black, labeled 3AS), 4A0DB (red, labeled 4AC), 4A0DS (dashed violet, labeled 4AS), 4A1DB (dotted blue), and finally 5A1DB (green). The spectra for the neutral water cluster are shown with black dashed lines. For clarity, the clusters contributing to the band between 1600 and 2500 cm^{-1} are explicitly labeled as 3AS (3A0DS), 4AC (4A0DB), and 4AS (4A0DS). Reproduced from ref 55 with permission. Copyright 2015 American Chemical Society

Europe PMC Funders Author Manuscripts

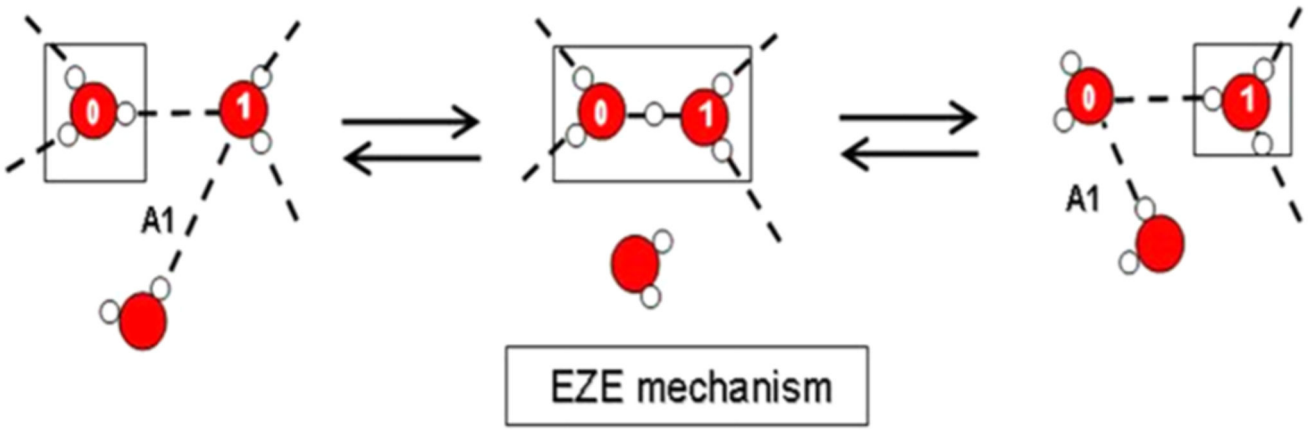

Figure 6.

Schematic depiction of the E–Z–E mechanism. Left: Oxygen 0 is the hydronium, and oxygen 1 is in its first solvation shell, accepting a HB (A1) from the second solvation shell. Center: The Zundel intermediate. Right: A new hydronium centered on oxygen 1. Reproduced from ref 68 by permission. Copyright 2008 American Chemical Society

Europe PMC Funders Author Manuscripts

Europe PMC Funders Author Manuscripts

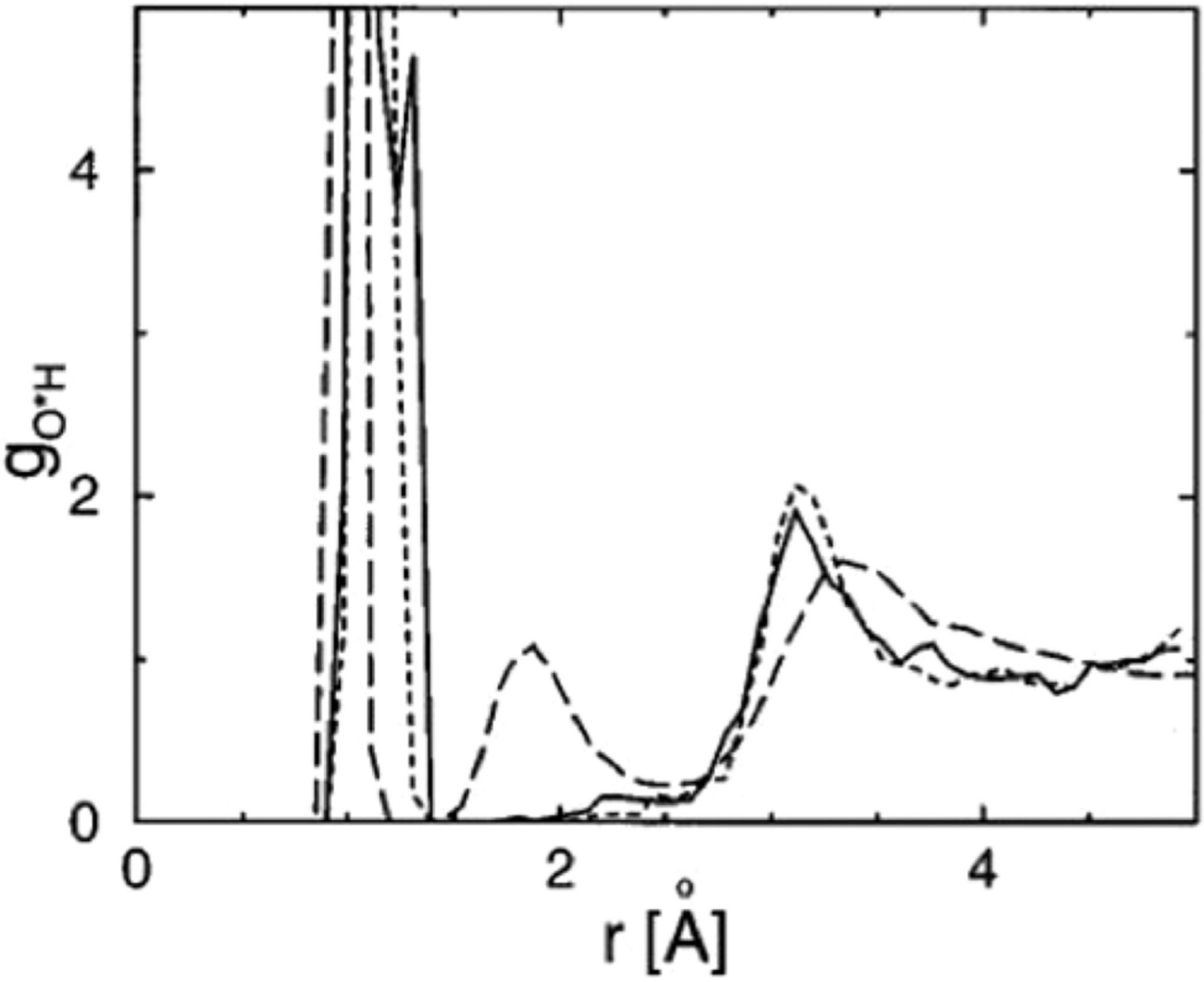

Figure 7.

O*−H radial distribution functions of the $H_9O_4^+$ (dotted line) and $H_5O_2^+$ (solid line) structures of H^+ in liquid water. The O* atoms correspond to the oxygen atoms hosting the proton. The dashed line gives the O–H radial distribution functions for pure water. Reproduced from ref 69 with permission. Copyright 1995 American Institute of Physics

Europe PMC Funders Author Manuscripts

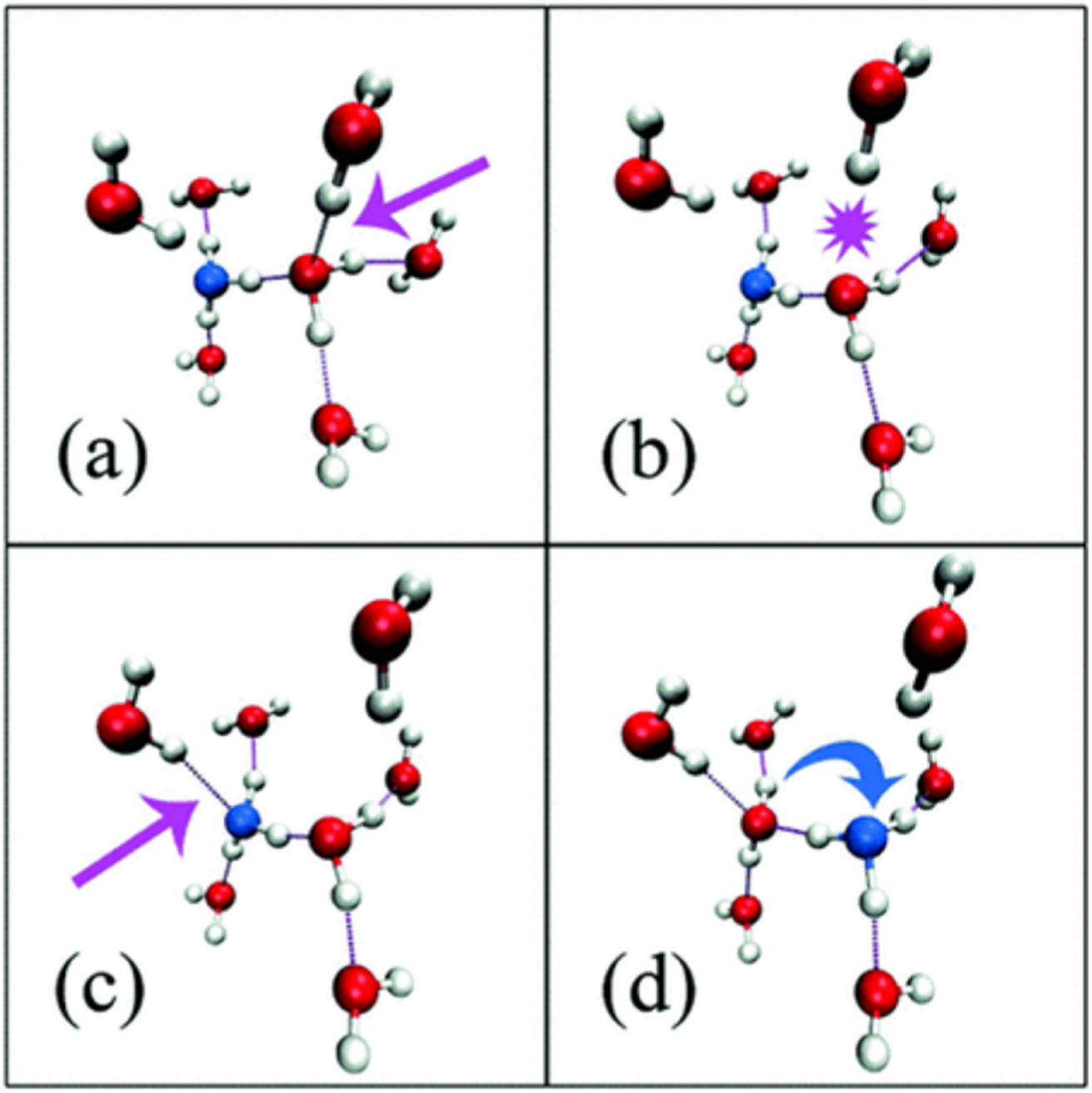

Figure 8.

Snapshots of an example proton-transfer event from the CPMD simulations. O* is blue, other oxygen atoms are red, hydrogen atoms are white, and HBs are purple. Panels a-d show how the PT step involves an almost simultaneous decrease and increase of the coordination number of the proton accepting and proton donating water molecules, respectively. Reproduced from ref 70 with permission. Copyright 2009 American Physical Society

Europe PMC Funders Author Manuscripts

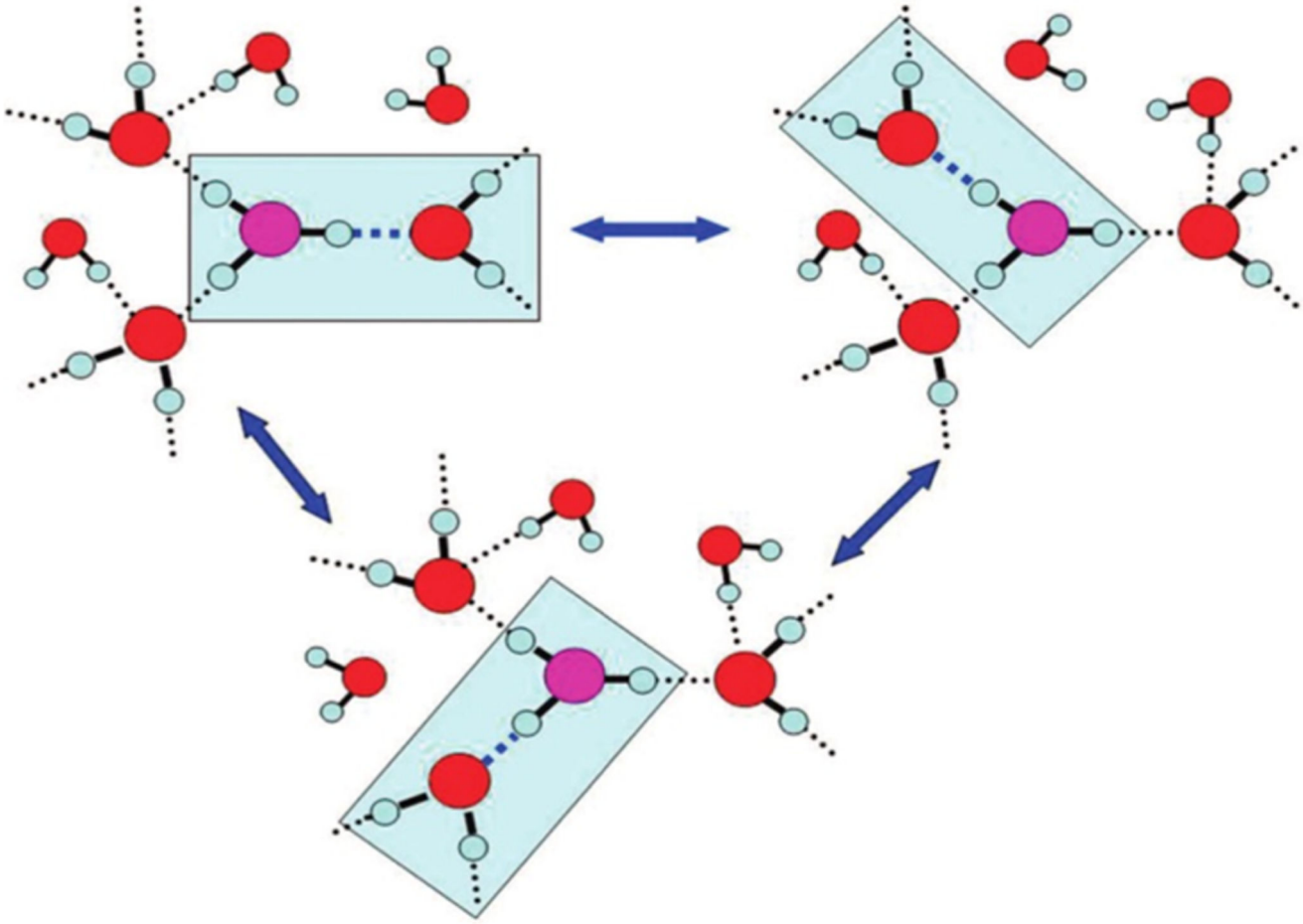

Figure 9.
Schematics of the special pair dance around a central hydronium ion (magenta-colored oxygen atom). The special partner, depicted as a triply coordinated water ligand, is interchanged following HB cleavage and formation events. Reproduced from ref 68 with permission. Copyright 2008 American Chemical Society

Europe PMC Funders Author Manuscripts

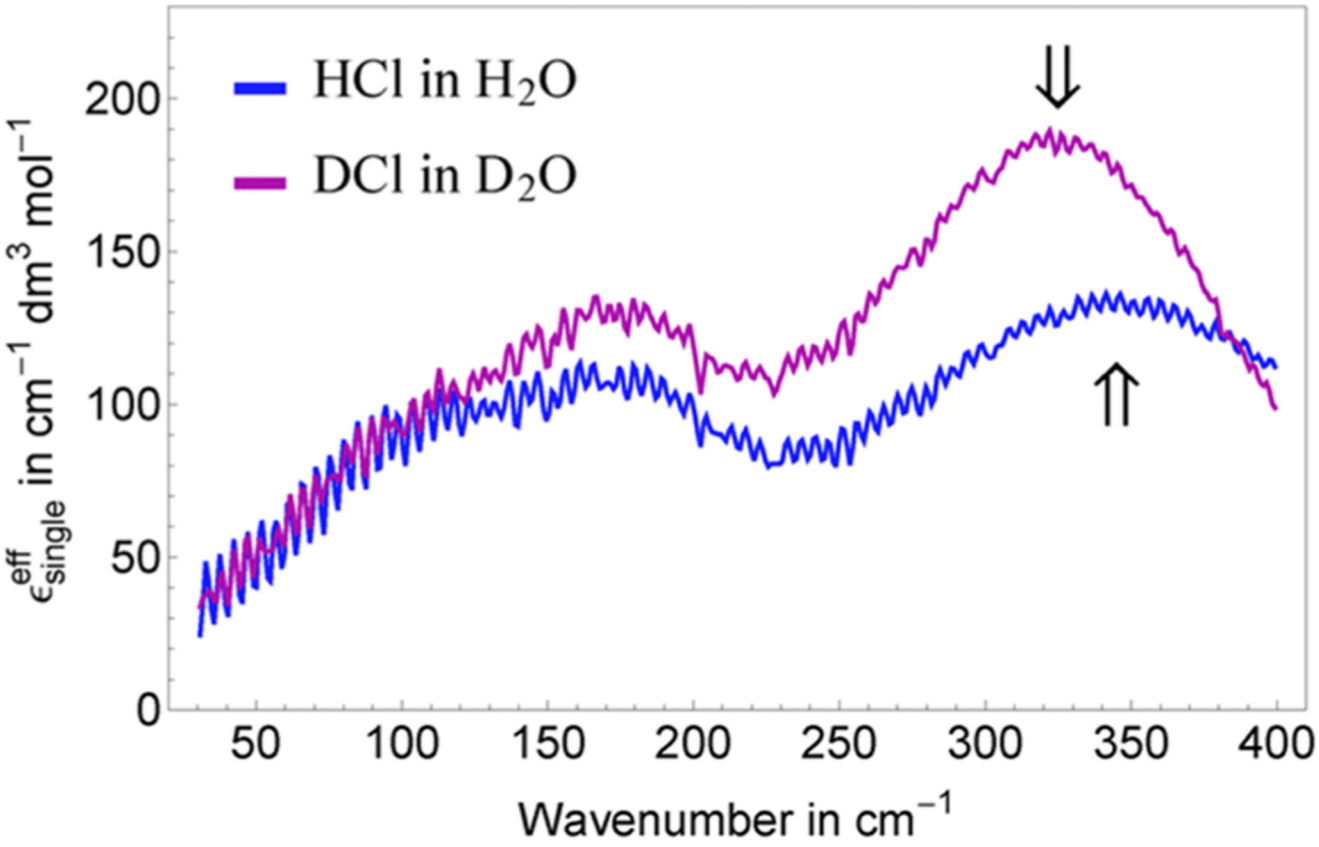

Figure 10.

Comparison of the effective ionic extinctions of HCl in H_2O and DCl in D_2O showing a slight red shift of the high-frequency resonance (from 340 to 320 cm^{-1}, arrows) that is ascribed to the SPD. Reproduced from ref 74 with permission. Copyright 2015 Royal Society of Chemistry

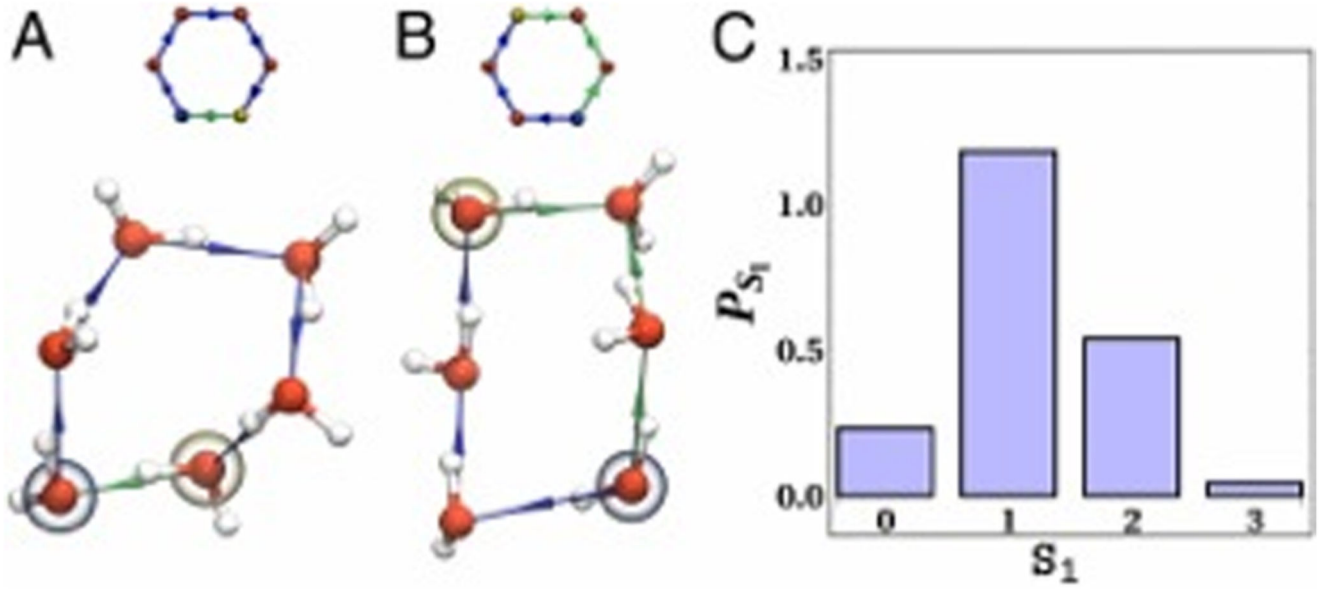

Figure 11.

Panels A and B show two directed six-membered rings obtained in liquid water. The ring in A is composed exclusively of water molecules that accept and donate a HB (DA waters), while that in B contains one water that donates two HBs (DD) and another that accepts two HBs (AA). The directional correlations within rings change, depending on the size and number of DD-AA pairs within the ring and create the architecture for water wires. The number of DD-AA pairs in the rings is quantified with the order parameter S_1. Panel C shows the distribution of the S_1 showing that most rings have one DD-AA pair. Reproduced from ref 61 with permission. Copyright 2013 National Academy of Sciences

Europe PMC Funders Author Manuscripts

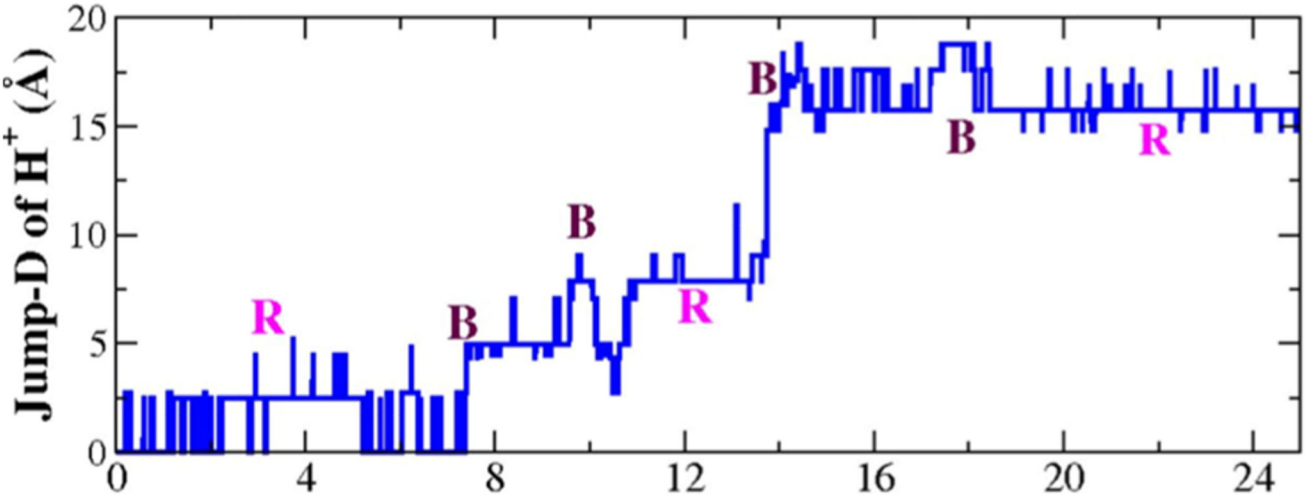

Figure 12.

Burst and rest behavior of the proton is shown for one trajectory. The *y* axis depicts the distance that the proton jumps with respect to a reference starting point at the beginning of the trajectory. The motion of the proton goes through periods of bursts (B), where it can jump rather long distances due to correlated proton hopping, followed by resting periods (R). Reproduced from ref 61 with permission. Copyright 2013 National Academy of Sciences

Europe PMC Funders Author Manuscripts

Europe PMC Funders Author Manuscripts

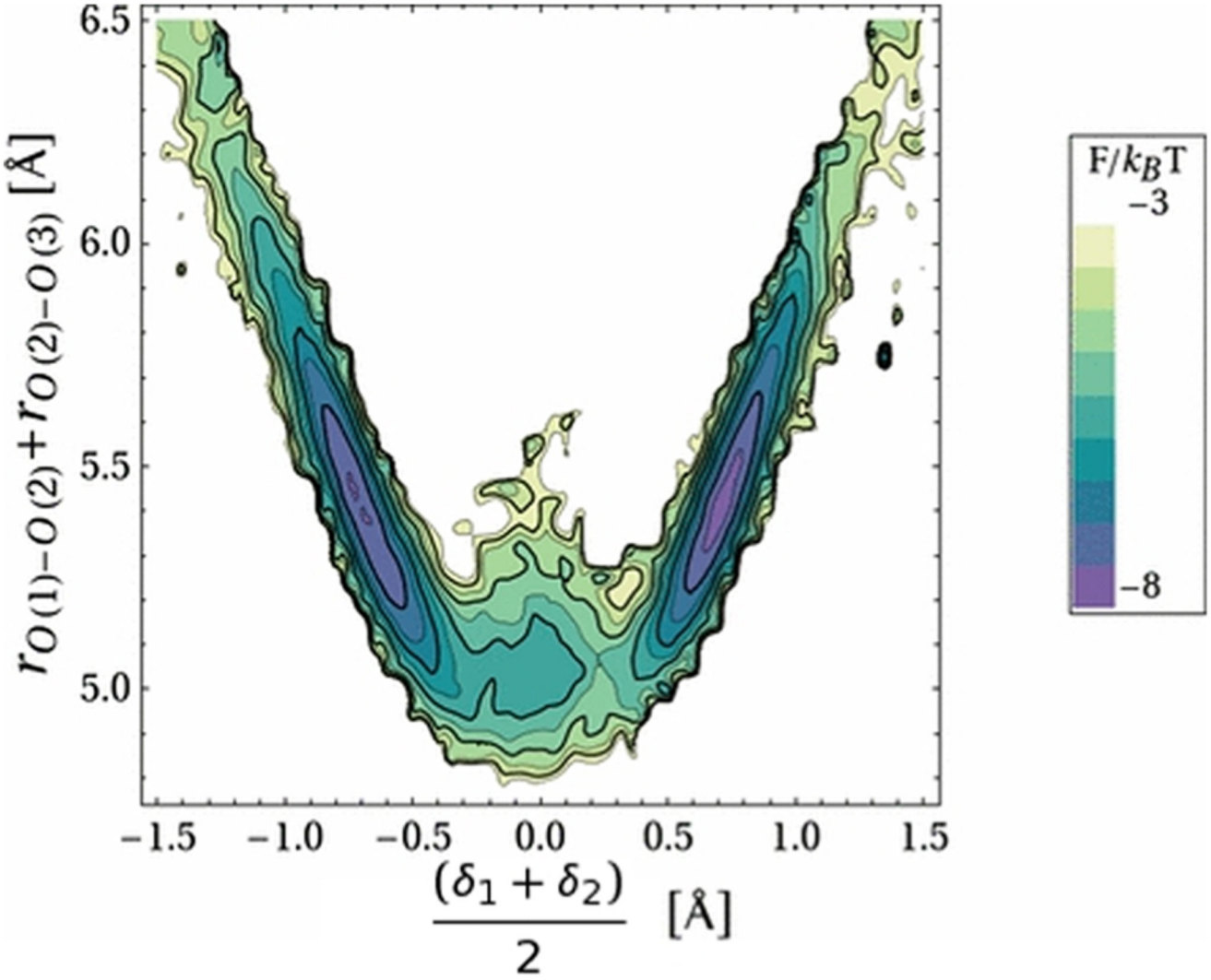

Figure 13.

Coupling between the average of two consecutive PT coordinates on the *x*-axis and the sum of the two HBs (the O–O distances) along which the PT events occur.[61] The double PT is coupled to the compression of the proton wire. Reproduced from ref 61 with permission. Copyright 2013 National Academy of Sciences

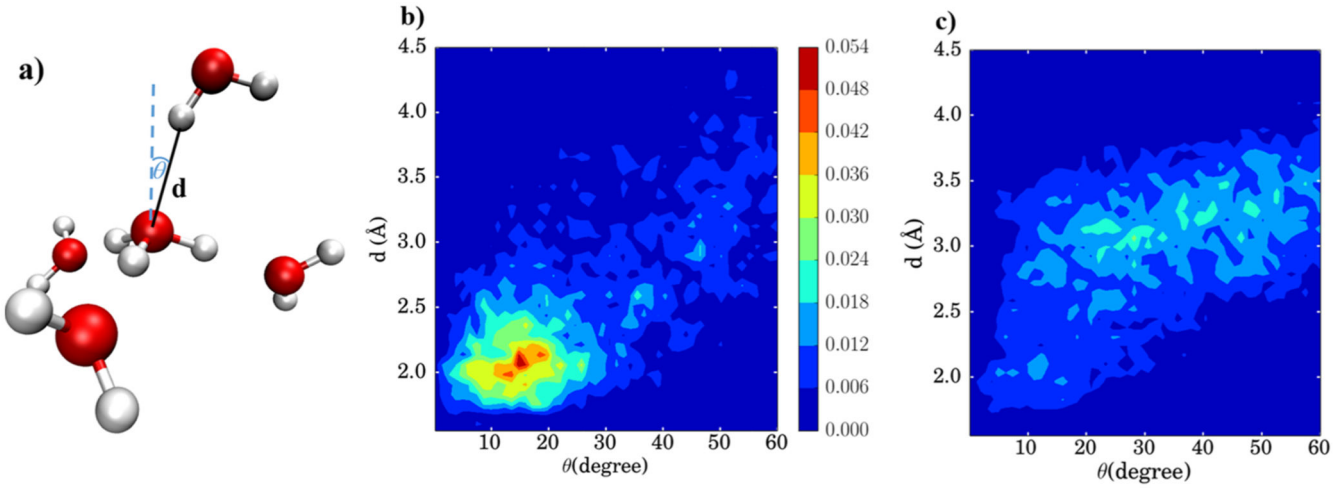

Figure 14.

Fourth water molecule (4WM) influence on PT burst dynamics. Panel a defines the distance, *d*, and angle, *θ*, between the 4WM hydrogen atom, the hydronium oxygen atom, and the normal to the plane of the H_3O^+ hydrogen atoms. Panel b shows the probability distribution in the (*d*,*θ*) plane during burst periods, while panel c shows it during rest periods. Reproduced from ref 79 with permission. Copyright 2015 Institute of Physics

Europe PMC Funders Author Manuscripts

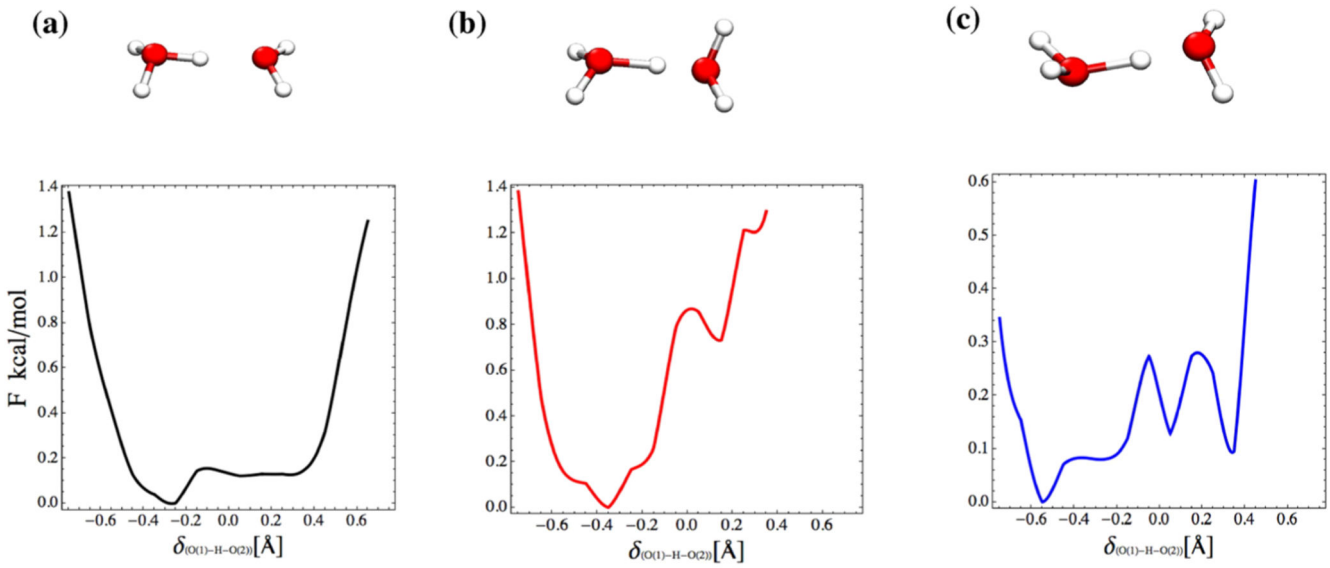

Figure 15.

Potential of mean force along the PT coordinate for three conformations of the inversion position of two water molecules between which the protons move. The snapshots on top of the free energy profiles are representative of the typical configurations used to generate these profiles. In all cases, we see that there is a tendency for the proton to be most localized on the left water, although the barriers associated with PT are on the order of $k_B T$. In panel a the lone-pairs of both oxygen atoms face upward, while in panel b left is up-inverted and right is down-inverted. This leads to quite a drastic change in the activation barrier for PT. On the other hand, in panel c the left water is down-inverted while the right is up-inverted. This introduces some additional roughness in the profile that is absent in both panels a and b. Reprinted from ref 80 with permission. Copyright 2014 Elsevier

Europe PMC Funders Author Manuscripts

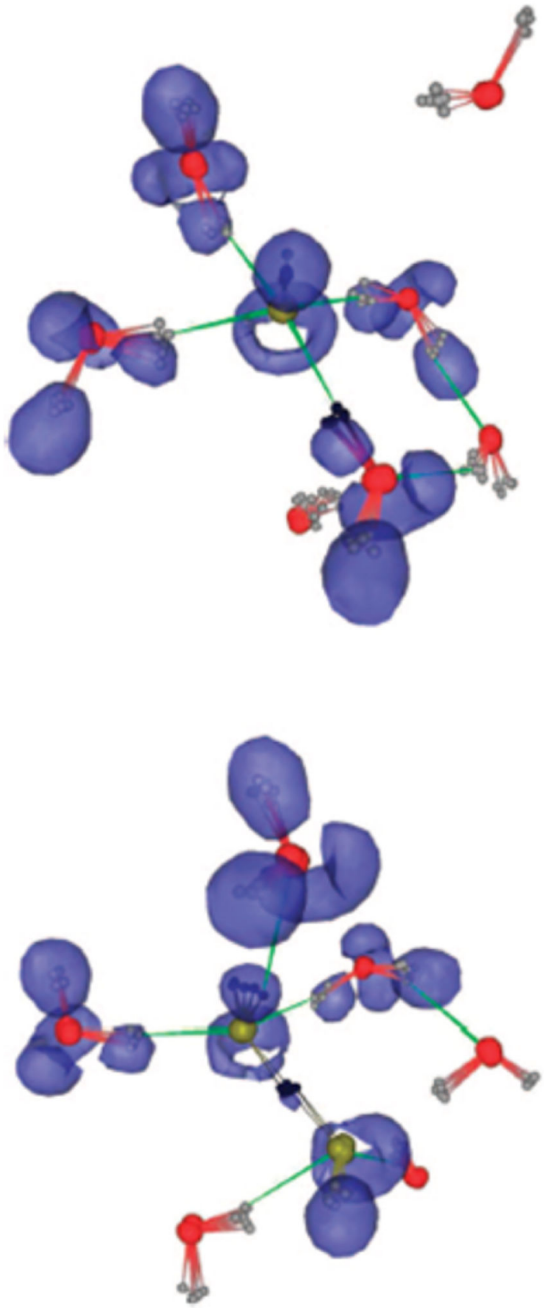

Figure 16.

Representative resting and active states of OH^- in bulk water, $OH^-(aq)$, within the dynamical hypercoordination mechanism (ref 4). The resting state (top) is the majority complex, with four HBs accepted by O* in an essentially square-planar arrangement. The active state (bottom) is a short-lived transient complex with three HBs accepted by O* and an additional HB donated by H' in a locally tetrahedral arrangement. O*, in yellow, is the oxygen atom identified as the OH^- ion and H' is the hydrogen atom attached to it. Electron density is depicted by the purple blobs. Note the ring of negative charge around O*,[48]

resembling the crescent of negative charge connecting the two lone pairs of a water molecule.[49] Reproduced from ref 48 with permission. Copyright 2002 Nature Publishing Group

Europe PMC Funders Author Manuscripts

Europe PMC Funders Author Manuscripts

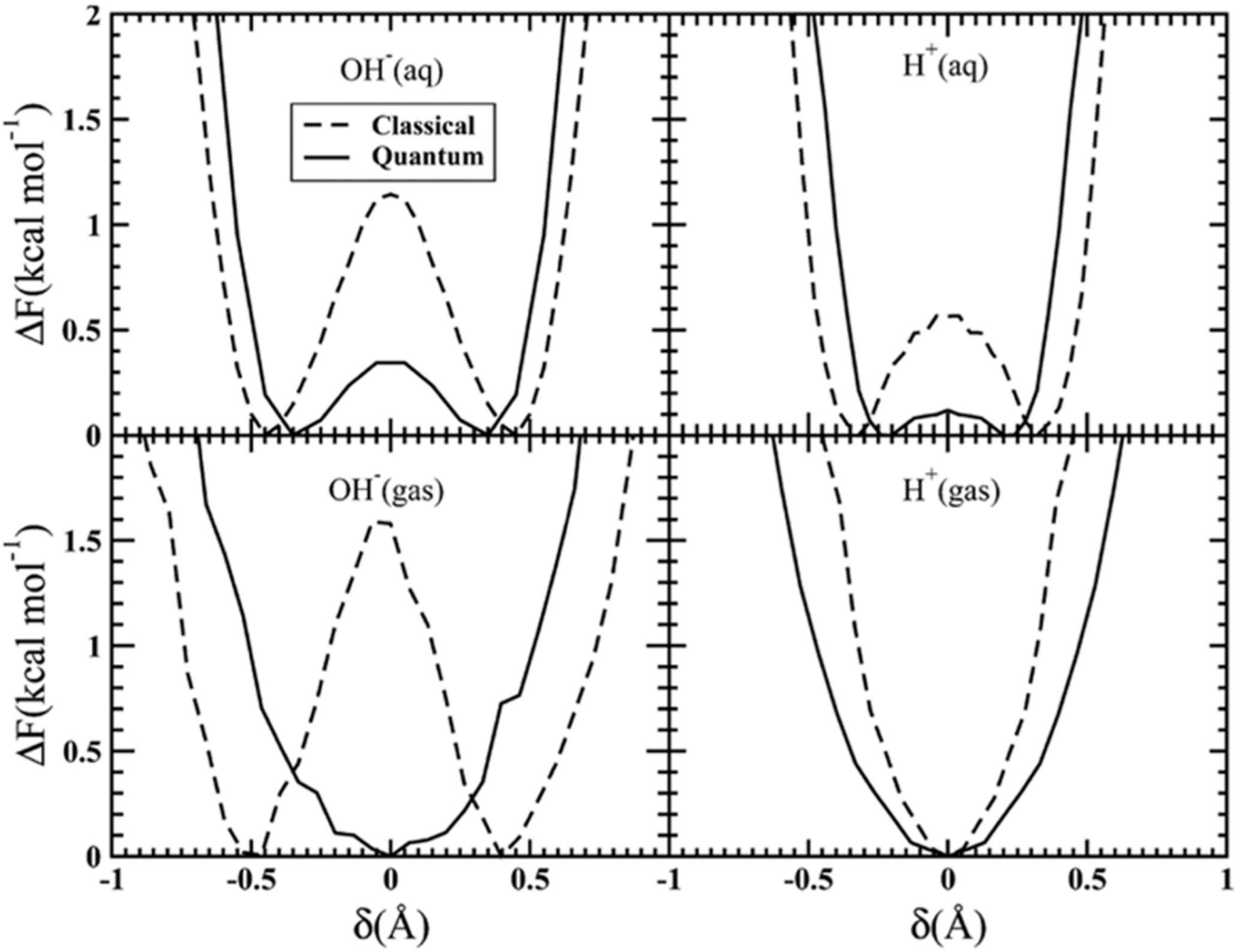

Figure 17.

Canonical (Helmholtz) free energy profile at 300 K along the proton transfer coordinate δ of the OH^- and H^+ systems (left and right panels, respectively) in bulk water (top) and the gas phase (bottom). Dashed lines depict the classical canonical ensemble, while solid lines are from the quantum simulations. Note that the thermal energy is $k_BT \approx 0.59$ kcal/mol at 300 K Reproduced from ref 4 with permission. Copyright 2010 American Chemical Society

Europe PMC Funders Author Manuscripts

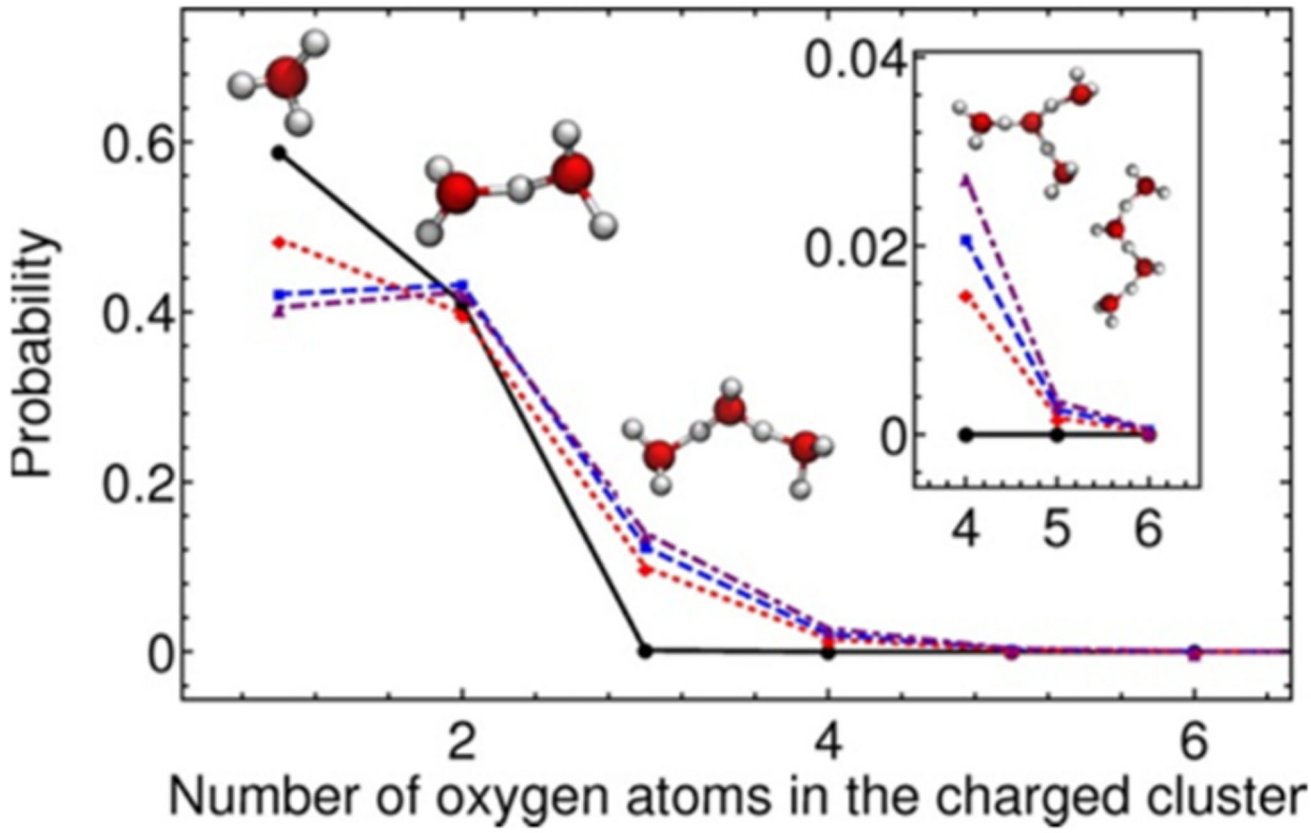

Figure 18.

Histogram of the number of constituents for the cluster containing the excess proton for three quantum simulations (red, blue, and purple dashed lines) and one classical simulation (black line). Here, a cluster corresponds to a motif built using a criterion based on the PT coordinate that connects species with high coordination numbers (see ref 45 for details) and that identifies the excess proton as localized on a cluster of n water molecules. Quantum fluctuations of the proton lead to situations where it is delocalized over more than two water molecules, most notably $n = 3$ and 4. Reproduced from ref 45 with permission. Copyright 2014 American Chemical Society

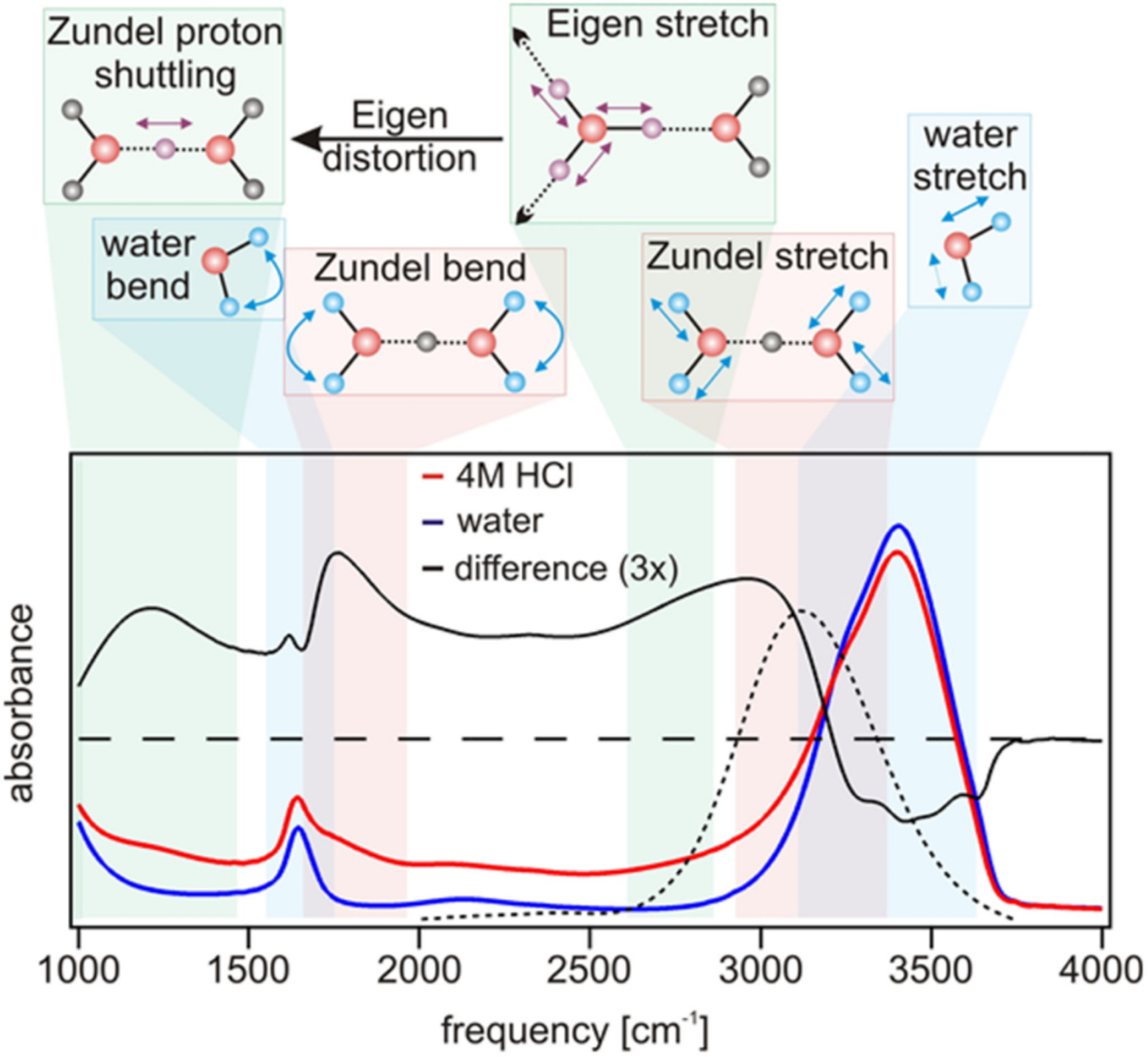

Figure 19.

FFT-IR spectra of water (blue line) and 4 M HCl (red line) with assignments of the different spectral regions to different structures of the solvated proton (cartoons). The vibrational modes shaded in green involve the excess proton (purple color), whereas the vibrations in bulk/flanking water molecules are shaded in red. Details of the assignments are discussed in the text. Reproduced from ref 99 with permission. Copyright 2015 American Association for the Advancement of Science

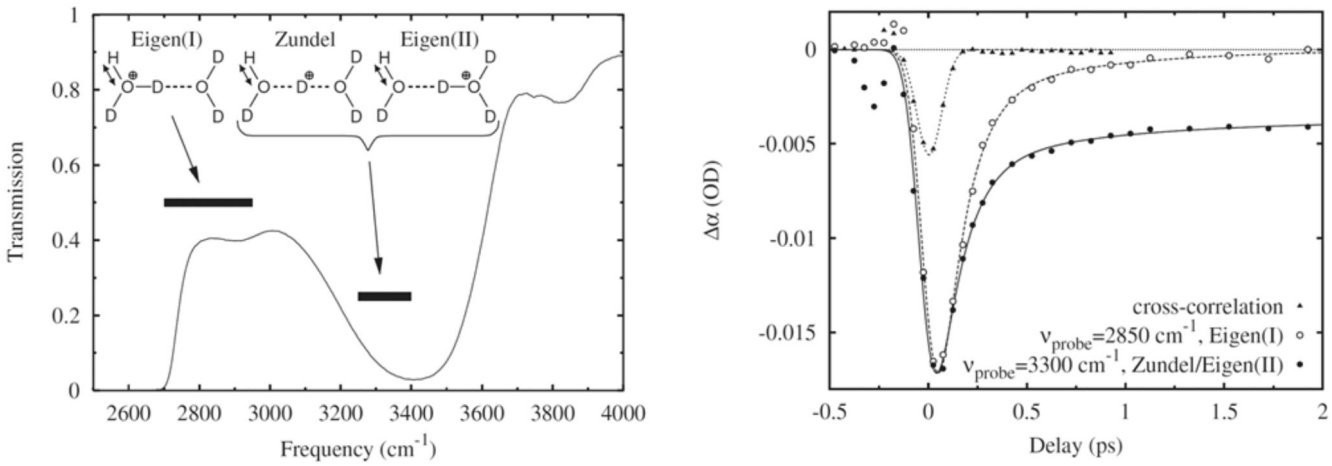

Figure 20.

Left panel: Infrared spectrum of a 5 M solution of HCl:DCl in HDO:D_2O, with a H:D ratio of 1:20. The bars indicate the frequency regions of the O–H-stretching modes of the E (I) and Z/E (II) structures. Right panel: Absorption change as a function of delay after resonant excitation (at 2935 cm^{-1}) of the proton O–H stretch vibrations of the E structure. The absorption change is shown for two probing frequencies, one resonant with the E (I) structure and one resonant with the Z and E (II) structures. The time constants are 120 fs and 0.7 ps for the dotted curve and 130 fs and 0.8 ps for the solid curve. From ref 100 with permission. Copyright 2006 American Physical Society

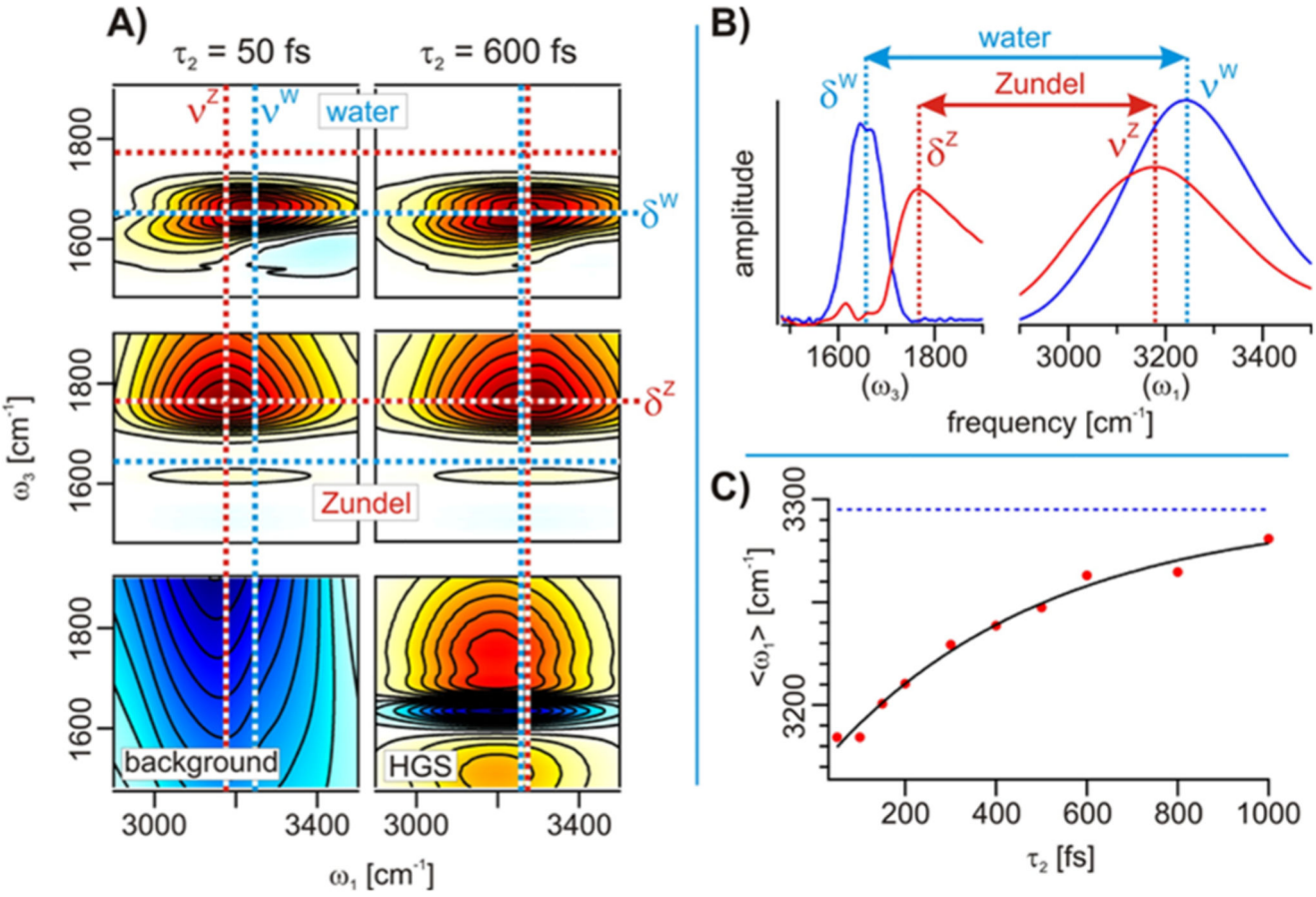

Figure 21.

Shape and time evolution of the stretch–bend cross-peaks following decomposition (Reproduced from ref 99. Copyright 2015 American Association for the Advancement of Science). (A) Presentation of the three dominant components for 2DIR spectra of 4 M HCl for waiting times (time elapsed after excitation) of τ_2 = 50 and 600 fs. Grid lines illustrate the Zundel (red) and water (blue) peak frequencies. (B) Projections of the stretch–bend cross peaks onto one frequency axis: ω_1 for stretch (υ) and ω_3 for bend (δ). These bleach signals are inverted to present a positive spectrum. (C) Evolution of the peak frequency of the Zundel stretch–bend cross peak in ω_1 with waiting time. The blue dotted line indicates the asymptotic value

Europe PMC Funders Author Manuscripts

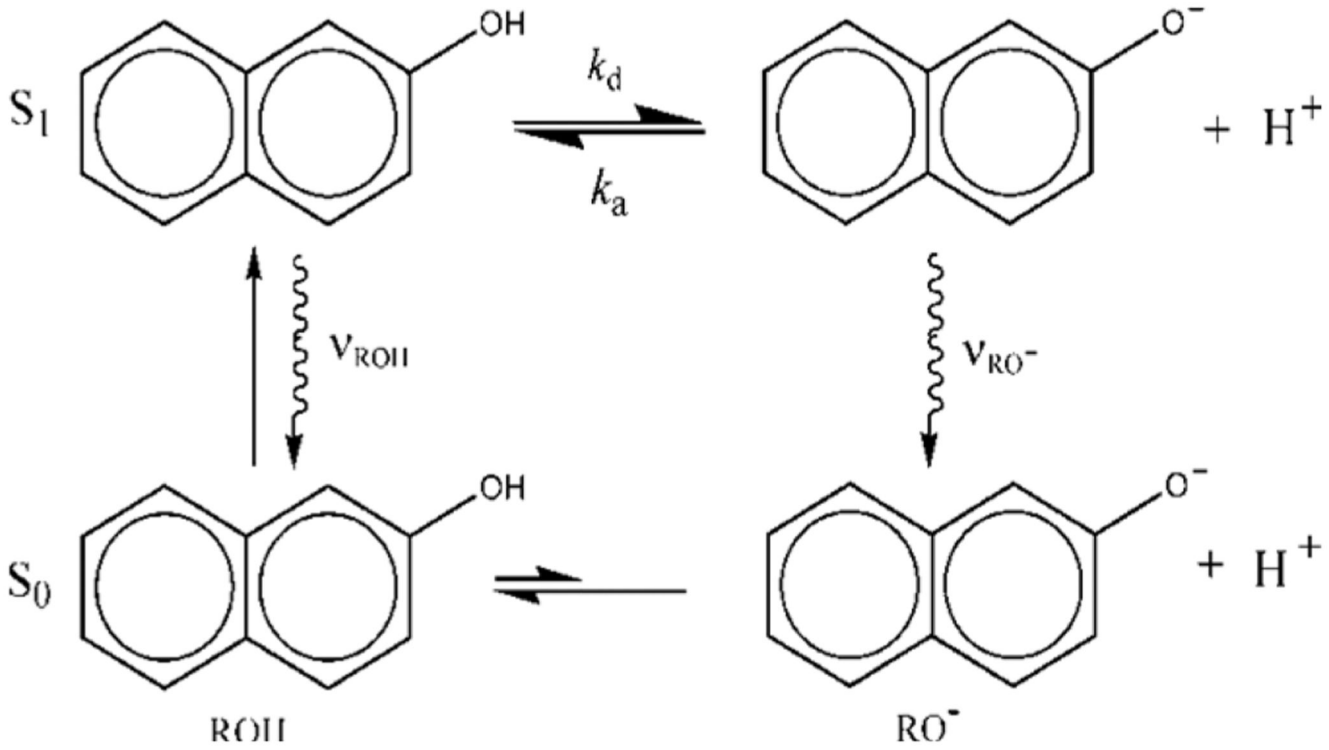

Figure 22.

Forster cycle of 2-naphthol.[104] The photoacid in its ground state (bottom left) is photoexcited (usually to S_2 and then relaxing very fast to S_1), ejects a proton to water (reversibly) to produce the conjugated photobase (upper right), and then decays radiatively (wiggly arrow), and also nonradiatively (not indicated), to form the ground-state RO^- base. The latter picks up a proton from solution and reprotonates (irreversibly) to regenerate the ground-state photoacid. Reproduced from ref 106 with permission. Copyright 2005 American Chemical Society

Europe PMC Funders Author Manuscripts

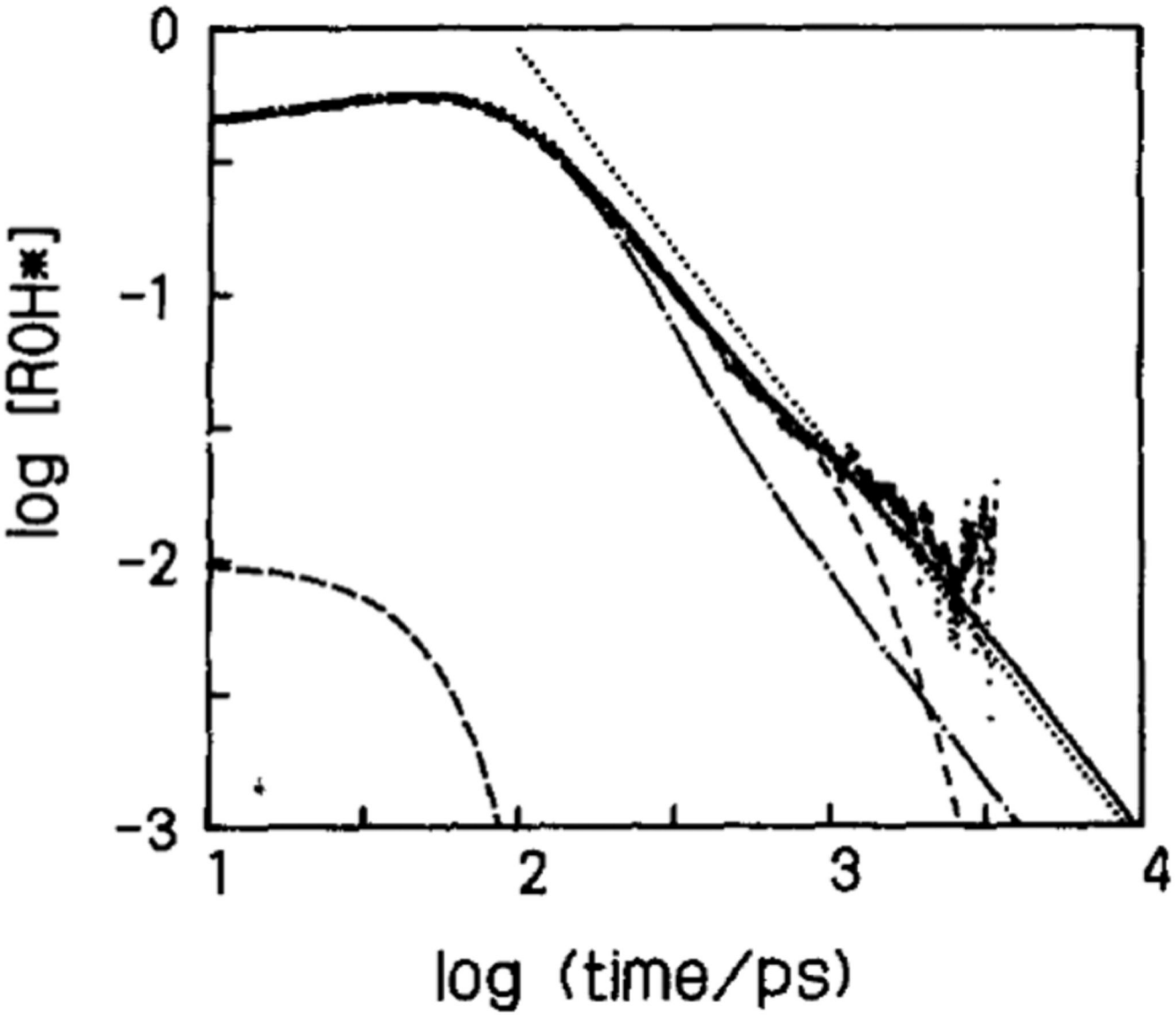

Figure 23.

First reported power-law kinetics in ESPT to water,[110111] from 8-hydroxypyrene-1,3,6-trisulfonate (HPTS) that was irradiated with a picosecond laser. The time-resolved fluorescence signal from the undissociated photoacid, detected by a streak-camera apparatus and corrected for its radiative lifetime, is depicted by dots. Irreversible proton dissociation would give rise to a single exponential decay, which is not the observed behavior. The reversibility of the reaction leads, in conventional chemical kinetics, to biexponential decay (upper dashed line) that does not fit the data at long times. The solution of the time-dependent Smoluchowski equation with reversible boundary conditions (convoluted with the instrument response function, lower dashed line) is depicted by the full line that goes through the data points. Its (analytically derived) asymptotic power-law behavior is the straight dotted line. Reproduced from ref 110 with permission. Copyright 1988 American Institute of Physics

Europe PMC Funders Author Manuscripts

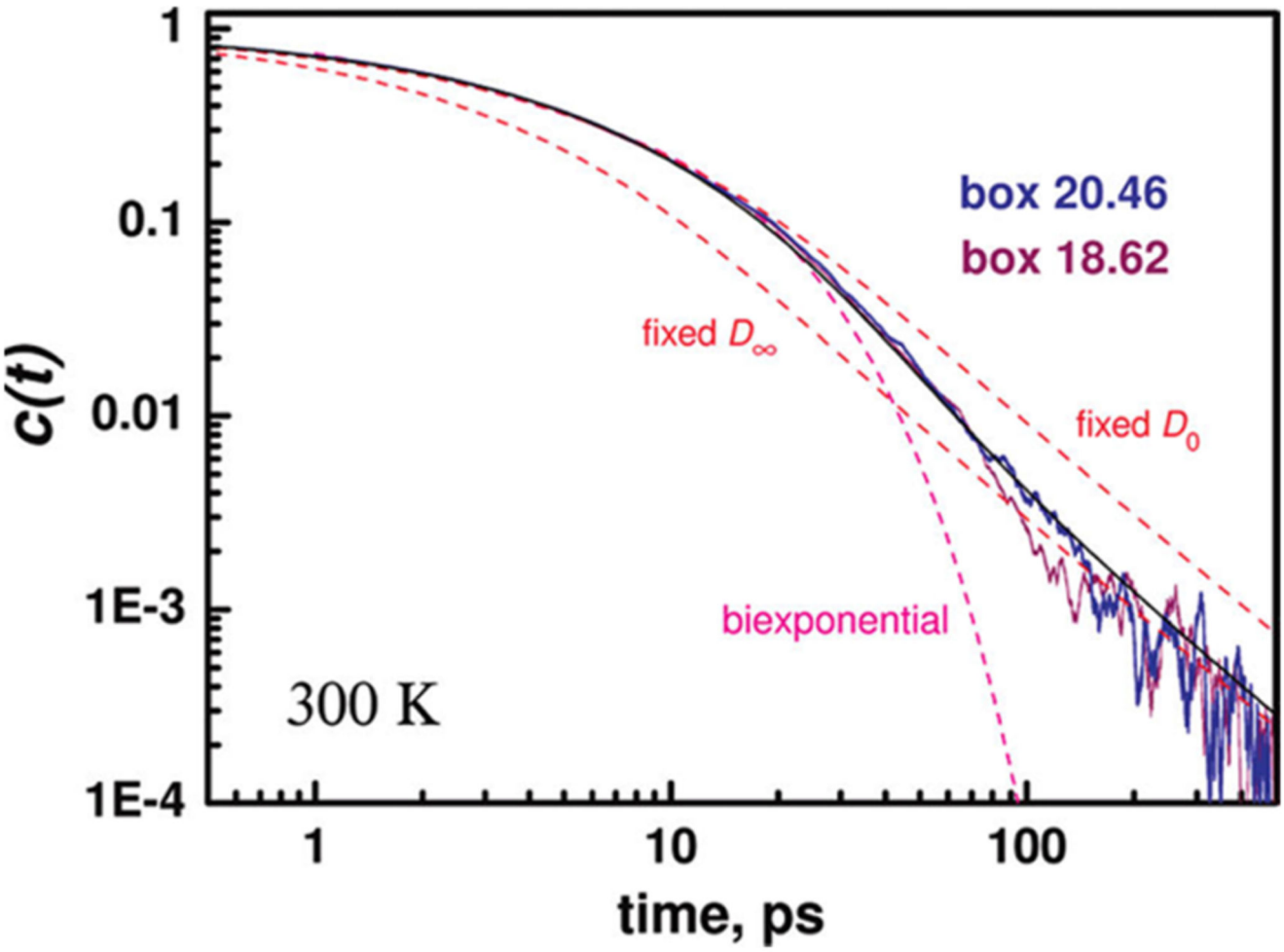

Figure 24.

Simulated (MS-EVB3) time evolution of the probability of the excess proton to reside on the oxygen atom (O*) to which it was initially bound (full lines), depicted on a log-log scale. A biexponential (dashed magenta line) clearly does not fit the data. A model with a fixed (small, D_0, or large, D_∞) diffusion constant also misses the data (dashed red lines). A model in which the diffusion constant increases (from D_0 to D_∞) as a function of r is in quantitative agreement with these simulations. Reproduced from ref 118 with permission. Copyright 2010 American Chemical Society

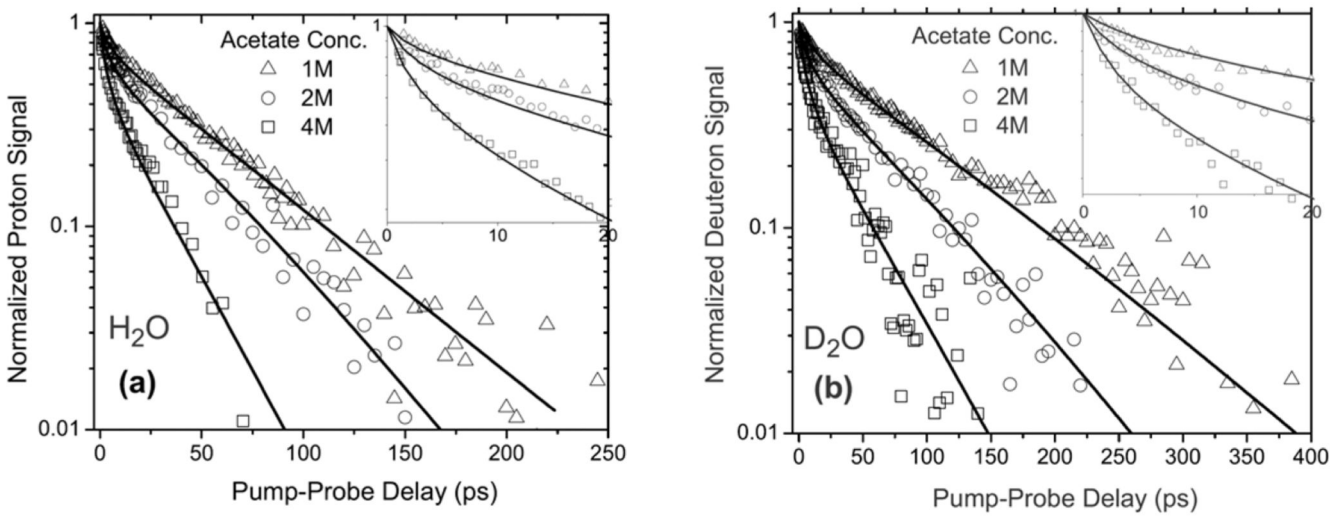

Figure 25.

Response of the proton/deuteron vibrations as a function of the pump-probe delay for solutions of 10 mM HPTS and 1, 2, and 4 M acetate in (a) H_2O and (b) D_2O. In the insets, the response measured in the first 20 ps is shown, illustrating the highly nonexponential character of the PT reaction. The solid lines are calculated using a conduction model in which the rate of transfer decreases by a constant factor for every additional water molecule in the short-living hydrogen-bonded water wire connecting the acid and the base. Reproduced from ref 123 with permission. Copyright 2008 American Chemical Society

Europe PMC Funders Author Manuscripts

Europe PMC Funders Author Manuscripts

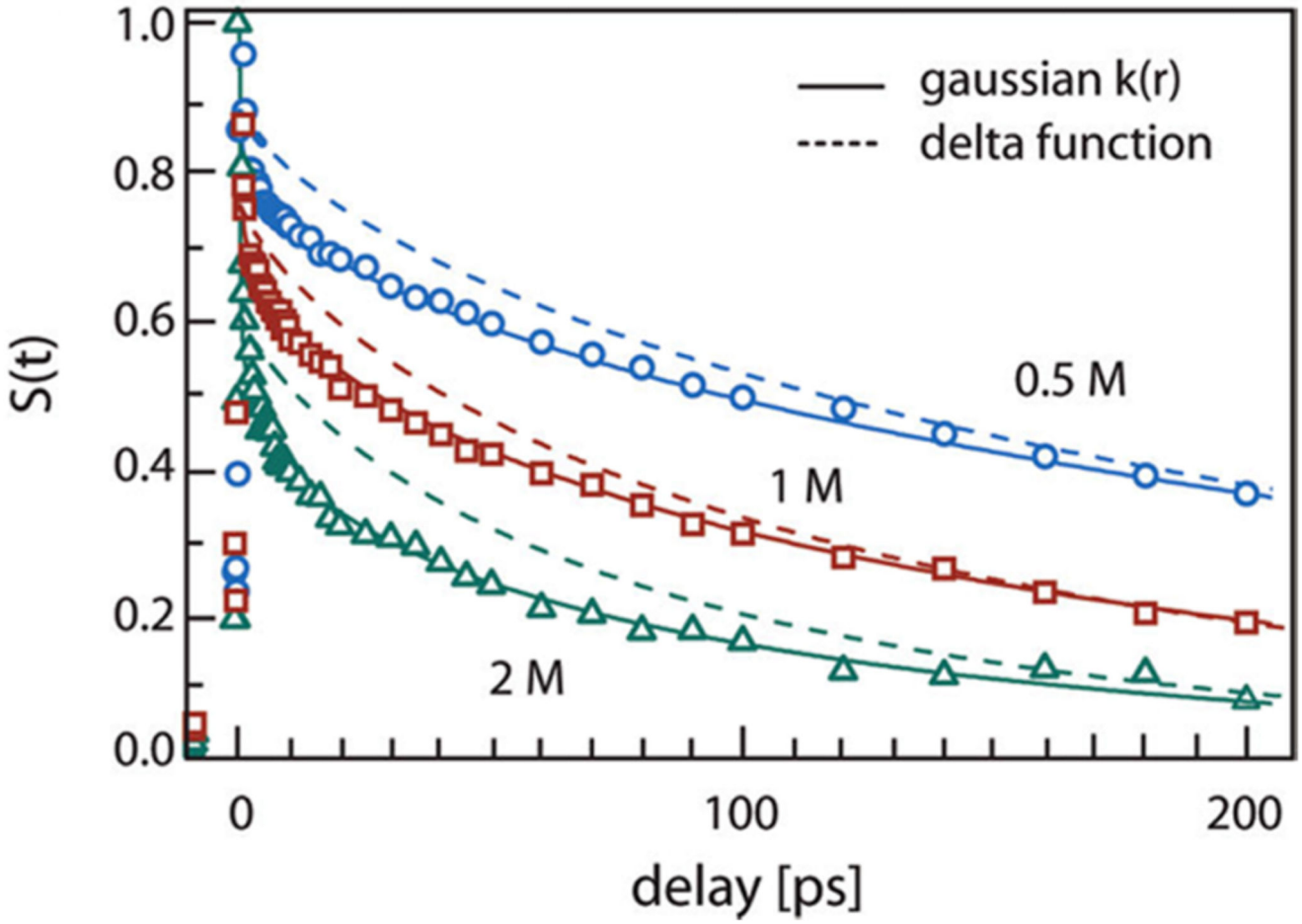

Figure 26.

Time-resolved infrared signal from excited HPTS in D_2O at 5 °C, at different acetate concentrations (symbols). Full lines are fits to the extended Smoluchowski model in which $k(r)$ has a Gaussian-like distance dependence. Reproduced from ref 124 with permission. Copyright 2009 American Chemical Society

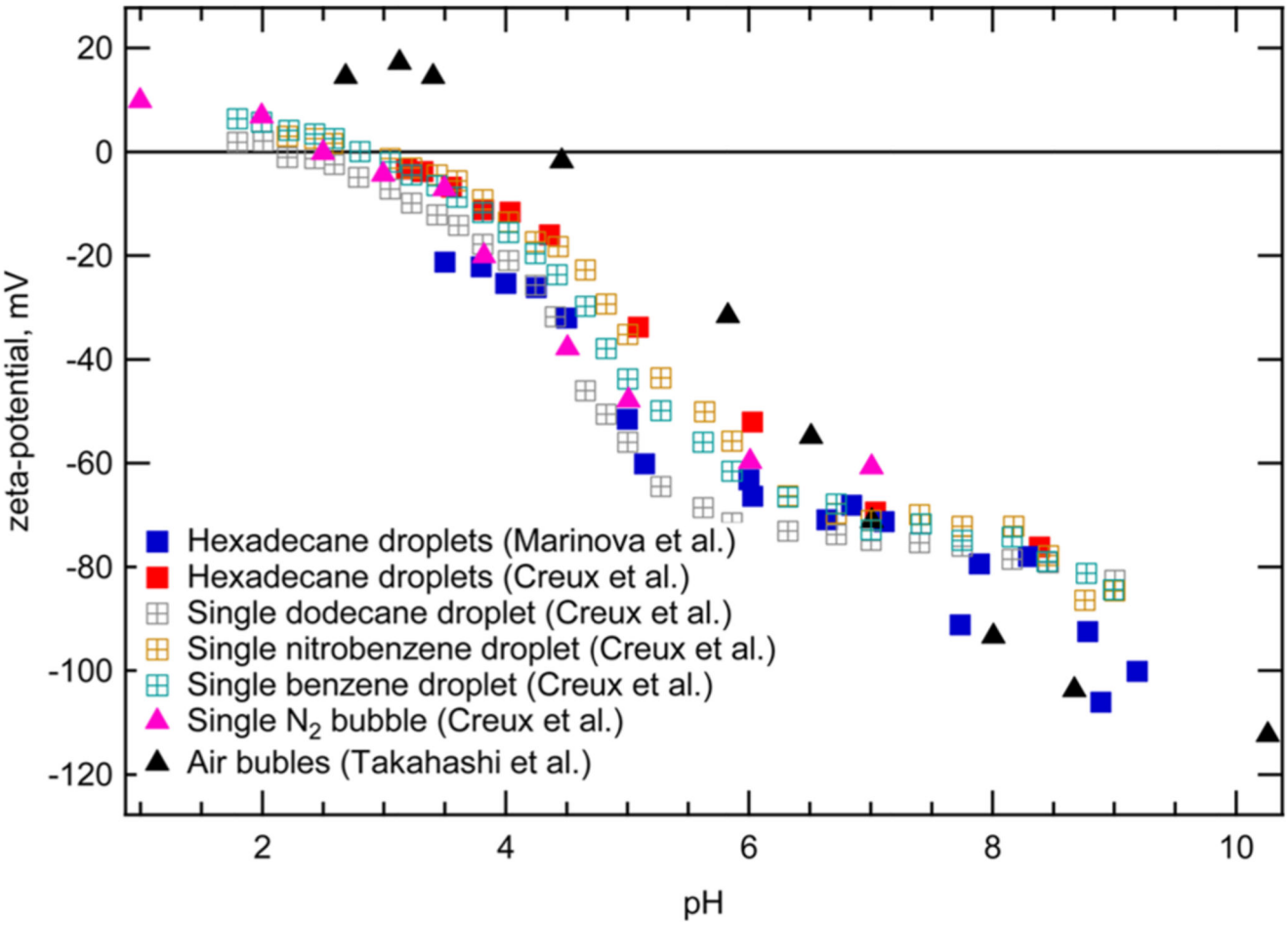

Figure 27.

ζ-potential of oil droplets[140139] and air[138] and N_2 [139] bubbles as a function of pH. pH control is achieved by adding either HCl or NaOH. The pH of the potential of zero charge is between 2.5 and 4.5

Europe PMC Funders Author Manuscripts

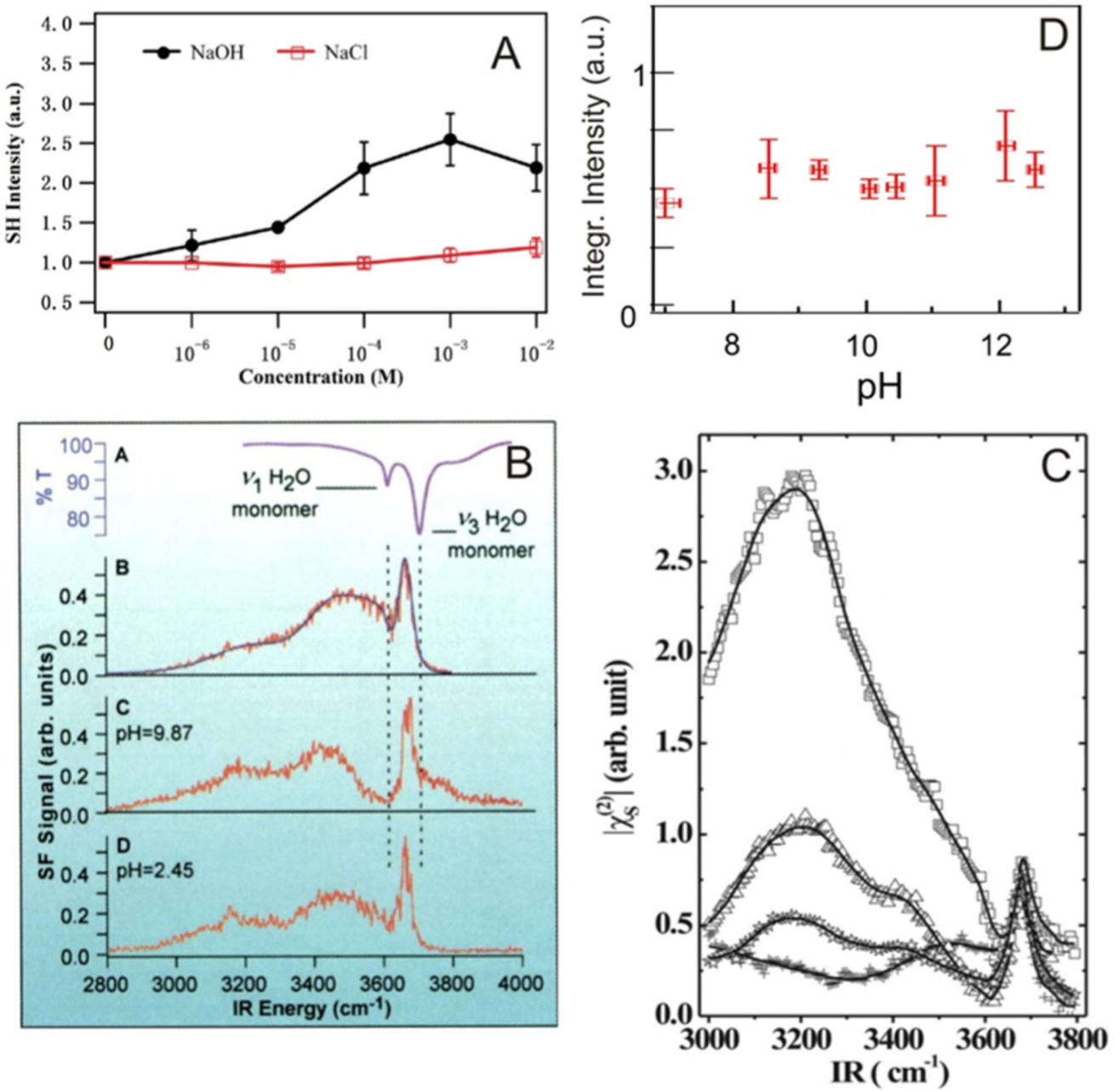

Figure 28.

pH-dependent SHG and SFG data for various interfaces: (A) pH-dependent nonresonant SHG intensity measured from the planar hexadecane/water interface (Reproduced from ref 149 with permission. Copyright 2015 Royal Society of Chemistry.); (B) SFG spectra obtained from the CCl_4/water interface (Reproduced from ref 155 with permission. Copyright 2001 American Association for the Advancement of Science.); (C) SFG spectra as a function of pH from the OTS/water interface [for pH values of 11 (squares), 7.8 (triangles), 6 (stars) and 2.3 (crosses)] (Reproduced from ref 156 with permission. Copyright 2009 Elsevier.); and (D) SFG scattering intensities from hexadecane nanodroplets in water

as a function of pH (Reproduced from ref 157 with permission. Copyright 2014 the National Academy of Sciences)

Europe PMC Funders Author Manuscripts

Europe PMC Funders Author Manuscripts

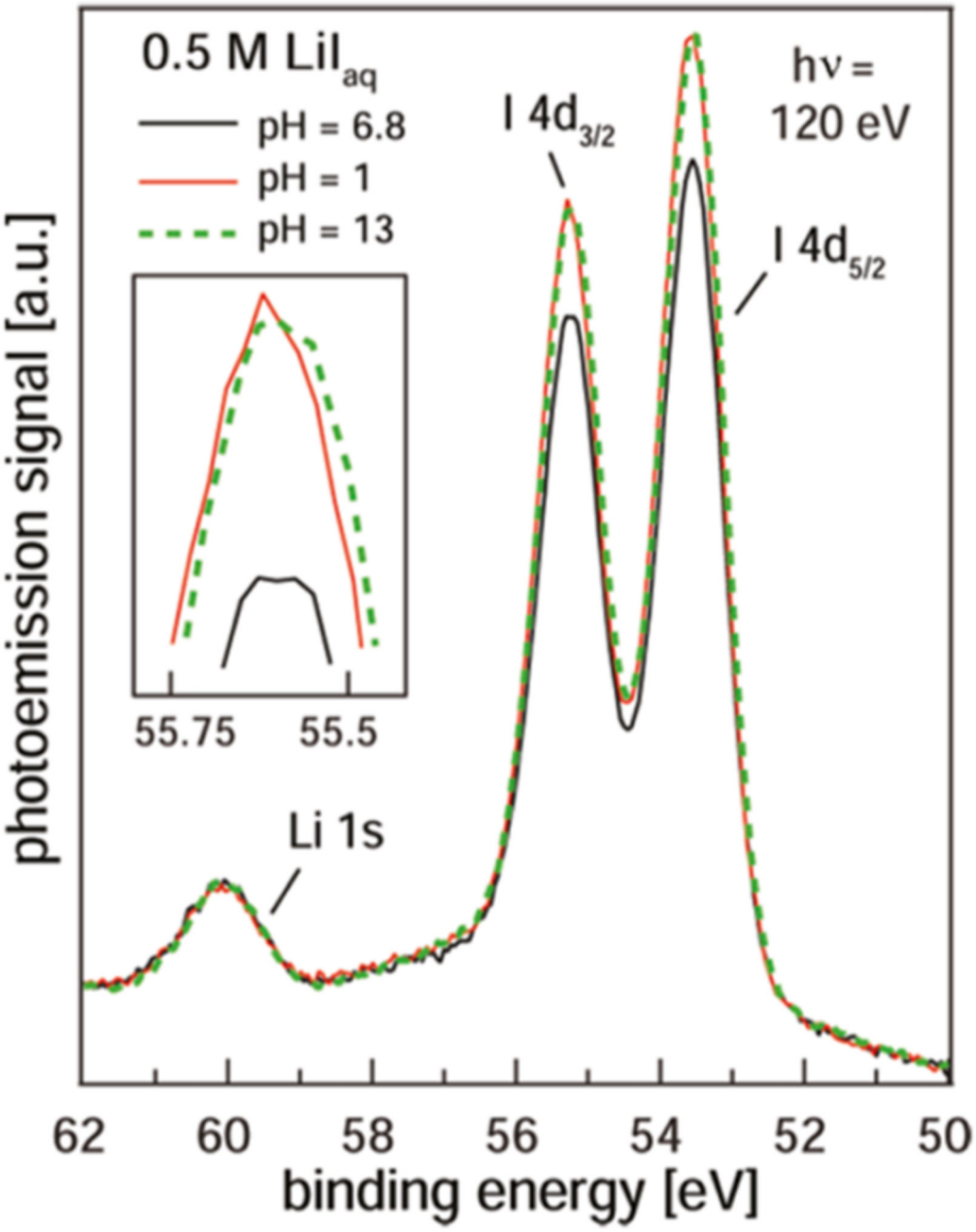

Figure 29.

XPS spectra of 0.5 M LiI aqueous solutions in the indicated energy range. Clearly, as illustrated in the inset, I^- surface propensity is enhanced in non-neutral solutions. Reproduced from ref 165 with permission. Copyright 2011 American Chemical Society

Europe PMC Funders Author Manuscripts

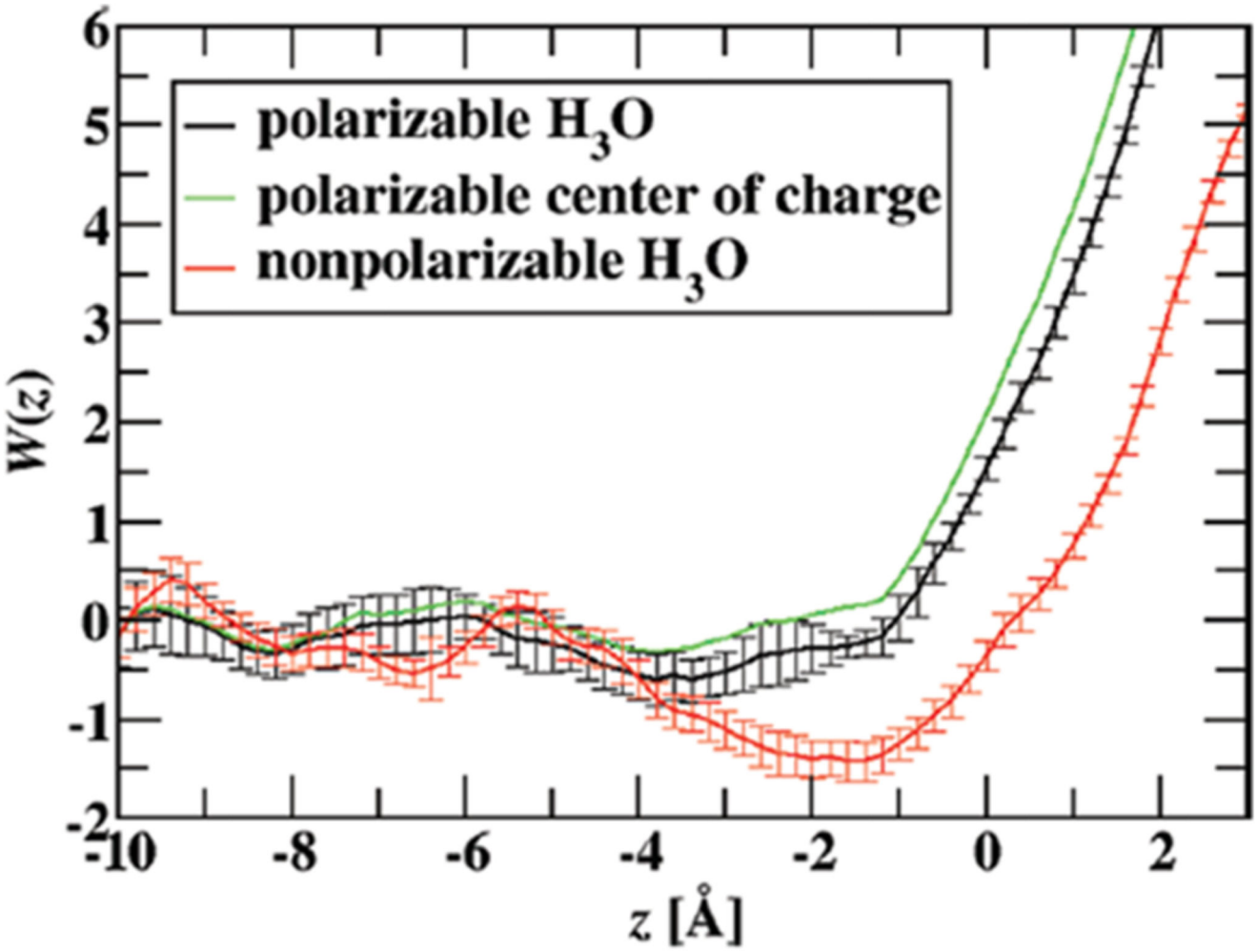

Figure 30.

Potentials of mean force calculated using an MS-EVB model of the proton with and without polarizability. Clearly accounting for polarizability creates a proton whose adsorption at the air/water interface is dramatically less favored. Reproduced from ref 177 with permission. Copyright 2012 American Chemical Society

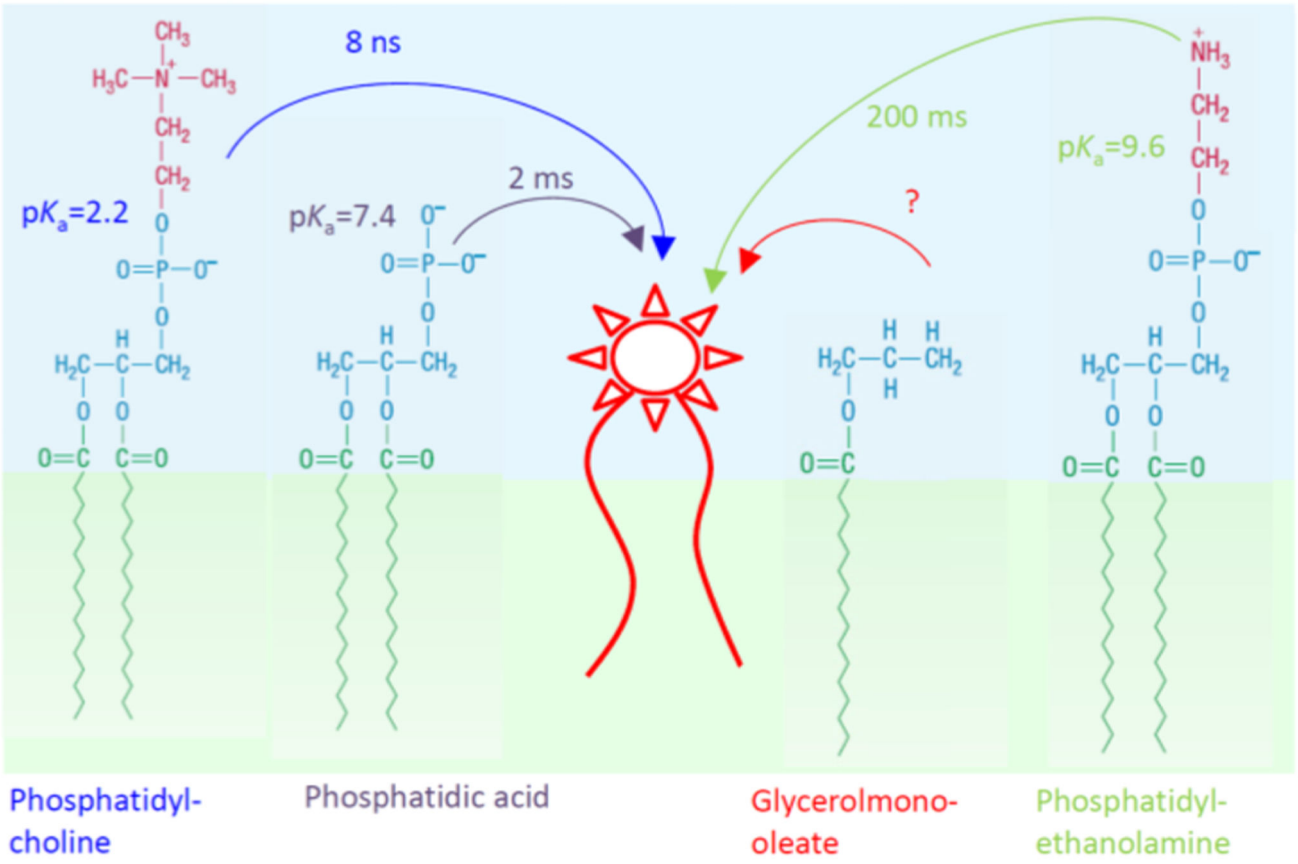

Figure 31.

Proton transfer to a lipid-anchored pH-sensitive dye. In equilibrium, the residence time of a proton on titratable residues can be calculated. If it was a determinant of proton mobility, the surface diffusion constants of protons on different lipids should differ by orders of magnitude

Europe PMC Funders Author Manuscripts

Europe PMC Funders Author Manuscripts

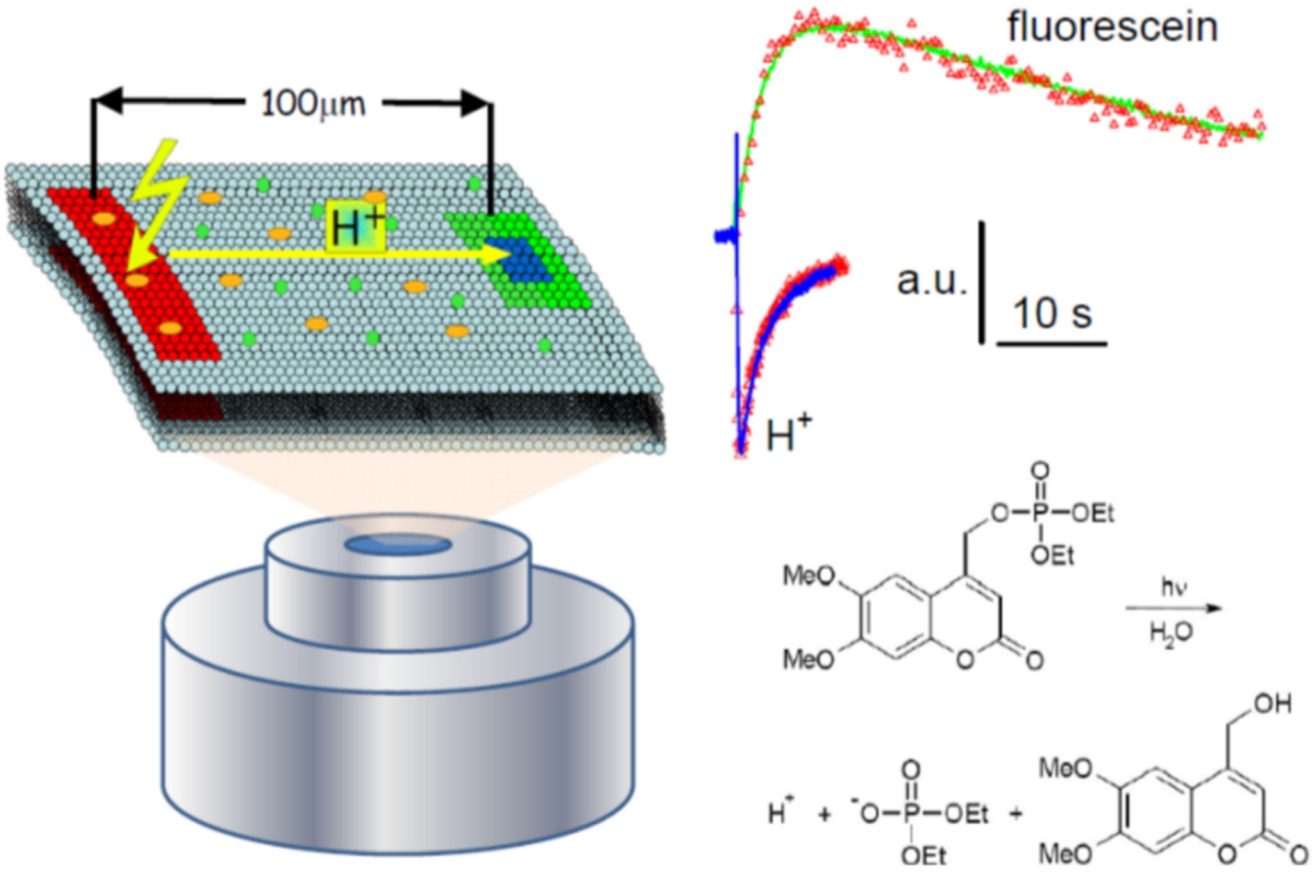

Figure 32.

Measurements of D_p. (Left) A horizontal planar lipid bilayer is placed on top of an inverse fluorescent microscope. A UV-flash releases the protons within the red area from a membrane-bound caged compound.[225] (Upper right) Proton arrival at a distant site (blue) is indicated by the drop in fluorescence intensity (blue line) of a lipid-anchored pH-dependent dye (excited in the green area). Photorelease of fluorescein from a caged compound in the red area and its fluorimetric detection in the blue area yielded a much slower diffusion constant (green line), indicating that fluorescein diffusion occurred via the aqueous bulk (Right upper panel taken from ref 218 with permission. Copyright 2003 Cell Press). Proton shuttling by buffer molecules would have yielded equally slow kinetics

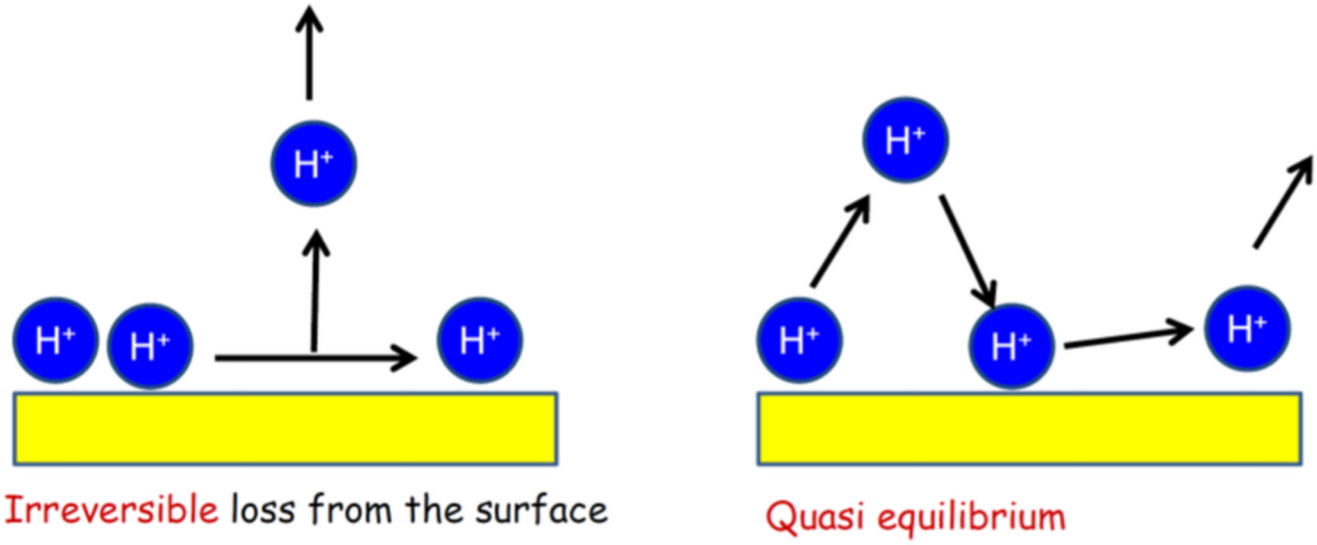

Figure 33.

Gibbs activation energy $\Delta G^{\ddagger}$ for proton surface-to-bulk release depends on whether the detached proton is irreversibly lost from the surface (left panel) or allowed to return to the surface (right panel). The term R_1 accounts for the two models in the equation for proton surface diffusion: $\sigma(x,t) = \sigma_o + A/(4\pi Dt)\exp(-x^2/(4Dt))R_1$ where σ(x,t), σ_0, A, and D are the are the proton surface density as a function of both time t and the distance x from the proton source, the initial proton surface density, a constant, and the proton surface diffusion coefficient, respectively. $R_1 = \exp(-tk_{off})$ for irreversible proton loss[228] and $R_1 = (1 + [(\pi Dt)^{-1/2}/L_0]^a)^{-1}$ in quasi-equilibrium, where L_0 and a are the distance over which surface and bulk protons are coupled and the dimensionality of the space orthogonal to the membrane surface where the detached protons diffuse (should be equal to 1), respectively.[229]

Europe PMC Funders Author Manuscripts

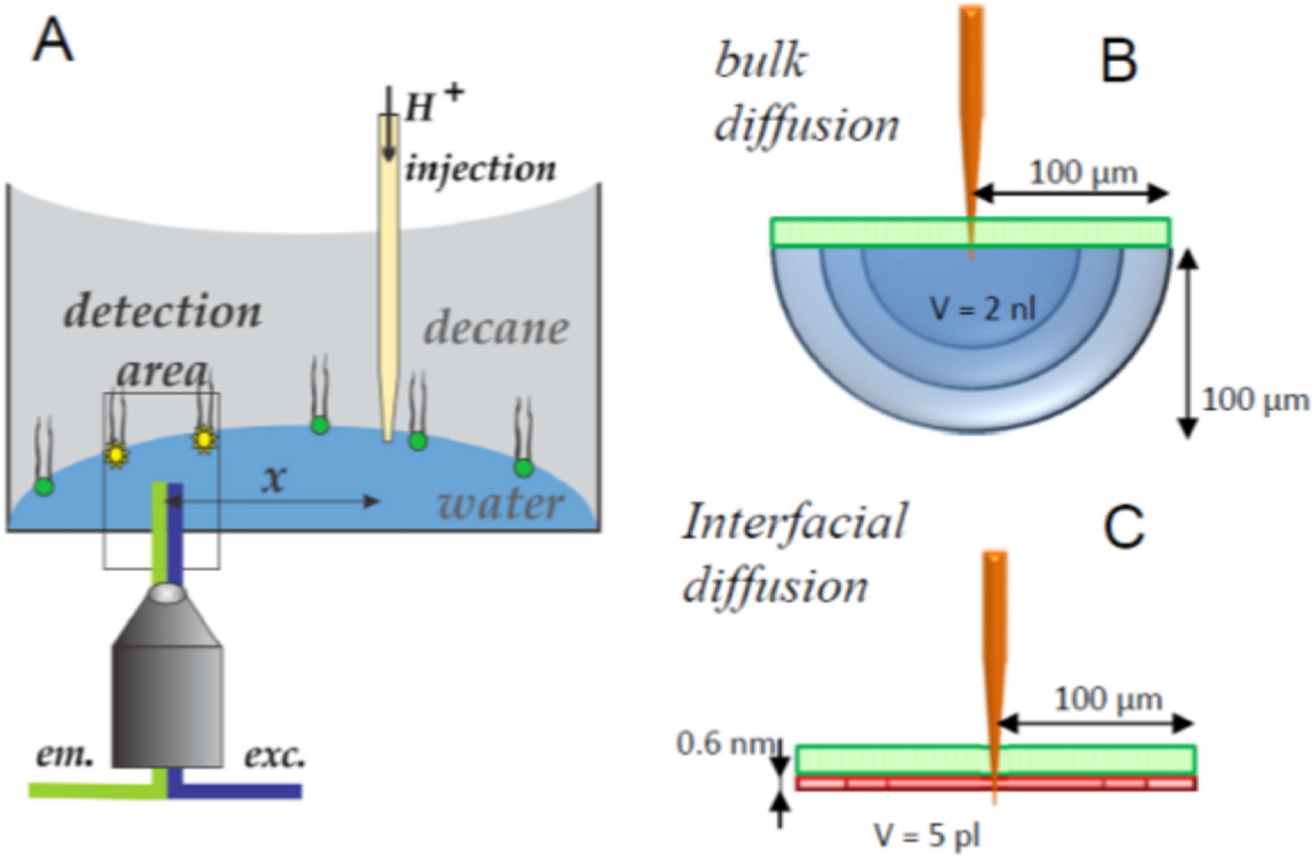

Figure 34.

Observation of interfacial proton migration along the decane/water interface. (A) Protons were microinjected via a glass pipet and their arrival at a distant spot was indicated by the pH response of sparsely located amphiphilic dye molecules.[230] (B) If the proton was traveling 100 μm by diffusion via bulk, proton microinjection to the surface should have decreased the pH from 6.3 to 5.3 in the buffer volume (V=2 nL) occupying the half-sphere beneath the water/decane interface. Taking into account the buffer capacity of 0.06 mM, this would have required 0.06 mM × 2 nL = 1.2×10^{-13} mole of protons. (C) Since only 2×10^{-16} mole of protons was injected, the protons must have moved within a thin layer (V=5 pL) adjacent to the interface to elicit the recorded pH drop 100 μm away from the source

Europe PMC Funders Author Manuscripts

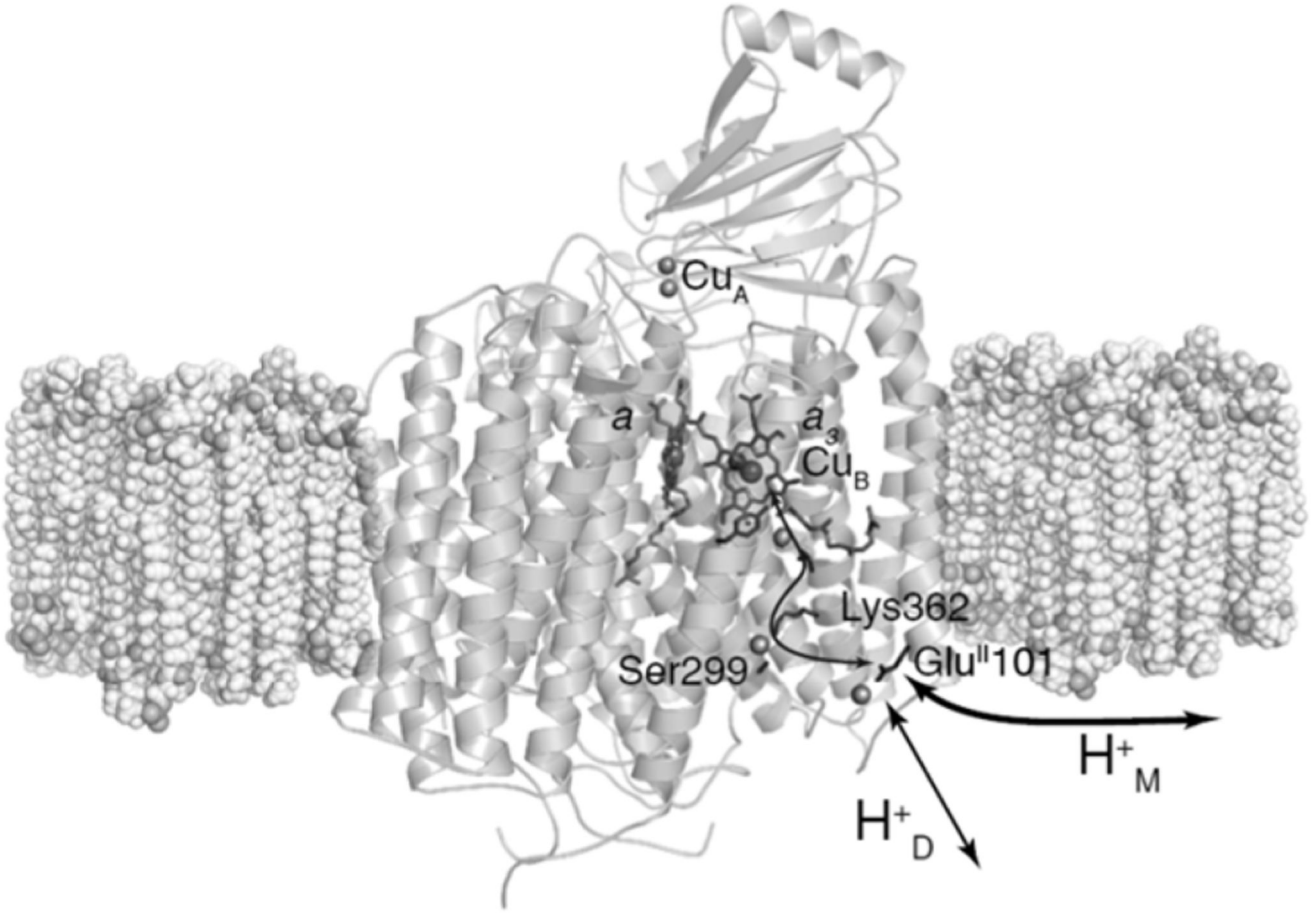

Figure 35.

One of the proton pathways in cytochrome c oxidase is wired via an acidic residue (Glu101) to the membrane surface. The proton influx H^+_M via the membrane surface exceeds several times the proton transfer H^+_D of the detergent-solubilized cytochrome c oxidase; serCuA, heme a, heme a3, and CuB are redox-active cofactors, and residue Lys362 (hydrogen bonded via a water molecule to SerI299) is a key element of the proton pathway. Reproduced from ref 232 with permission. Copyright 2010 National Academy of Sciences

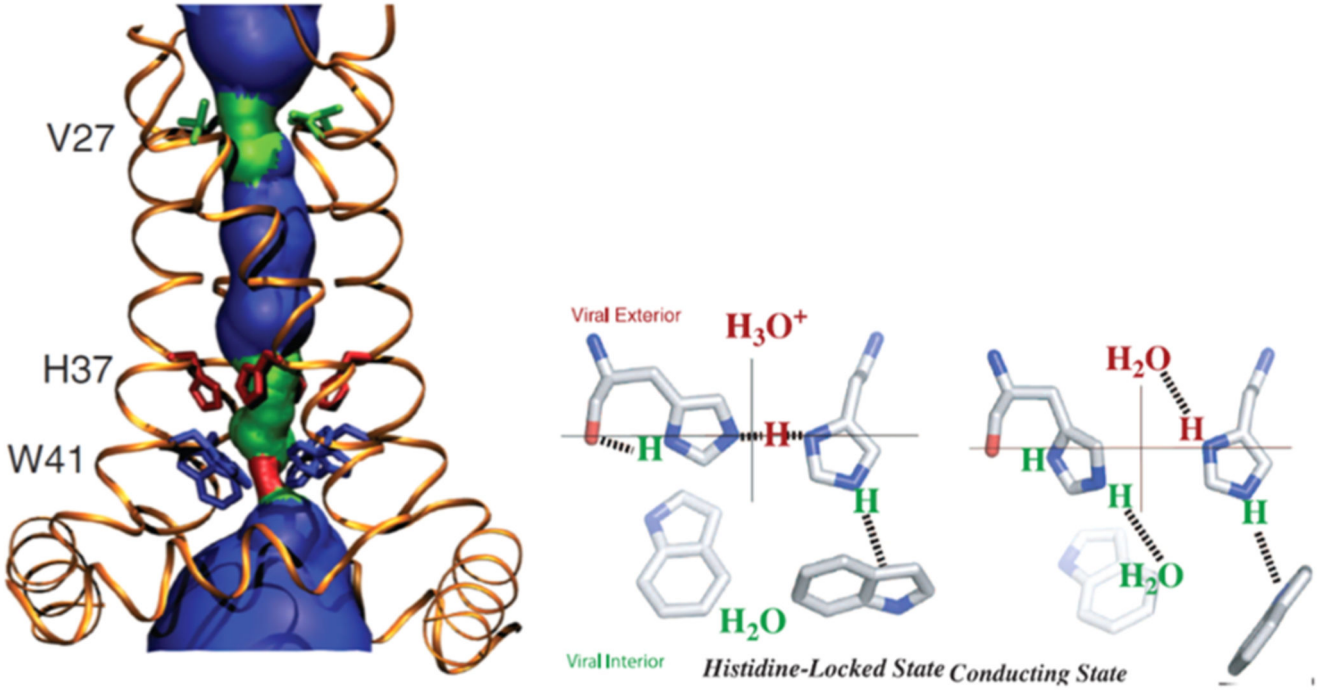

Figure 36.

Homotetrameric proton channel formed by the M2 protein from influenza A. His37 mediates the shuttling of protons across a central barrier between the N- and C-terminal aqueous pore regions. Two of the four histidines and tryptophans are shown. Upon PT to the inter-residue HB, the transition from the locked to the open conformation takes place.[244]

Europe PMC Funders Author Manuscripts

Europe PMC Funders Author Manuscripts

Table 1

Comparison of Different Computational Methods for Vibrational Spectroscopy

	method	anharmonic effects	temp effects	NQE
static	harmonic NM	no	no	yes
	VPT2	quartic	no	yes
	VSCF	yes	no	yes
dynamic	DFT-BOMD	yes	yes	no
	DFT-CPMD	yes	yes	no
	MCTDH	yes	yes	yes